

**THE UNIVERSITY OF WESTERN ONTARIO
DEPARTMENT OF CIVIL AND
ENVIRONMENTAL ENGINEERING**

Water Resources Research Report

**City of London: Vulnerability of Infrastructure to
Climate Change**

**Background Report #1
Climate and Hydrologic Modeling**

**By:
Hyung-II Eum
and
Slobodan P. Simonovic**

**Report No: 068
Date: August 2009**

**ISSN: (print) 1913-3200; (online) 1913-3219;
ISBN: (print) 978-0-7714-2844-9; (online) 978-0-7714-2845-6;**



City of London: Vulnerability of Infrastructure to Climate Change

Background Report 1 – Climate and Hydrologic Modeling

August, 2009

Prepared by

Hyung-II Eum

and

Slobodan P. Simonovic

Executive summary

The climate is changing and these changes may induce severe impacts on both, global and local scales. The Public Infrastructure Engineering Vulnerability Committee (PIEVC) established by Engineers Canada conducted an assessment of the vulnerability of Canadian Public Infrastructure to changing climatic conditions. The major conclusion of the assessment is that water resources infrastructure failures due to the climate change will be common across Canada. As a follow up, the City of London took an initiative to evaluate the impacts of climate change on its municipal infrastructure. An original systematic procedure is used to gather and examine available data in order to develop an understanding of the relevant climate effects and their interactions with infrastructure. The key steps of the procedure include: (i) Inventory of infrastructure components; (ii) Data gathering and sufficiency; (iii) Qualitative vulnerability assessment; (iv) Quantitative vulnerability assessment; and (v) Prioritization of the infrastructure components based on the level of risk. The assessment work is based on the results of the previously completed climate change impact study and focuses on infrastructure vulnerability to flooding.

Assessment methodology requires identification of climate loading on the municipal infrastructure. Climate and hydrologic modeling methodology and results are presented in this report as the basis for the impact assessment work. A weather generator model combined with principle component analysis (WG-PCA) and HEC-HMS hydrologic model are used in this study. The WG-PCA model is used to generate two different climate scenarios named: (a) historic scenario and (b) wet scenario, representing the lower and the upper bound of potential climate change, respectively. Generated meteorological data (precipitation and temperature) is used with the hydrologic model (HEC-HMS) and transformed into flow at multiple locations within the study region. Lastly, the flow frequency analysis is conducted to provide input into a hydraulic model that is used in mapping the floodplains for two climate scenarios considered (Sredojevic and Simonovic, 2009).

Using 43-years of historical data from 1964 to 2006 at 15 stations in the Upper Thames River basin, the WG-PCA generates a feasible future scenario of precipitation and temperature for 200 years – the historic climate scenario. The historic data is used to represent the business-as-usual condition that assumes there is no change in the social-economic-climatic system in the future. This scenario simulates climate change that may occur as a consequence of the already existing conditions and is considered in this study as the lower bound of climate change impact on the region under consideration. The second climate scenario employs CCSRNIES global climate model (GCM) with B21 emission scenario for time slice of 2040-2069 together with the historical data to generate a feasible future scenario we named in this work as a wet climate scenario – upper bound of climate change impact on the region under consideration. The results demonstrate the WG-PCA regenerates well the 25th, 50th, 75th percentile statistical values of precipitation and temperature for the historic scenario. Use of data perturbation process within the weather generator model generates data out of the range of values within the observed data. For the wet scenario, the WG-PCA generates the future that reflects the monthly climate shift of GCM model used (CCSRNIES B21) in the study.

The generated annual precipitation extreme values for 200 years are processed to extract the largest annual flood event for the entire basin and corresponding annual peak flow is used in flood frequency analysis. An assumption introduced in this work is that the largest floods are generated from extreme precipitation events. Several probability distributions including Gumbel, LP3, and GEV are utilized in this study. The flood frequency analysis results obtained using Gumbel distribution for the historic and the wet climate scenarios are compared with the current data used by the Upper Thames River Conservation Authority (UTRCA) for flood plain management. The difference exists between the current data and the data generated for two scenarios, as expected, and the direction of change varies with the location in the basin.

During the work on this study, the major deficiency in observed flow data is noticed across the basin – specially for the locations within the City of London. Therefore, continuous monitoring system at the

various sites in the basin is needed to provide the accurate hydrologic information that should enhance the results of modeling work. If and when the new observed data is collected, the hydrologic modeling analysis can be enhanced and consequently flood flow frequency analysis can be verified

Contents

City of London: Vulnerability of Infrastructure to Climate Change	- 1 -
Executive summary	- 2 -
List of Figures	- 7 -
List of Tables	- 9 -
1. Introduction.....	- 10 -
2. Climate modeling	- 12 -
2.1 The Weather Generator (WG) model	- 13 -
2.1.1 The K-NN Weather Generator (WG) algorithm	- 13 -
2.1.2 The WG algorithm with principle component analysis (WG-PCA)	- 16 -
2.2 The K-NN WG model used in this study.....	- 17 -
2.3 Results of the climate modeling	- 25 -
2.3.1 Precipitation.....	- 25 -
2.3.2 Temperature.....	- 34 -
2.3.3. Conclusions.....	- 39 -
3. Hydrologic modeling	- 40 -
3.1 The HEC-HMS hydrologic model.....	- 42 -
3.2 Input data for the HEC-HMS model.....	- 43 -
3.2.1 Spatial interpolation of model input data (inverse distance method, IDM).....	- 43 -
3.2.2 Temporal disaggregation of model input data	- 45 -
3.3 Delineation of model sub-basins and model calibration.....	- 49 -
3.3.1 Delineation of the sub-basins within the City of London	- 50 -
3.3.2 Model calibration	- 54 -
3.4 Application of the HEC-HMS model to future climate scenarios	- 66 -
3.5 Flood frequency analysis	- 69 -
4. Conclusions.....	- 81 -

References..... - 83 -

Appendix 1: Flood frequency at various locations..... - 87 -

Appendix 2: HEC-HMS hydrologic model parameters..... - 93 -

Appendix 3: Description of CD enclosed..... - 96 -

Appendix 4: List of Previous Reports in Series - 98 -

List of Figures

Figure 2.1 Schematic map of meteorological stations in the basin	19 -
Figure 2.3 Maximum temperature corresponding to different α values at the London station	22 -
Figure 2.4 Minimum temperature corresponding to different α at the London station	23 -
Figure 2.5 Comparison of the generated and the observed precipitation value for the historic scenario	26 -
Figure 2.6 Comparison of the generated and the observed precipitation value for the wet scenario	28 -
Figure 2.7 Monthly average change in total precipitation at the three representative stations for the wet scenario	29 -
Figure 2.8 Flood occurrence vectors	31 -
Figure 2.9 Number of annual maximum precipitation events within 200 years	33 -
Figure 2.10 Maximum temperature at the representative stations for the historic scenario	35 -
Figure 2.11 Minimum temperature at the representative stations for the historic scenario	36 -
Figure 2.12 Maximum temperature at the representative stations for the wet scenario	37 -
Figure 2.13 Minimum temperature at the representative stations for the wet scenario	38 -
Figure 3.1 Three modules of the HEC-HMS model.....	42 -
Figure 3.2 Hyetographs of an annual extreme event for the historic scenario	47 -
Figure 3.3 Hyetographs of an annual extreme event for the wet scenario	48 -
Figure 3.4 HEC-HMS model with 34 sub-basins.....	49 -
Figure 3.5 Locations used in the sub-watershed delineation process	51 -
Figure 3.6 Delineation of 4 main sub-watersheds in the City of London.....	52 -
Figure 3.7 Delineation of the Thames River into sub-watersheds within the City of London.....	53 -
Figure 3.8 The HEC-HMS model structure.....	53 -
Figure 3.9 Example of a set of water-surface profiles between section <i>A</i> and <i>B</i> of a channel.....	55 -
Figure 3.10 Relationships between storage and outflow for the sub-watersheds in the basin	56 -
Figure 3.11 Relationships between storage and outflow for the main stream (Upper Thames River) ...	58 -
Figure 3.12 Calibration results for the main stations in the basin	60 -

Figure 3.13 Calibration results for the Byron station (July 2000).....	- 61 -
Figure 3.14 Rainfall hyetograph for three creeks	- 63 -
Figure 3.15 Streamflow check points of the previous sub-watershed study	- 65 -
Figure 3.16 Time distribution of 24 hrs SCS synthetic storm.....	- 65 -
Figure 3.17 Hydrographs of an event for the historic scenario	- 67 -
Figure 3.18 Hydrographs of an event for the wet scenario	- 68 -
Figure 3.19 Procedure of flood frequency analysis	- 70 -
Figure 3.20 Flood frequency analyses for two climate scenarios	- 75 -
Figure 3.21 Procedure of flood frequency analysis in previous works.....	- 78 -
Figure 3.22 Flood frequency for two climate scenarios	- 79 -

List of Tables

Table 2.1 Monthly changes in precipitation and temperature between the historic and the GCM scenarios	- 20 -
Table 2.2 Accuracy of cross-correlation for two WG models	- 21 -
Table 2.3 Seasonal standard deviation for maximum and minimum temperature	- 24 -
Table 2.4 The MDMP and dispersion (\bar{r}) (Julian calendar)	- 32 -
Table 3.1 Characteristics of potential hydrologic models for use in this study	- 41 -
Table 3.2 Location information for 15 measurement stations in the Upper Thames River basin	- 44 -
Table 3.3 Synthetic storms and peak flows in the sub-basins	- 62 -
Table 3.4 Peak flow (m ³ /sec) simulation results	- 62 -
Table 3.5 Peak flow at the Dingman Creek check points	- 64 -
Table 3.6 Goodness-of-fit test for the main locations	- 74 -

1. Introduction

The climate is changing and these changes may induce severe impacts on both, global and local scales. The Public Infrastructure Engineering Vulnerability Committee (PIEVC) established by Engineers Canada conducted an assessment of the vulnerability of Canadian Public Infrastructure to changing climatic conditions. The major conclusion of the assessment is that water resources infrastructure failures due to the climate change will be common across Canada. Consequently, the water infrastructure vulnerability should be identified as one of four priority areas to be reviewed as part of the first National Engineering Assessment.

The main objective of this study is to provide an engineering assessment of the vulnerability of London's public infrastructure to changing climate conditions. An original systematic procedure is used to gather and examine available data in order to develop an understanding of the relevant climate effects and their interactions with infrastructure. The key steps of the procedure are: (i) Inventory of infrastructure components; (ii) Data gathering and sufficiency; (iii) Qualitative vulnerability assessment; (iv) Quantitative vulnerability assessment; and (v) Prioritization of the infrastructure components based on the level of risk. The presented work is based on the results of the previously completed climate change impact study and focuses on infrastructure vulnerability to flooding. The elements of infrastructure under consideration include: buildings within and adjacent to the flood lines, roads, bridges, culverts, wastewater treatment plants, storm water management network, etc. The study is limited to the boundaries of the City of London.

Climate and hydrologic modeling methodology and results are presented in this report as the basis for the impact assessment work. A weather generator model combined with principle component analysis (WG-PCA) and HEC-HMS hydrologic model are used in this study. The WG-PCA model is used to generate two different climate scenarios: (a) historic scenario and (b) wet scenario. Generated meteorological data (precipitation and temperature) is used with the hydrologic model (HEC-HMS) and

transformed into flow at multiple locations within the city. Lastly, the flow frequency analysis is conducted to provide input into a hydraulic model that is used in mapping the floodplains for two climate scenarios considered (Sredojevic and Simonovic, 2009).

The report is organized in two major parts: (i) the climate model and (ii) the hydrologic model. The climate model section starts with the theory of the WG model and the formulation of input data. Then, the results of two different climate scenarios (historic and wet), generated by the WG model are presented. In hydrologic model section, the description of the HEC-HMS model, input and output data is provided. The presentation of the model calibration and verification follows. The results of the hydrologic model analyses for 2 different scenarios are provided and frequency analysis of flow data is described. The report concludes with insights from the climate and hydrologic analyses.

2. Climate modeling

Stationarity—the idea that natural systems fluctuate within an unchanging variability—is a foundational concept in water resources management. The stationarity assumption has long been compromised by human disturbances in river basins. Flood risk, water supply, and water quality are affected by water infrastructure, channel modifications, drainage works, and land-cover and land-use change. Two other (sometimes indistinguishable) challenges to stationarity have been externally forced, natural climate changes and low-frequency, internal variability. Planners have tools to adjust their analyses for known human disturbances within river basins, and justifiably or not, they generally have considered natural change and variability to be sufficiently small to allow stationarity-based water resources management. **Stationarity is dead** because substantial anthropogenic change of Earth's climate is altering the means and extremes of precipitation, evapotranspiration, and rates of discharge of rivers (Milly et al, 2008). Warming augments atmospheric humidity and water transport. This increases precipitation, and possibly flood risk, where prevailing atmospheric water-vapor fluxes converge. New tools are required to address this challenge.

The General Circulation Models (GCMs) provide the range of feasible future climate scenarios employing various emission scenarios categorized into 4 families (A1, A2, B1, and B2) that explore economic and technological driving forces, a wide range of demography and green-house gas emissions (IPCC, 2000). However, GCMs have inevitable drawback that their spatial resolution is too coarse for assessment of regional impacts of climatic change.

Downscaling procedures, therefore, are necessary to apply at regional scales. A various forms of Weather Generators (WG) have been used as a statistical downscaling approach. The WG models can take two forms: 1) parametric form (Nicks et al., 1990; Parlange and Katz, 2000), and 2) non-parametric form (Sharma et al., 1997; Wilks and Wilby, 1999; Mehrotra and Sharma, 2007). Due to the difficulty of parametric weather generators with regards to fitting model parameters and some problems induced by

the parameters, the non-parametric methods are preferred in hydrologic practice. Among non-parametric methods, the K-NN (K-Nearest Neighbor) technique for generating synthetic weather data has been successfully applied in practice (Young, 1994; Lall and Sharma, 1996; Lall et al., 1996; Rajagopalan and Lall, 1999; Buishand and Brandsma, 2001; Yates et al., 2003).

Sharif and Burn (2006) proposed the improved K-NN technique to generate data that will be out of the historical range by the introduction of a perturbation process. In addition, Eum and Simonovic (2008) extended the work of Sharif and Burn by combining the WG model with the principle component analysis to decrease the calculation burden (new model is named WG-PCA). Sharif and Burn (2006), Prodanovic and Simonovic (2006a, 2006b), and Eum and Simonovic (2008) have applied K-NN technique successfully in the Upper Thames River Basin, Canada using three daily input meteorological variables (precipitation, maximum temperature, and minimum temperature) and same output variables. They have also investigated the accuracy of generated monthly averaged values of meteorological variables. Therefore, in this study the improved WG-PCA algorithm has been implemented. It incorporates a probability bandwidth (Sharma et al., 1997; Sharma and O'Neill, 2002) that limits generation of unacceptable values of meteorological variables. The following sections present the theory of K-NN WG model and the improved WG-PCA model used in this study.

2.1 The Weather Generator (WG) model

2.1.1 The K-NN Weather Generator (WG) algorithm

The K-NN algorithm starts by randomly generating the day 1, normally Jan 1st, from the observed data set and a specified number of days similar in characteristics to the current day. Using resampling procedure, one of the days from the data set with similar statistical characteristics with current day is selected to represent the weather for the next day. The nearest neighbor algorithm (a) uses a simple computational procedure, and (b) preserves well both, temporal and spatial correlation among the input

data. Yates et al. (2003) applied K-NN algorithm successfully with three variables to diverse areas of United States. Their version of the algorithm has a limitation that the newly generated data stay within the range of observed minimum and maximum value.

Sharif and Burn (2006) modified the K-NN weather generator algorithm of Yates et al. (2003) by incorporating a perturbation process for weather variables that generates extremes outside the range of historically observed data. The modified K-NN algorithm with p variables and q stations proposed by Sharif and Burn (2006) has the following steps:

- 1) Calculation of regional means of p variables (x) across all q stations for each day in the historic record:

$$\overline{X}_t = [\overline{x}_{1,t}, \overline{x}_{2,t}, \dots, \overline{x}_{p,t}] \quad \forall t = \{1, 2, \dots, T\} \quad (2.1)$$

where

$$\overline{x}_{i,t} = \frac{1}{q} \sum_{j=1}^q x_{i,t}^j \quad \forall i = \{1, 2, \dots, p\} \quad (2.2)$$

- 2) Computation of the potential neighbors of size $L = (w + 1) \times N - 1$ days long for each variable p with N years of historical record and selected temporal window of size w . All days within that window are selected as potential neighbors to the current feature vector. Among the potential neighbors, N data corresponding to the current day are eliminated in the process to prevent the possibility of generating the same value as that of the current day.
- 3) Computation of the regional means for all potential neighbors selected in step 2) across all q stations for each day.
- 4) Computation of the covariance matrix, C_t , for day t using the data block of size $L \times p$.
- 5) Random selection of the first time step value for each variable p from all current day values in the record of N years.
- 6) Computation of the Mahalanobis distance expressed by Eq. (2.3) between the mean vector of the current days (\overline{X}_t) and the mean vector of all nearest neighbor values (\overline{X}_k), where $k = 1, 2, \dots, L$.

$$d_k = \sqrt{(\bar{X}_t - \bar{X}_k) C_t^{-1} (\bar{X}_t - \bar{X}_k)^T} \quad (2.3)$$

where T represents the transpose matrix operation, and C^{-1} represents inverse of covariance matrix.

- 7) Selection of the number of $K = \sqrt{L}$ nearest neighbors out of L potential values.
- 8) Sorting the Mahalanobis distance d_k from smallest to largest, and retaining the first K neighbors in the sorted list (they are referred to as the K Nearest Neighbors). Then, use a discrete probability distribution giving higher weights to closest neighbors for resampling out the set of K neighbors (Lall and Sharma, 1996). The weights are calculated for each k neighbor using the following Eq. (2.4) and (2.5).

$$w_k = \frac{1/k}{\sum_{i=1}^K 1/i} \quad (2.4)$$

where $k = 1, 2, \dots, K$. Cumulative probabilities, p_j , are given by:

$$p_j = \sum_{i=1}^j w_i \quad (2.5)$$

- 9) Generating random number $u(0,1)$ and comparing it to the cumulative probability p_j to determine the nearest neighbor of current day. If $p_1 < u < p_K$, then day j for which u is closest to p_j is selected. On the other hand, if $u < p_1$, then the day corresponding to d_1 is selected, and if $u = p_K$, then the day corresponding to d_K is selected. Once the nearest neighbor is selected, the weather of selected day is used for all stations in the region. This is how the K-NN algorithm preserves the cross-correlation among variables within the region under consideration.
- 10) This step is added by Sharif and Burn (2006) to generate variables outside the range of historical data by perturbation. First, estimation of (a) a conditional standard deviation σ for K nearest neighbors, and (b) bandwidth λ (Sharma et al., 1997) is performed using Eq. (2.6):

$$\lambda = 1.06 \sigma K^{-1/5} \quad (2.6)$$

Then, the perturbation process follows according to Eq. (7):

$$y_{i,t}^j = x_{i,t}^j + \lambda \sigma_i^j z_t \quad (2.7)$$

where $x_{i,t}^j$ is the value of the weather variable obtained from the original K-NN algorithm; $y_{i,t}^j$ is the weather variable value from the perturbed set; z_t is normally distributed random variable with zero mean and unit variance, for day t . To prevent the negative values for bounded variables (i.e. precipitation), the largest acceptable value of $\lambda_a = x_{*,t}^j / 1.55\sigma_*^j$ is employed (Sharma and O'Neill, 2002), where * refers to a bounded weather variable (Sharif and Burn, 2006). If the value of the bounded weather variable, computed previously, is still negative, then a new value of z_t is generated.

2.1.2 The WG algorithm with principle component analysis (WG-PCA)

Eum and Simonovic (2008) have improved the K-NN WG model to reduce the dimension of Mahalanobis distance matrix expressed by Eq. (2.3). This modification allows the use of various available variables without the increase of computational burden. The WG-PCA algorithm reduces the dimension of the mean vector of the current days (\bar{X}_t) and the mean vector of all nearest neighbor values (\bar{X}_k) in Step (6) from previous section. In that way only the variance of the first principle component is required to calculate the Mahalanobis distance. The WG-PCA modifies the Step (6) of the algorithm presented in the previous section as follows:

- (a) Calculation of eigenvector and eigenvalue for the covariance matrix (C_t).
- (b) Finding the eigenvector related to the largest eigenvalue that explains the largest fraction of the variance described by the p variables.
- (c) Calculation of the first principle component with the eigenvector found in step (b) using Eq. (2.8) and Eq. (2.9):

$$PC_t = \bar{X}_t \mathbf{E} \quad (2.8)$$

$$PC_k = \bar{X}_k \mathbf{E} \quad (2.9)$$

where PC_t and PC_k are the values of current day and the nearest neighbor transferred by the eigenvector from step (b), respectively; and \mathbf{E} is the eigenvector related to the largest eigenvalue. After calculating the PC_t and PC_k with one-dimensional matrix obtained by Eq (2.8) and (2.9), the Mahalanobis distance is computed using Eq. (2.10):

$$d_k = \sqrt{(PC_t - PC_k)^2 / \text{Var}(\mathbf{PC})} \quad \forall k = \{1, 2, \dots, K\} \quad (2.10)$$

where $\text{Var}(\mathbf{PC})$ represents the variance of the first principle component for the K nearest neighbors.

The perturbation process introduced by Sharif and Burn (2006) may generate high (or low) values of meteorological variables that are not acceptable in practice. Previous studies (Sharif and Burn, 2006; Eum and Simonovic, 2008) have employed the bandwidth corresponding to the probability of generating a negative value for precipitation. However, no procedure was in place for unacceptably high (or low) value of temperature. Therefore, in this study we investigate impacts of the bandwidth corresponding to several α probability values for temperature as shown in Eq. (2.11).

$$\begin{aligned} \lambda' &= \lambda \quad \text{if } F_{N(\mu_i, \lambda^2 \sigma_i)}(y_i \leq y_i^{\text{low}}) \leq \alpha/2 \text{ and } F_{N(\mu_i, \lambda^2 \sigma_i)}(y_i \leq y_i^{\text{high}}) \geq 1 - \alpha/2 \\ &= \lambda' \quad \text{if } F_{N(\mu_i, \lambda^2 \sigma_i)}(y_i \leq y_i^{\text{low}}) > \alpha/2 \text{ or } F_{N(\mu_i, \lambda^2 \sigma_i)}(y_i \leq y_i^{\text{high}}) < 1 - \alpha/2 \end{aligned} \quad (2.11)$$

where, λ' is a transformed bandwidth, y_i^{low} and y_i^{high} is a low and a high bound for variable y_i , respectively.

2.2 The K-NN WG model used in this study

This study employs daily precipitation, maximum temperature, and minimum temperature for 15 stations in the basin (Fig. 2.1) for the period from 1964 to 2006 ($N = 43$) to generate feasible future weather scenarios using the WG-PCA model described in the previous section. Among 15 stations used in this study, only three locations are selected to show the comparison of WG results in this report (data for

other locations are available upon request): (1) Stratford for illustrating the characteristic of the northern part of the basin, (2) London for south-western part, and (3) Woodstock for south-eastern part of the basin. For application of the WG-PCA, this study used the temporal window of 14 days ($w = 14$) and 43 years of historical data - 569 days as the potential neighbors ($L = (w + 1) \times N - 1 = 569$) for each variable.

This study incorporated a GCM climate change scenario with the WG-PCA model to represent the upper bound of climate change that may occur in the region. Based on the results of the previous research study (as documented by Prodanovic and Simonovic, 2006a) the CCSRNIES B21 scenario provided by the Canadian Climate Impacts Scenarios group at the University of Victoria (<http://www.cics.uvic.ca>) has been selected to investigate the impacts on high flows in the Upper Thames River basin and named wet climate scenario in this report. This study employs the CCSRNIES B21 (wet) scenario for the time slice of 2040-2069 representing climate condition for the 2050s. To include the impact of climate change in the K-NN WG model, the observed historical data is modified by adding (in the case of temperature) or multiplying (in the case of precipitation) the average change between the reference scenario and the future climate scenario to the regional observed historical data at a specific station. The monthly change for the wet scenario for precipitation and temperature variables is shown in Table 2.1. The wet scenario shows the increase in precipitation during the period from January to September. Specially, the precipitation during the spring season from March to June is significantly higher. Note that temperature for wet scenarios is higher for all months (reflection of global warming).

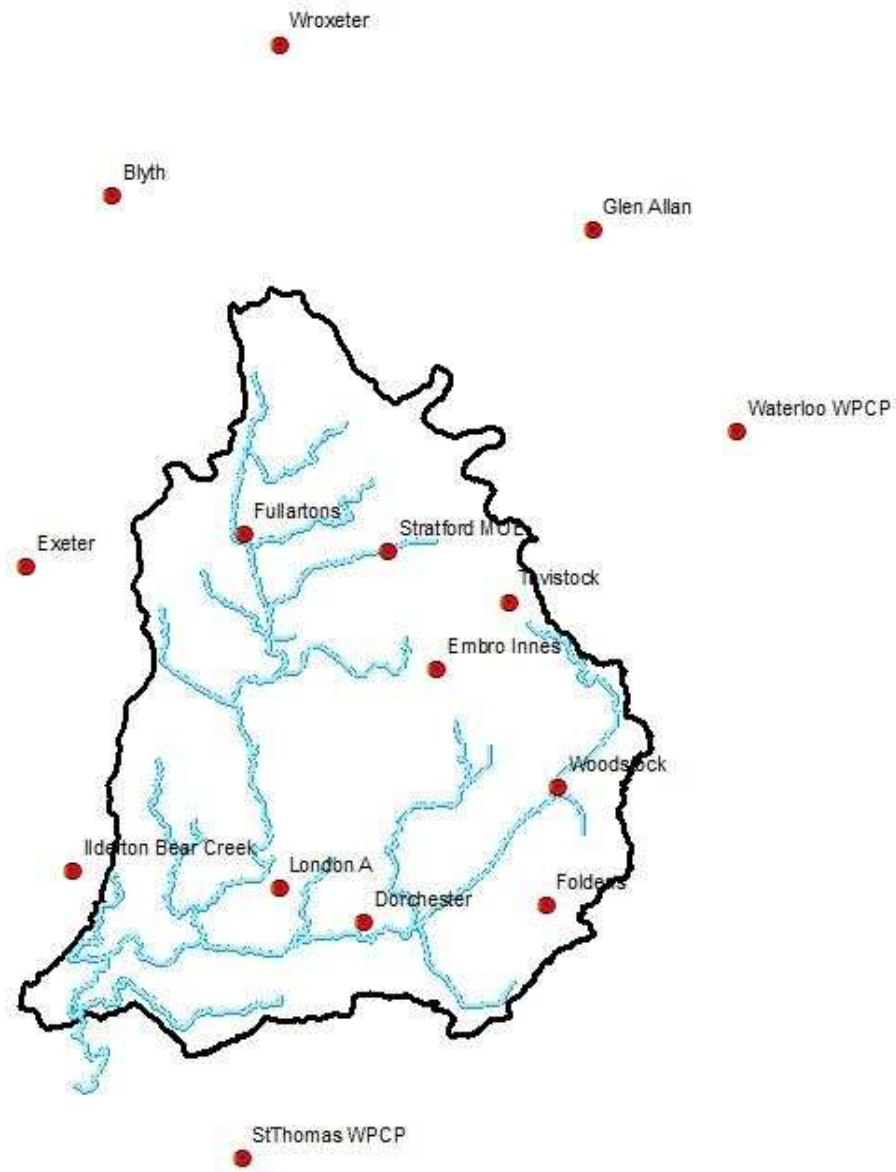


Figure 2.1 Schematic map of meteorological stations in the basin

Table 2.1 Monthly changes in precipitation and temperature between the historic and the GCM scenarios

Month	Wet	
	Precipitation (Percentage change)	Temperature (Difference in °C)
Jan	0.1767	4.43
Feb	0.0638	3.29
Mar	0.1507	4.52
Apr	0.2284	5.78
May	0.2414	4.50
Jun	0.1855	3.32
Jul	0.0503	3.59
Aug	0.0788	4.09
Sep	0.0427	2.11
Oct	-0.1151	3.11
Nov	-0.1555	4.64
Dec	-0.031	1.43

To avoid generation of negative precipitation value at a station, the previous study regenerated a random number for that station until positive values are obtained. This study uses the same random number for all stations in order to minimize the bias. Table 2.2 shows the sum of square error for monthly cross-correlation of precipitation. By employing the same random number at all stations, monthly cross-correlation is improved for 40.2 %. Figure 2.2 shows the results of cross-correlation analysis for the two WG-PCA models.

In addition, this study introduces a bandwidth λ for various probability level α values for temperature variables to alleviate generation of unacceptably high or low values of temperature. Five α values: 6 %, 5%, 4%, 1%, and 0.05 % are tested in this study. Then, the seasonal daily temperatures are compared as shown in Figure 2.3 and Figure 2.4.

Table 2.2 Accuracy of cross-correlation for two WG models

Contents	WG used in earlier study	WG used in this study
Sum of square error	0.42	0.25
Improvement (%)	-	40.2

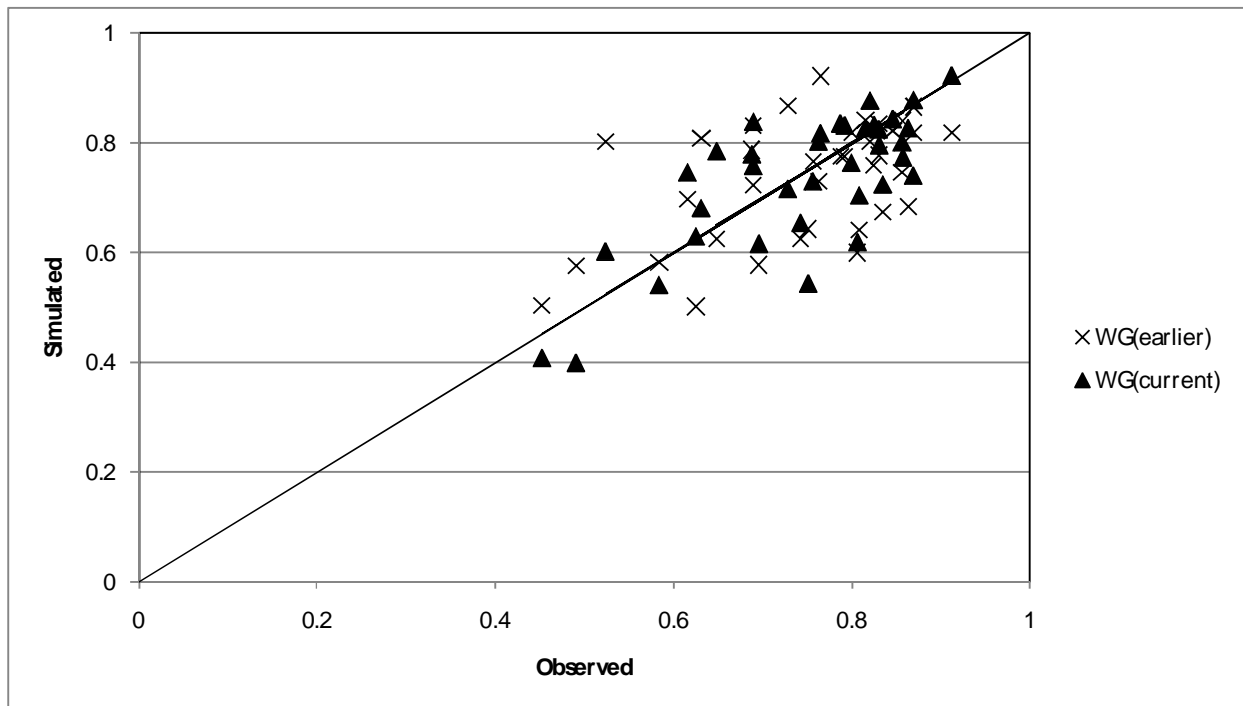
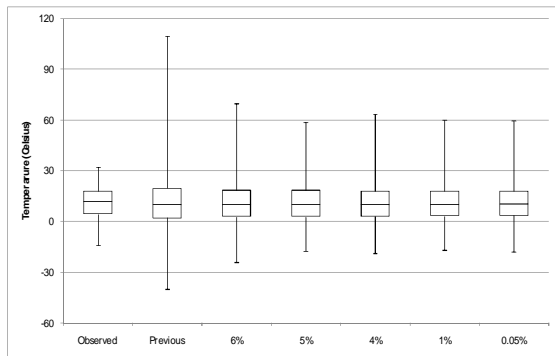
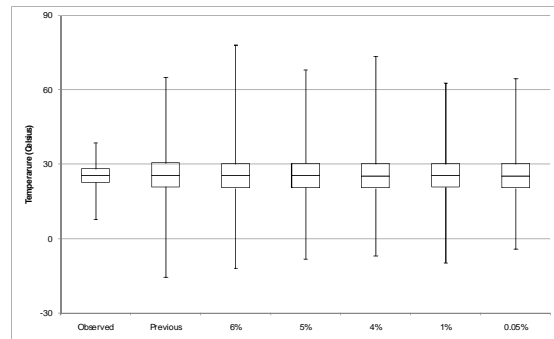


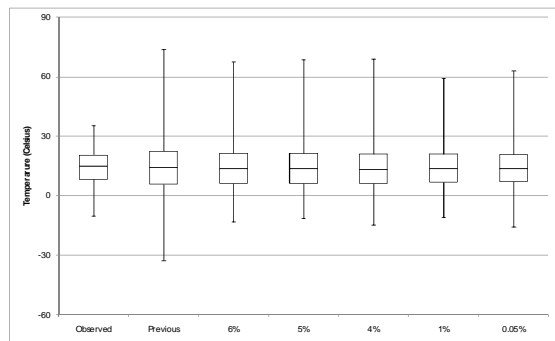
Figure 2.2 Cross-correlation results for data obtained by two WG models



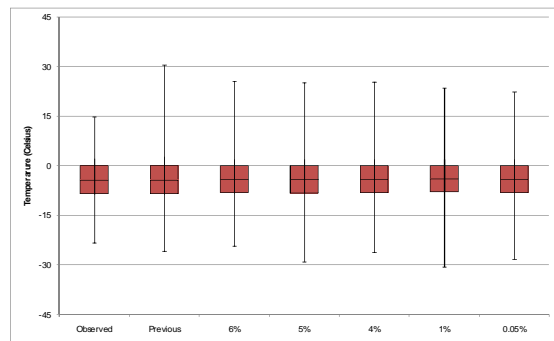
(a) Spring



(b) Summer

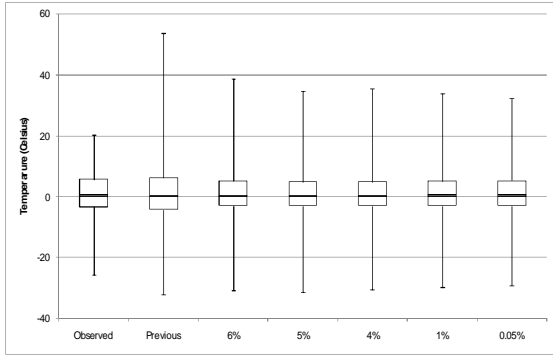


(c) Autumn

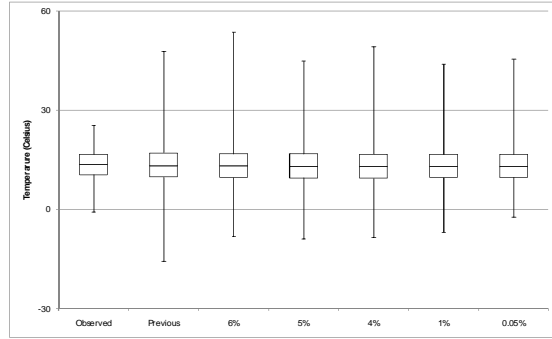


(d) Winter

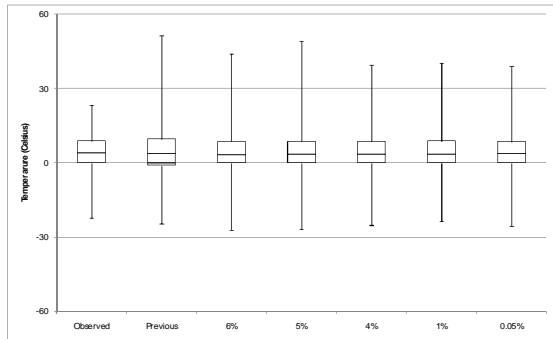
Figure 2.3 Maximum temperature corresponding to different α values at the London station



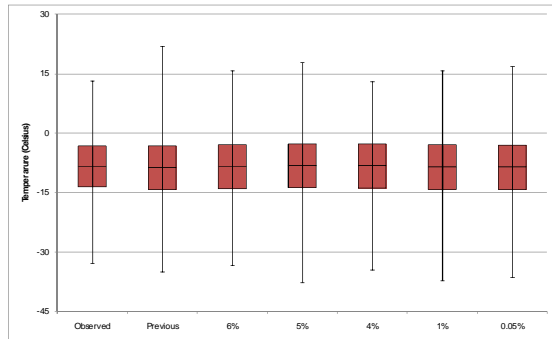
(a) Spring



(b) Summer



(c) Autumn



(d) Winter

Figure 2.4 Minimum temperature corresponding to different α at the London station

As expected, the variability of daily temperature value decreases with decrease in α value, but the level of decrease varies with season. In specific, the impact of bandwidth introduction is more significant during spring and autumn. In the perturbation process of the K-NN algorithm, a variable is generated by combination of a bandwidth, a standard deviation, and a random number as shown in Eq. (2.7) in previous section. In addition, a bandwidth is inversely proportional to a standard deviation as shown in Eq. (2.12). Therefore, a larger standard deviation makes a bandwidth smaller and consequently the variability of a variable is smaller.

$$\lambda_a = x_i / z_\alpha \sigma_i \quad (2.12)$$

Table 2.3 shows the standard deviation of the observed historical data for four seasons at the three representative stations. Compared to other seasons, spring and autumn seasons are more sensitive to a bandwidth (have larger standard deviations). On the basis of these results, this study selected the bandwidth corresponding to probability $\alpha=0.01$ (1%).

Table 2.3 Seasonal standard deviation for maximum and minimum temperature

Variable	Station	Spring	Summer	Autumn	Winter
Maximum Temperature	London	8.7	4.0	7.9	5.6
	Stratford	8.8	4.2	8.1	5.5
	Woodstock	8.7	4.1	8.0	5.5
Minimum Temperature	London	6.9	4.1	6.4	6.6
	Stratford	7.3	4.2	6.5	6.5
	Woodstock	7.0	4.2	6.5	6.7

The WG-PCA model (improved as discussed above) has been used with two climate scenarios that define the range of potential climate change within the region of interest. The baseline (lower bound) of

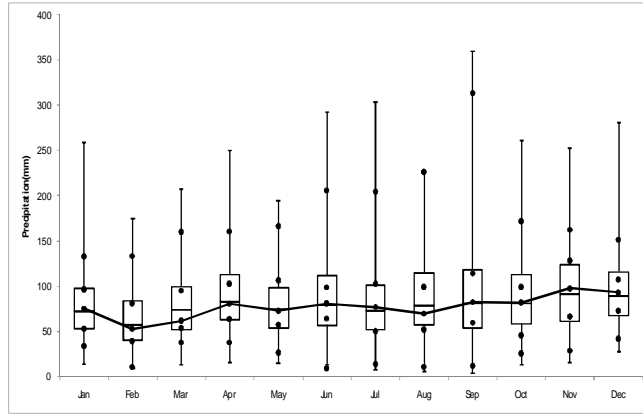
climate change is represented using the observed historic data with perturbation. The upper bound of potential climate change is represented using the wet scenario that is obtained by combining historic data with the GCM output, CCSRNIES B21. In this study 200-year of weather data (precipitation, minimum and maximum temperature) is generated to be used as input into the hydrologic model.

2.3 Results of the climate modeling

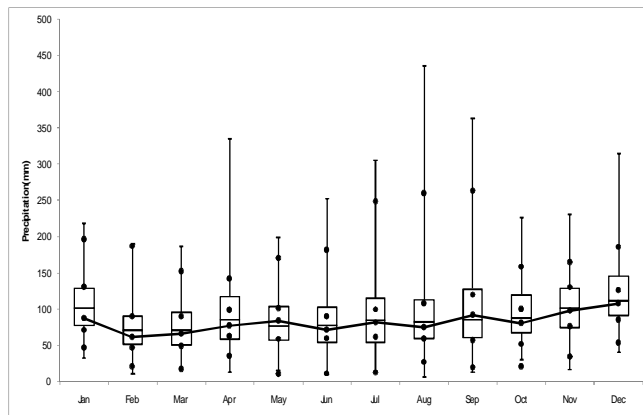
Climate modeling performed in this study results in 200 years of daily values for three meteorological variables: 1) precipitation; 2) maximum temperature; and 3) minimum temperature, for the historic and wet climate scenarios. All variables generated by the WG-PCA model are compared with the observed historical data for verification purposes. The discussion of the comparison follows.

2.3.1 Precipitation

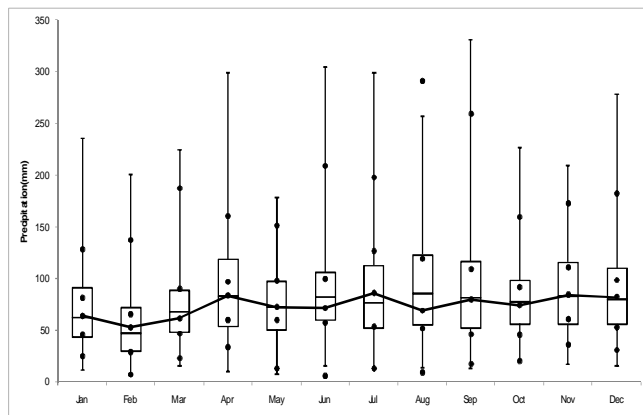
The WG-PCA model is first used with 43 years of observed data (1964 to 2006) to simulate the future – historic climate scenario – in which is the current climate assumed to provide the basis for future change. This scenario, as pointed earlier, is considered to provide the lower bound of potential climate change. The underlining assumption in this scenario is that neither mitigation nor adaptation measures will be introduced into the social-economic-climatic system and the future state of the system will be the consequence of already existing conditions within the system (concentration of green-house gasses, population growth, land use, etc.). Figure 2.5 shows the comparison between the generated and observed precipitation data for the historic scenario. The synthetic data generated using WG-PCA model are shown using the box plot while dots represent the percentile values of the observed data corresponding to the minimum, 25th, 50th, 75th, and maximum are , from the bottom to the top, respectively. The median value of the observed historical data is shown as the solid line. The results confirm that the WG-PCA regenerates well the percentile values of the observed data, specially the 25th, 50th, 75th percentile value. In addition, due to the implementation of the perturbation step in the WG-PCA algorithm the generated data includes values outside of the observed minimum and maximum value.



(a) London



(b) Stratford

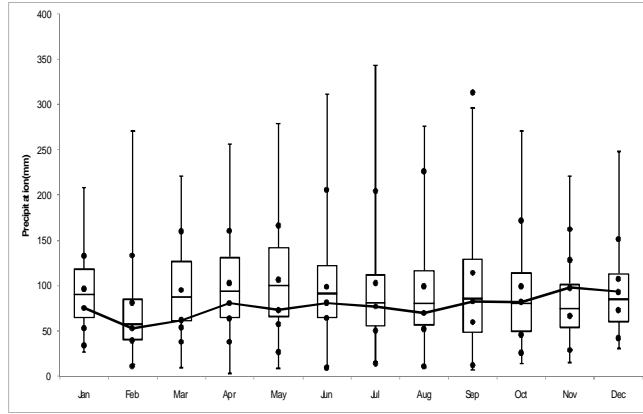


(c) Woodstock

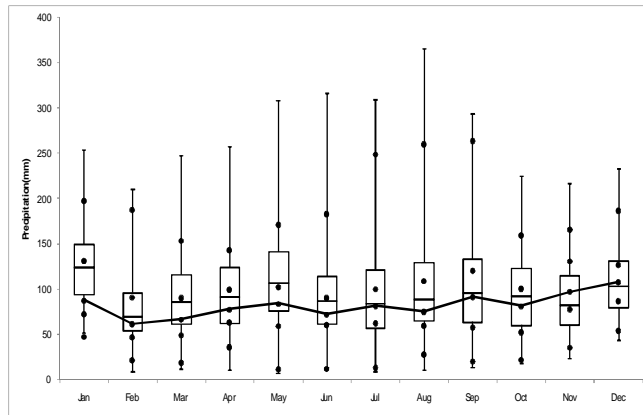
Figure 2.5 Comparison of the generated and the observed precipitation value for the historic scenario

The second phase of the climate modeling analysis uses WG-PCA with the wet climate scenario that combines CCSRNIES B21 GCM output with the observed data. Figure 2.6 shows the precipitation results for the wet scenario. According to the climate shift as shown in Table 2.1, the amount of precipitation from January to September is increased. Most often floods in the Upper Thames River basin result from the combination of snowmelt and intensive precipitation during the period between December and April. In addition, the summer frontal storms may produce severe flooding too.

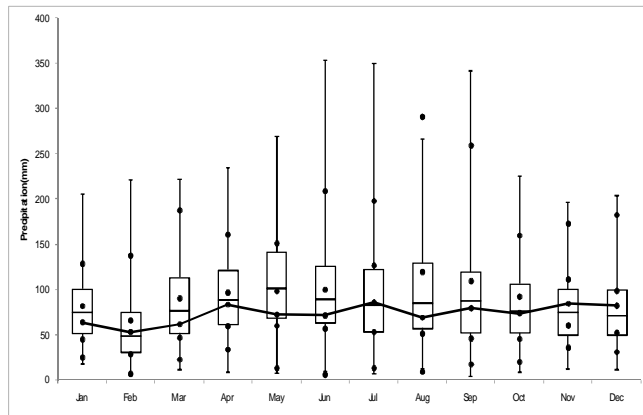
Figure 2.7 presents the average monthly change of total precipitation at the three representative stations selected in this study for the wet scenario. The significant change is observed during the spring season, from March to June, with the highest change occurring in May. It is clear that the increase in precipitation may be the cause of increase in frequency and severity of floods under the wet climate scenario.



(a) London



(b) Stratford



(c) Woodstock

Figure 2.6 Comparison of the generated and the observed precipitation value for the wet scenario

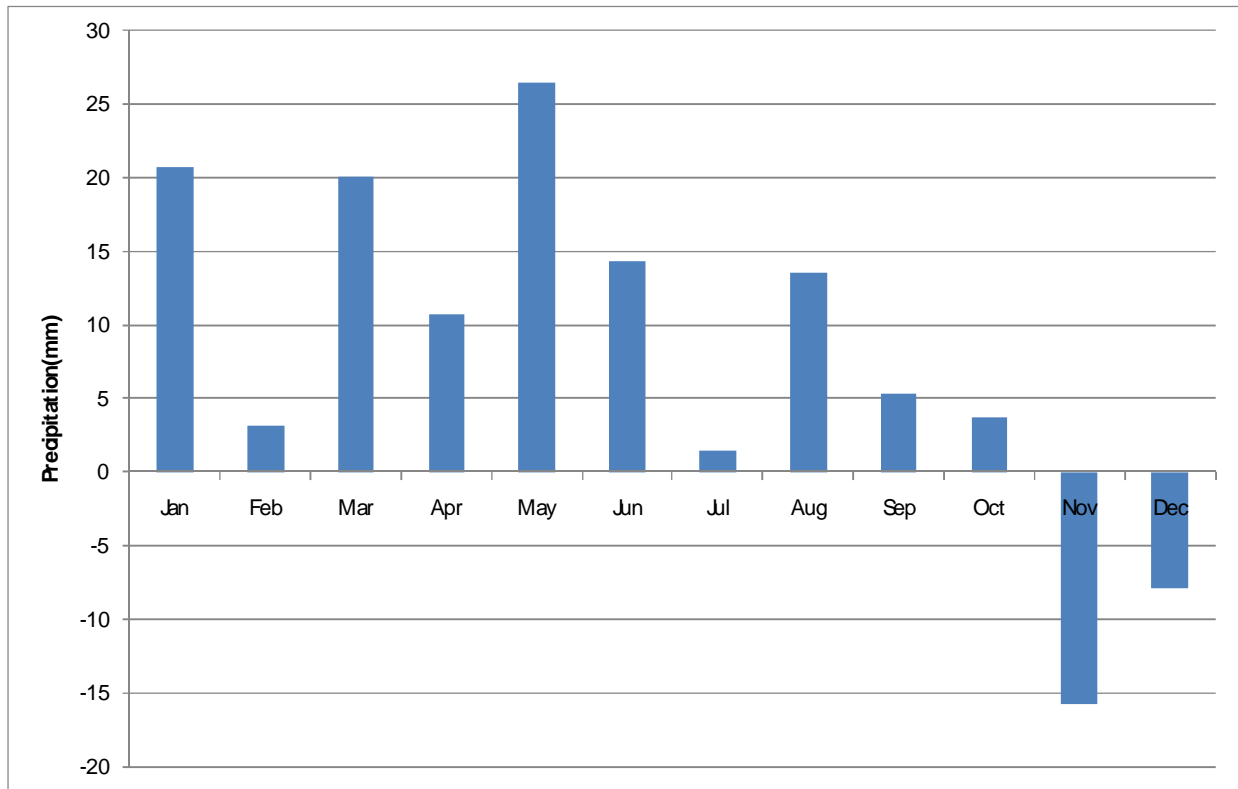


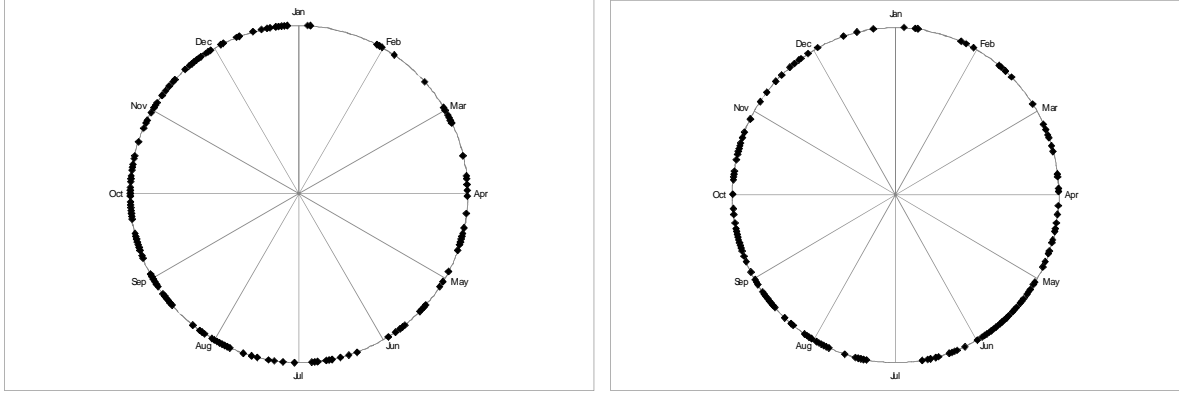
Figure 2.7 Monthly average change in total precipitation at the three representative stations for the wet scenario

Further comparison between the generated and observed data has been done using the maximum precipitation seasonality analysis to investigate the change in timing of the maximum precipitation occurrence. The main advantage of this approach is that the date data used in the maximum precipitation seasonality are practically error-free and are more robust than precipitation magnitude data. The maximum precipitation seasonality is conducted by means of directional statistics (directional mean and variance) that use individual dates of the maximum precipitation occurrence as a directional variable (Fisher, 1993).

The Julian day of the maximum precipitation occurrence (Day_i) is converted to an angular value (θ_i) using Eq. (2.13):

$$\theta_i = Day_i \frac{2\pi}{N_D} \quad 0 \leq \theta_i \leq 2\pi \quad (2.13)$$

where N_d is the number of days in a year. From Eq. (2.13), a date of the maximum precipitation occurrence represents a vector with unit magnitude and a direction given by θ_i . This study selects the annual maximum precipitation events on the basis of the total precipitation amount calculated at each station using a 5 day moving window and assuming that the annual maximum precipitation results in annual maximum flood. Fig. 2.8 shows the maximum precipitation occurrence vectors calculated using Eq. (2.13). In the historic scenario, maximum precipitations are occurring mainly from October to December and July to September due to winter snow storms and summer storms, respectively. For the wet scenario, on the other hand, floods are concentrated mainly within the period from March to October.



(a) Historic scenario

(b) Wet scenario

Figure 2.8 Maximum precipitation occurrence vectors

The directional mean ($\bar{\theta}$) and the mean day of maximum precipitation (MDMP) are calculated as shown in Eq. (2.14) and (2.15).

$$\bar{\theta} = \tan^{-1}\left(\frac{\bar{y}}{\bar{x}}\right); \quad \bar{x} \neq 0; \quad \text{MDMP} = \bar{\theta} \frac{N_D}{2\pi} \quad (2.14)$$

$$\bar{x} = \frac{1}{n} \sum_{i=1}^n \cos(\theta_i); \quad \bar{y} = \frac{1}{n} \sum_{i=1}^n \sin(\theta_i) \quad (2.15)$$

where n is the number of samples for a given site. A convenient measure of dispersion (variability) of the individual dates of the maximum precipitation occurrence around the mean value can be defined as shown in Eq. (2.16) where the variable \bar{r} represents a dimensionless dispersion measure. Because the higher value of dispersion indicates less variability, \bar{r} is used as a measure of lack of dispersion.

$$\bar{r} = \sqrt{\bar{x}^2 + \bar{y}^2} \quad (2.16)$$

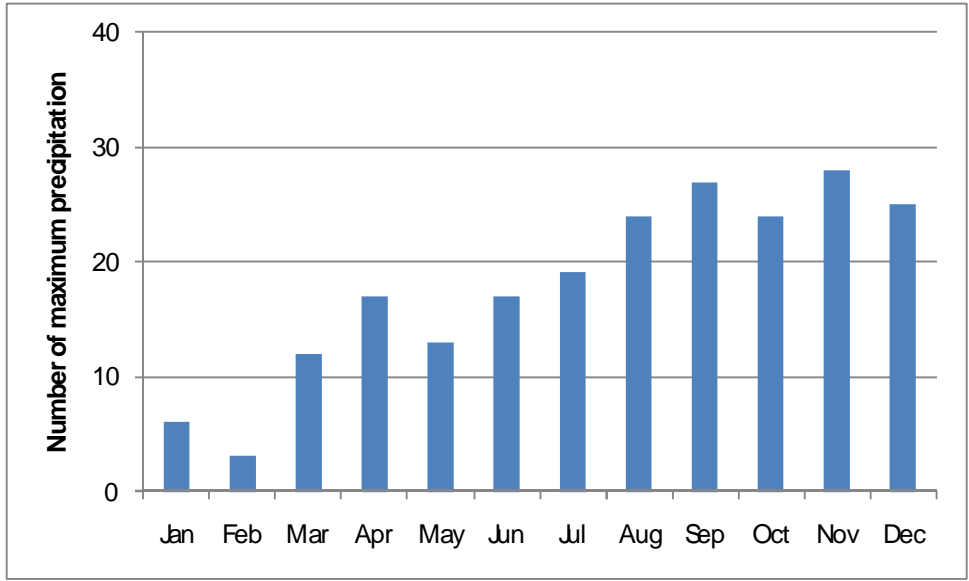
The MDMP and dispersion (\bar{r}) are calculated using Eq. (2.14) and (2.16) and the Julian calendar. Table 2.4 shows the results for two climate scenarios. In table 2.4, “All stations” shows the annual peak

precipitation amount calculated by adding the precipitation at all stations within the region. “London” shows the annual precipitation peak value for the London station only.

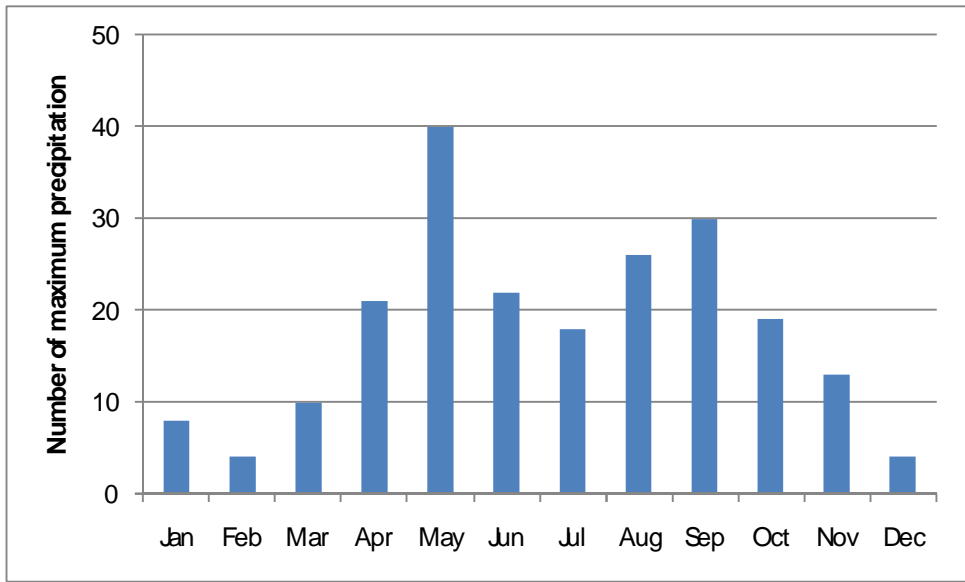
Table 2.4 The MDMP and dispersion (\bar{r}) (Julian calendar)

Station	MDMP		\bar{r}	
	Historic	Wet	Historic	Wet
All stations	262.7 (Sep. 20 th)	194.8 (Jul. 14 th)	0.26	0.31
London	242.7 (Aug. 31 st)	180.9 (Jun. 30 th)	0.20	0.30
Stratford	234.6 (Aug. 23 rd)	188.3 (Jul. 8 th)	0.28	0.29
Woodstock	223.3 (Aug. 12 th)	186.9 (Jul. 6 th)	0.25	0.32

The results show that the mean day of maximum precipitation (MDMP) for the historic scenario is 53.1 days later on average than for the wet scenario while the dispersion is lower than for the wet scenario. That means that the range of the maximum precipitation occurrence day for the historic scenario is wider and the maximum precipitation could occur earlier due to the climate change. Figure 2.9 shows monthly distribution of maximum precipitation occurrence for 200 years. As the results of MDF and dispersion in Table 2.4 show, the time of the maximum precipitation occurrence for the historic scenario is spread out from March to December and mainly from August to December. On the other hand, the the maximum precipitation occurrence for the wet scenario is concentrated mainly to spring (April to June) and summer (August to September).



(a) Historic scenario

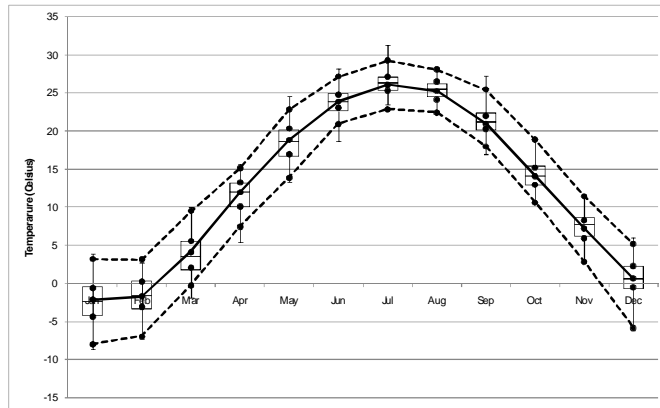


(b) Wet scenario

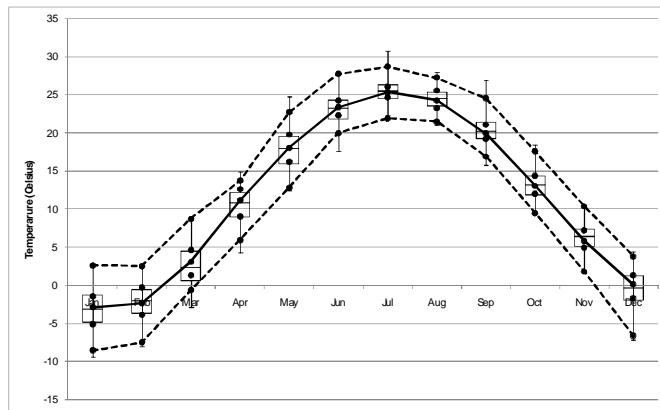
Figure 2.9 Number of annual maximum precipitation events within 200 years

2.3.2 Temperature

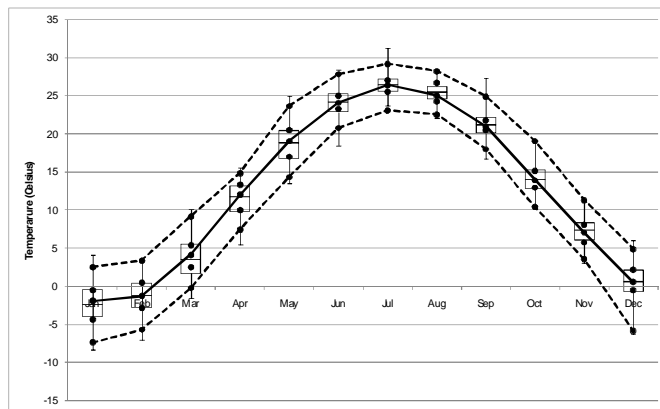
In addition to precipitation, maximum and minimum temperature at 15 stations is generated in this study for the period of 200 years using the WG-PCA model. The results of comparison between generated and observed maximum and minimum temperature for the historic climate scenario are shown in Figures 2.10 for maximum temperature and 2.11 for minimum temperature, respectively. The results for the wet climate scenario are shown in Figures 2.12 and 2.13. The increase in temperature is observed for all months in the case of the wet climate scenario. This is the indication that the WG-PCA model generates temperature with desired statistical attributes. Maximum and minimum temperature is higher by 5.7 °C and 5.2°C on average over all months, respectively. IPCC (2007) reports that warming of the winter months is faster than warming of the summer months. Results of our study confirm the findings of IPCC. The average increase in maximum temperature in winter season (November to April) is 6.2 °C and in summer season (May to October) is 5.2°C for the representative stations. The change in minimum temperature for the two seasons is 5.9 °C and 4.6°C, respectively. These results, therefore, prove that climate change impact on temperature is more significant during the winter season, 1.15 °C on average, than during the summer season.



(a) London

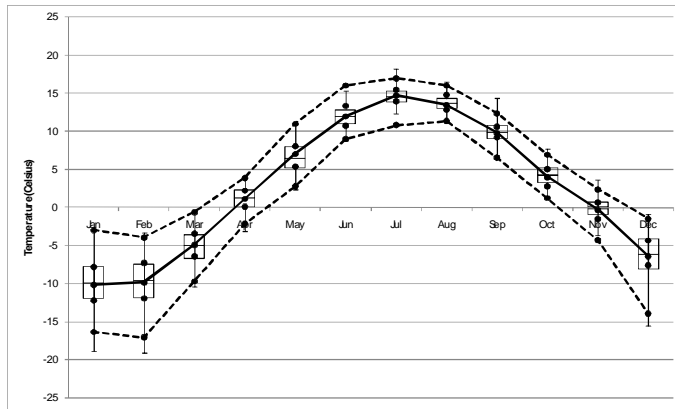


(b) Stratford

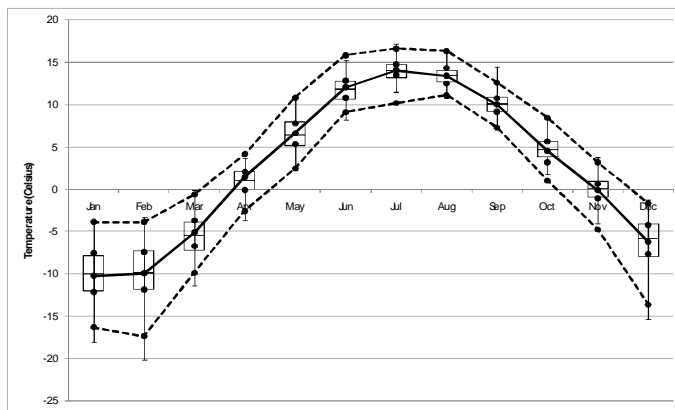


(c) Woodstock

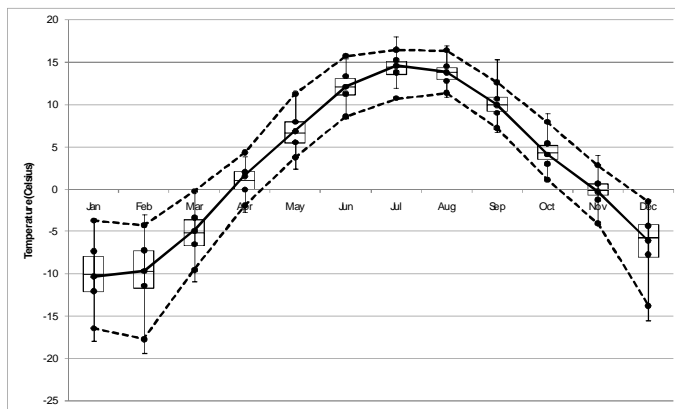
Figure 2.10 Maximum temperature at the representative stations for the historic scenario



(a) London

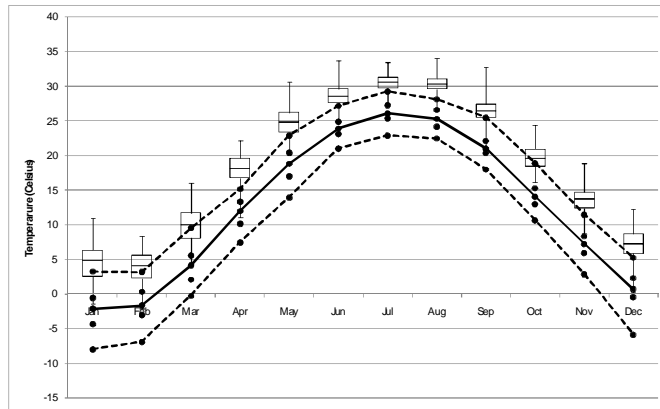


(b) Stratford

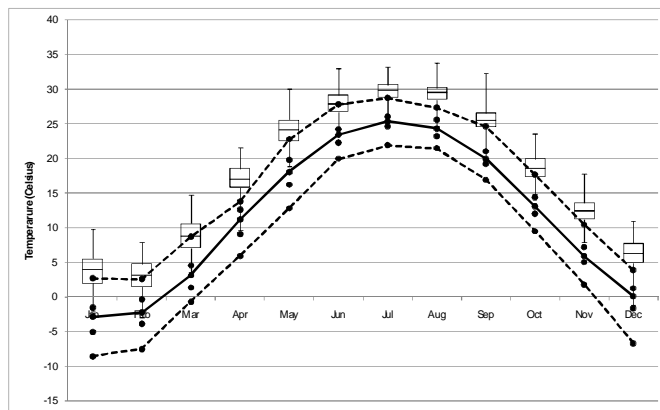


(c) Woodstock

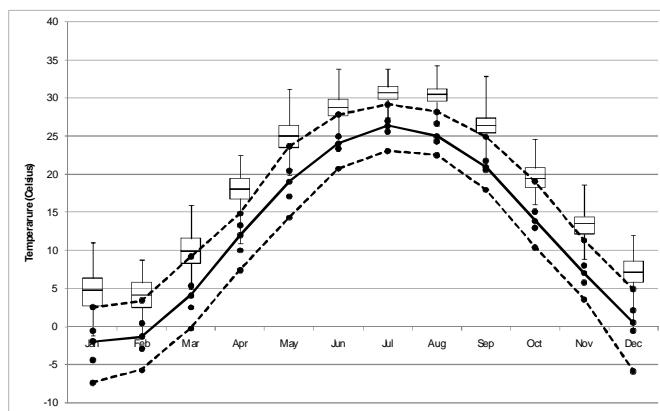
Figure 2.11 Minimum temperature at the representative stations for the historic scenario



(a) London

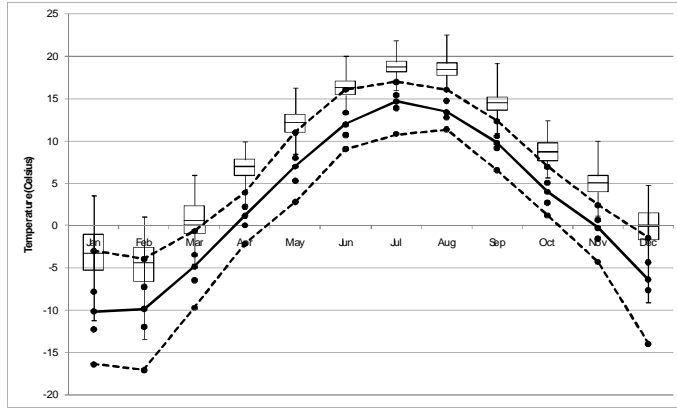


(b) Stratford

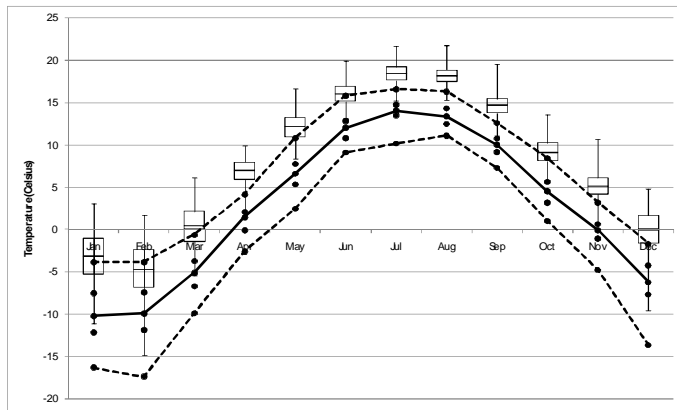


(c) Woodstock

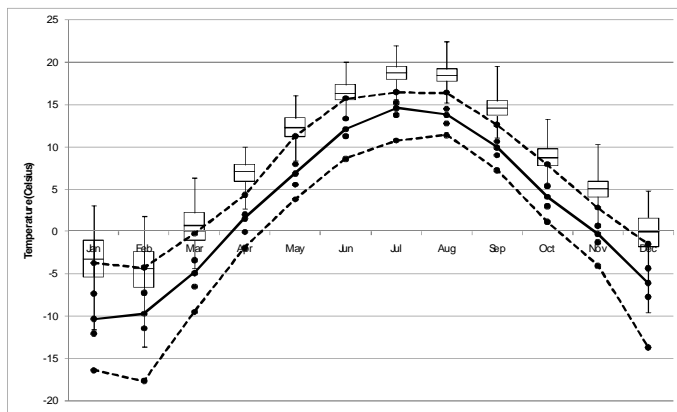
Figure 2.12 Maximum temperature at the representative stations for the wet scenario



(a) London



(b) Stratford



(c) Woodstock

Figure 2.13 Minimum temperature at the representative stations for the wet scenario

2.3.3. Conclusions

Based on the analysis of climate modeling results we conclude that all the meteorological variables considered in this study are satisfactorily generated. Therefore, they can be used to assess the vulnerability of municipal infrastructure for the City of London. The results for historic and wet climate scenarios show that both meteorological variables, precipitation and temperature, increase during the spring season (March to June). Therefore, more frequent and more severe flooding, resulting from the snowmelt and precipitation, might be expected in the future.

3. Hydrologic modeling

The meteorological variables generated by the WG-PCA model, precipitation and temperature in this study, are used as input into a hydrologic model to further assess the impacts of climate change on the hydrologic conditions in the basin. Hydrologic models are mathematical representations of rainfall-runoff processes within a basin. They provide essential information, such as peak flow and total run-off, for each sub-basin and support for the water resources management activities in the basin. Therefore, the selection of an appropriate hydrologic model is a very important step in the climate change impacts assessment process. Results of the hydrologic modeling are directly used in hydraulic analyses that finally provide for the assessment of vulnerability of infra-structure to climate change in a basin.

This study investigates the advantages and drawbacks of several hydrologic model candidates considered for use in this study. Table 3.1 shows the comparison of the models frequently used in the North America. Among these models, the HEC-HMS is acceptable over all criteria used in the selection process. In addition, Cunderlik and Simonovic (2004; 2005) have developed and successfully applied the two versions of the HEC-HMS model for the Upper Thames River basin: 1) continuous model and 2) event model. In spite of the fact that HEC-HMS is not “the best” model for the use in urban watersheds, (i) availability of the calibrated model for the Upper Thames River basin, (ii) limited modelling time and resources available for the study, and (iii) limited flow data for most sub-watersheds within the City of London boundaries, led to the selection of this model for the use in our study. Selection of the HEC-HMS model for hydrologic analyses in this study has some other advantages too: previously developed model structure, shorter model development time, easy modification of model structure, etc.

Table 3.1 Characteristics of potential hydrologic models for use in this study

Criterion	HEC-HMS	SWMM	MIKE11	OTTHYMO
Temporal scale	Flexible*	Flexible	Flexible	Flexible (limited window size)
Spatial scale	Flexible**	Small Area	Flexible	Flexible
Processes modeled:				
Event simulation	Yes	Yes	Yes	Yes
Continuous simulation	Yes	Yes	Yes	No
Snow acc. and melt	Yes	Yes	Yes	Yes
Interception and Infiltration	Yes	Yes	Yes	Yes
Evapotranspiration	Yes	Yes	Yes	Yes
Reservoir routing	Yes	Yes	Yes	Yes
Cost	Public Domain	Public Domain	USD 10,000	The first copy for \$2,999
Set-up time	Medium	Long	Medium	Medium
Expertise	Medium	High	High	Medium
Technical support	Annual subscription	Third-party vendors	DHI software support center	On-line help System
Documentation	Good	Good	Good	
Ease of use	Medium	Difficult	Medium	Medium

* the time scale can range from one minute to one month

** the spatial scale can range from small to large

3.1 The HEC-HMS hydrologic model

The hydrologic model employed in this study is a semi-distributed model based on the US Hydrologic Engineering Center's Hydrologic Modeling System (HEC-HMS version 3.3) that consists of three modules as shown in Figure 3.1: (i) meteorologic module (ii) basin module; and (iii) control module. The meteorologic module is a place for the user to describe basin input processes such as the hourly or daily precipitation data, evapotranspiration and others. The basin module is for describing the main physical processes occurring within a basin such as reservoirs and sub-basins. Lastly, the control module is used to set the starting (and ending) dates and time horizon to simulate.

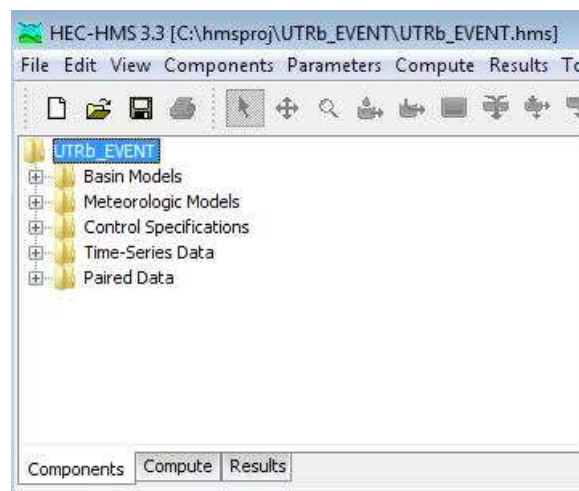


Figure 3.1 Three modules of the HEC-HMS model

HEC-HMS hydrologic model can be used as event-driven or continuous-process model depending on the goal of a study. The main goal of this study is to assess the impacts of climate change, specifically flooding, on the municipal infrastructure for the City of London. Previous work in the Upper Thames River Basin concluded that “The increased precipitation scenario (called wet scenario in this report) is identified as the critical scenario for the assessment of risks associated with the occurrence of floods in the basin” (Cunderlik and Simonovic, 2007, page 574). In addition they

state that “A single-event hydrologic modeling should be used for simulating storm and frontal rainfall induced floods” (Cunderlik and Simonovic, 2004, page 26). Therefore, the event-driven HEC-HMS model is used in this assessment. Event-driven models are designed to simulate basin response for individual precipitation-runoff events, so generally moisture balance accounting process is simplified and evapotranspiration is not included in the model. Their emphasis is placed on infiltration and surface runoff, and their main objective is the evaluation of direct runoff. They have serious limitations in estimating runoff from the snowmelt. The event model is however, well suited for the analysis of extreme flood events as requested in this study.

3.2 Input data for the HEC-HMS model

The weather generator (WG) model, presented earlier, generates daily precipitation and temperature variables at 15 stations within the Upper Thames River basin. However, the HEC-HMS requires extreme precipitation data with at least hourly resolution. In addition, spatial resolution of model input data has to be adjusted too. The meteorological input data (precipitation) is available at 15 stations within the basin and required for each sub-basin in the Upper Thames River basin. Therefore, the temporal disaggregation and the spatial interpolation schemes are implemented to provide the necessary input data.

3.2.1 Spatial interpolation of model input data (inverse distance method, IDM)

The spatial interpolation uses the inverse distance method (IDM), quite common in the hydrologic practice (Lapen and Hayhoe, 2003). IDM takes a higher weighting factor for target locations closer to the measurement locations. Eq. (3.1) shows how the interpolated data at a given location Z , is calculated from the measured data.

$$Z = \frac{\sum_{i=1}^n Z_i w_i}{\sum_{i=1}^n w_i}, \quad w_i = \frac{1}{d^p} \quad (3.1)$$

where Z_i is known observed data value at a station i , d_i is the distance from the station i to the required location, and p is the exponent. The higher value of p , the more weight is placed on the stations closer to the required location. Normally, the value of $p = 2$ is used in practice. So, the same value has been adopted in this study. The spatial interpolation, based on the inverse distance method and the location information for 15 measurement stations as shown in Table 3.2, is applied to obtain the meteorological data for each sub-basin.

Table 3.2 Location information for 15 measurement stations in the Upper Thames River basin

Station	Latitude	Longitude
Blyth	43.72	-81.37
Dorchester	43.00	-81.02
Embro	43.25	-80.92
Exeter	43.35	-81.50
Foldens	43.02	-80.77
Fullarton	43.38	-81.20
Glen Allan	43.67	-80.72
Ilderton	43.05	-81.42
London	43.02	-81.15
St Thomas	42.77	-81.21
Stratford	43.37	-81.00
Tavistock	43.32	-80.82
Waterlood	43.47	-80.52
Woodstock	43.13	-80.77
Wroxeter	43.87	-81.15

3.2.2 Temporal disaggregation of model input data

The weather generator model used in the study produces meteorological variables with daily temporal resolution that is not sufficient for intense rapidly changing storms. The disaggregation procedure is implemented to convert daily data into hourly. The method of fragments (Svanidze, 1977) has been used as the most popular method for disaggregation of precipitation data. The main idea of the method is that the fragments are the hourly fractions of daily precipitation, thus they sum to unity as shown in Eq. (3.2).

$$p_i = w_i P, \quad w_i = \frac{o_i}{\sum_{i=1}^n o_i} \quad (3.2)$$

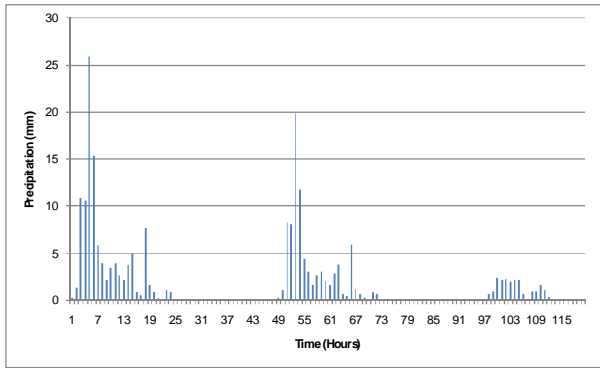
where p_i represents a new disaggregated precipitation value, w_i is a fragment to be calculated for hour i , o_i is a hourly data from the observed hourly time series chosen to produce fragments, and n is the number of hours in the time series (e.g. 12 hours or 24 hours). In our case $n = 24$.

For producing accurate hourly data from a daily data by fragments, the choice of the observed hourly time series is a key task. Therefore, Srikanthan and McMahon (1982) suggested choosing the series that most closely matches with characteristics of data being disaggregated, e.g. total precipitation. Choosing a closely matching set of fragments will ensure that precipitation events are generated with the proper shapes and characteristics. Another issue with method of fragments is the repetition of series in the case of short observation period. Porter and Pink (1991) proposed a method of synthetic fragments to overcome the repetition using K-NN method. Wójcik and Buishand (2003) proposed another method that chooses a randomly selected fragment set from the k closest matches instead of choosing only one fragment set that the most closely matches. Wey (2006) suggested a new method of fragments to properly reproduce the characteristics of the original observed data, e.g. seasonality. Her work has been used in the climate change impact study conducted for the Upper Thames River basin and used as the background for the work presented here. Wey (2006) disaggregated only days which receive more than 25 mm of rain in

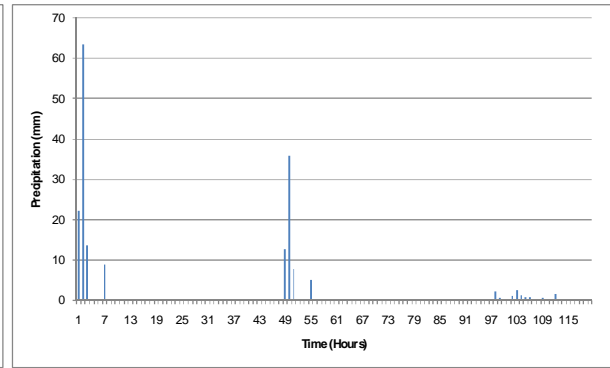
order to reduce the computational burden. Following the work of Wey (2006), this study disaggregates daily data into hourly using the following procedure:

1. Extract the events from the observed historical hourly data set from 1984 to 2003. Events are considered separate if there is no-precipitation between them for more than 5 hours.
2. When a precipitation value is different from zero, i.e., precipitation event occurs, select neighbors from the historical events extracted in Step 1 on the basis of total precipitation. The ratios of lower bound and upper bound for total precipitation to select the neighbors are 0.8 and 1.2, respectively. In addition, the temporal window is 60 days, e.g. if current day is 15th Jan, then temporal window is from 1st Jan to 30th Jan. All days within the temporal window are regarded as potential neighbors to the current feature vector.
3. Select a historical event among the neighbors using random process.
4. According to the hourly time sequence of the selected historical event, disaggregate a daily precipitation value into hourly using Eq. (3.2).

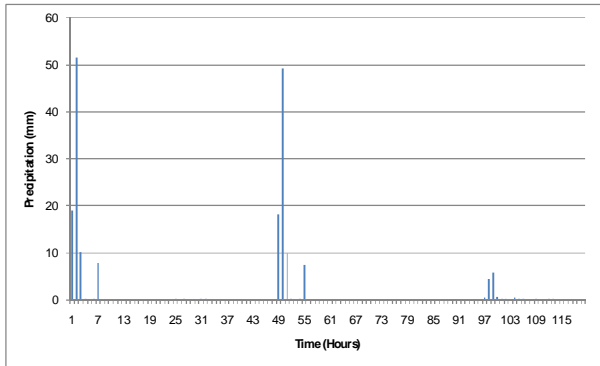
This study generates daily data for 200 years and in any given year there are a number of events. The main objective of this study is to perform the flood frequency analysis of extreme annual flood events. Therefore, we select 5-day annual extreme event that produces the largest annual event (200 events altogether) for the entire basin. Fig. 3.2 and Fig. 3.3 show the extreme flood hyetographs at six stations that represent upper, middle, and low regional characteristics in the basin. The results for other stations are available upon request.



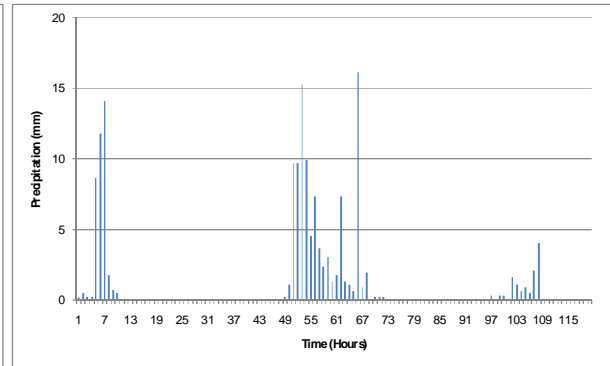
(a) Blythe



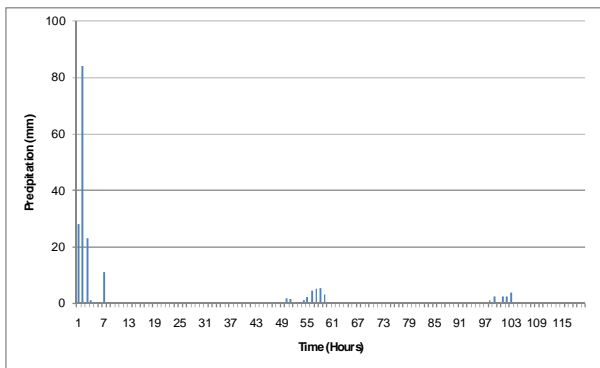
(b) Dorchester



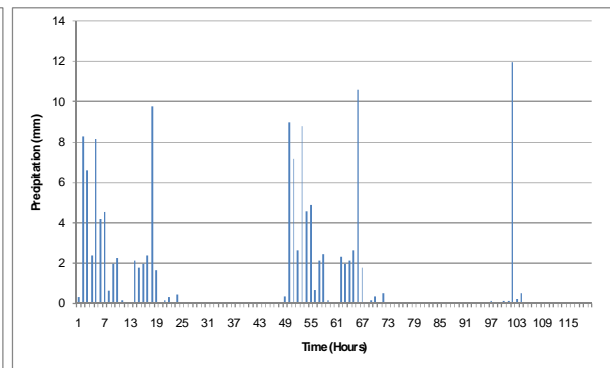
(c) London



(d) Stratford

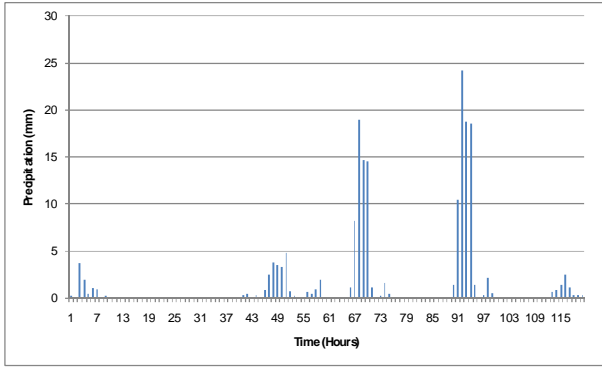


(e) StThomas

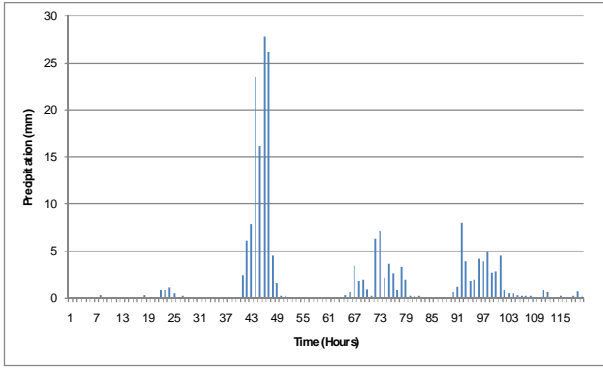


(f) Woodstock

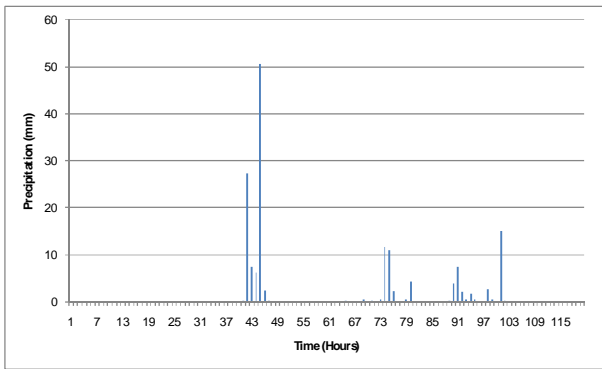
Figure 3.2 Hyetographs of an annual extreme event for the historic scenario



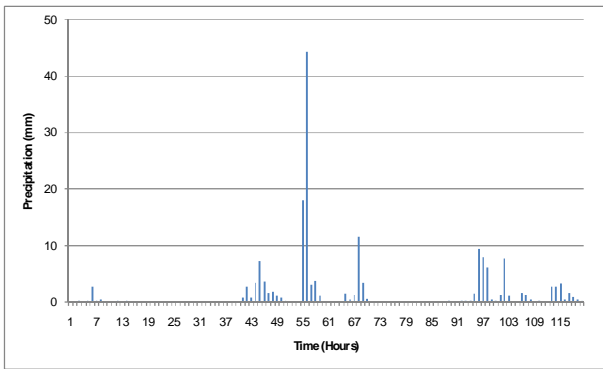
(a) Blythe



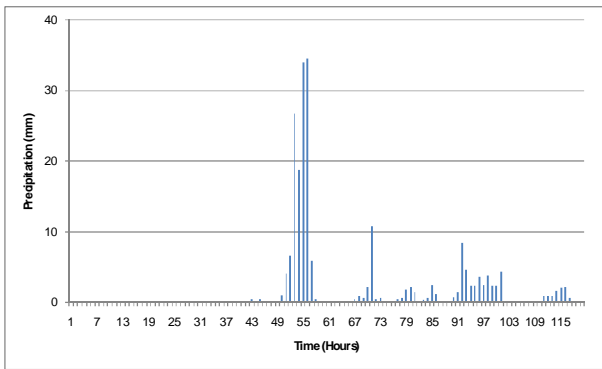
(b) Dorchester



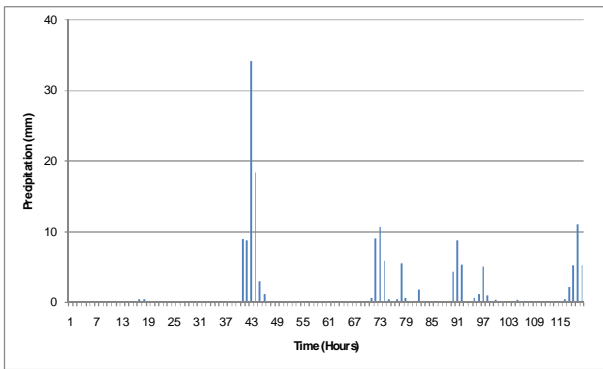
(c) London



(d) Stratford



(e) StThomas



(f) Woodstock

Figure 3.3 Hyetographs of an annual extreme event for the wet scenario

3.3 Delineation of model sub-basins and model calibration

Cunderlik and Simonovic (2004) have developed the HEC-HMS model with 34 sub-basins (Figure 3.4) for the Upper Thames River basin and successfully applied the model to assess climate change impacts on the main control points in the basin. The aim of this study is to assess the vulnerability of municipal infrastructure to climate change in the City of London, which requires detailed description of the hydrologic conditions within the City of London. The procedure implemented here involves nesting of additional sub-basins (for better spatial resolution within the City boundaries) into original model structure that includes 34 sub-basins for the whole basin. The watershed delineation process in the City of London includes the Medway Creek, Stoney Creek, Pottersburg Creek, Dingman Creek as well as the main Thames river channel.

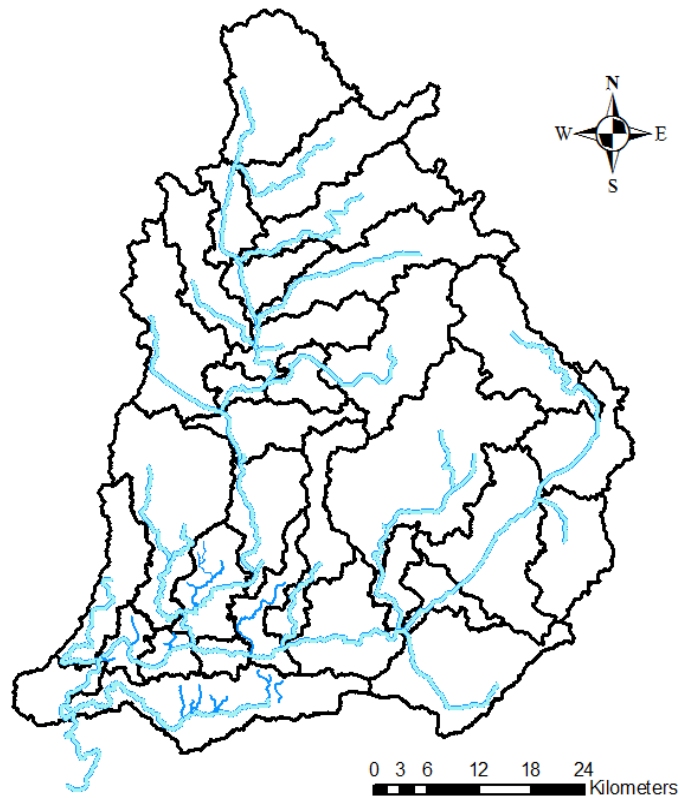
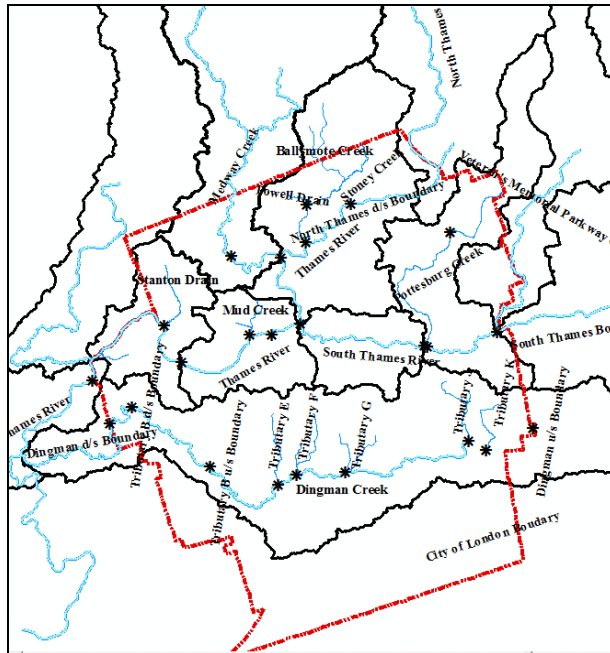


Figure 3.4 HEC-HMS model with 34 sub-basins

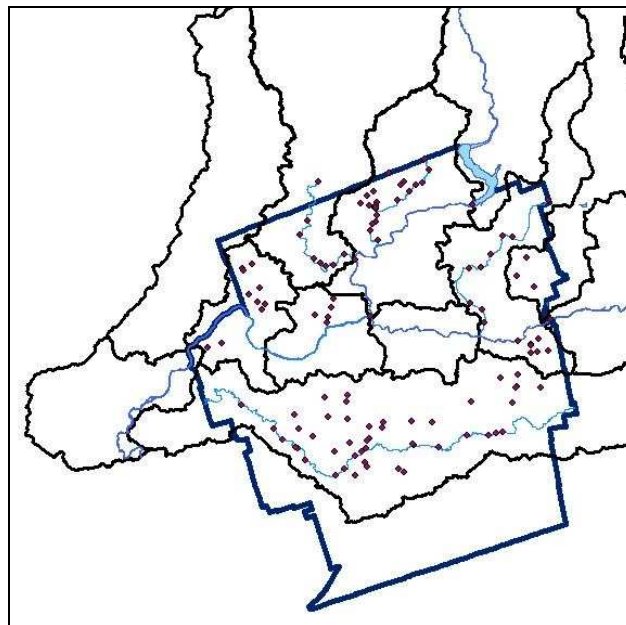
3.3.1 Delineation of the sub-basins within the City of London

To establish the proper spatial model resolution within the City of London, all locations that require streamflow data are identified by the City and combined with the required locations for the hydraulic model (HEC-RAS) used for calculation of water surface elevation. Figure 3.5 (a) shows points of the interest to the City (stars) and the City boundary (dotted line). Figure 3.5 (b) shows all the locations required for hydraulic model analyses.

Taking into consideration all locations of interest the territory of the City has been delineated into sub-watersheds as shown in Fig. 3.6 and Fig. 3.7. There are four major sub-watersheds in the city: Medway Creek, Stoney Creek, Pottersburg Creek, and Dingman Creek, which are divided into 5, 6, 4, and 16 sub-watersheds, respectively (Fig. 3.6). In addition to four sub-watersheds, this study also delineates the main river basin within the city. At the end, the complete HEC-HMS model used in this study consists of 72 sub-basins, 45 reaches, 49 junctions, and 3 reservoirs (Fig. 3.8).



(a) Locations of interest to the City of London



(b) Locations that require flow data for hydraulic analyses

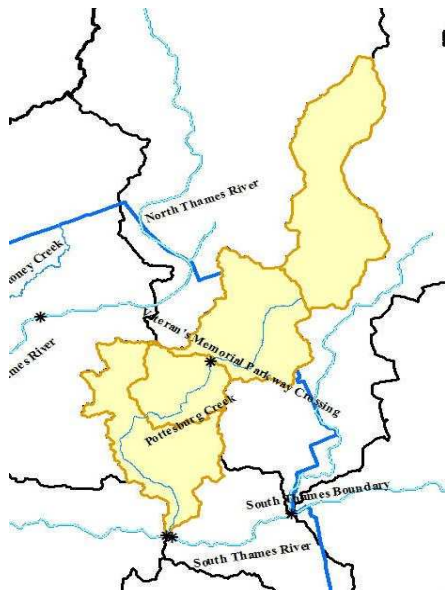
Figure 3.5 Locations used in the sub-watershed delineation process



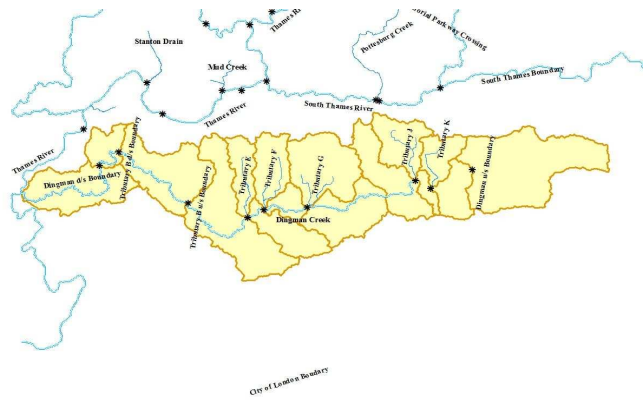
(a) Medway Cr.



(b) Stoney Cr.



(c) Pottersburg Cr.



(d) Dingman Cr.

Figure 3.6 Delineation of 4 main sub-watersheds in the City of London

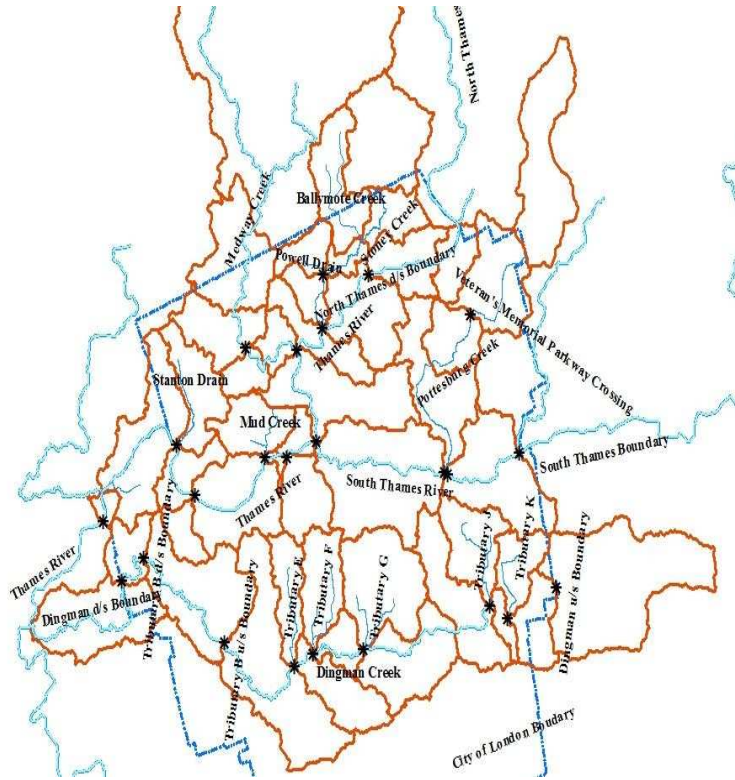


Figure 3.7 Delineation of the Thames River into sub-watersheds within the City of London

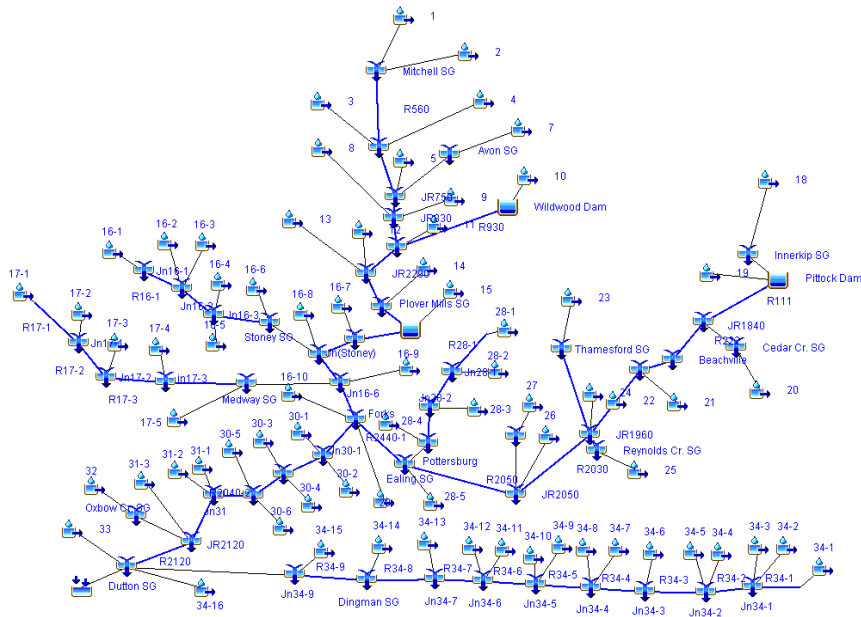


Figure 3.8 The HEC-HMS model structure

3.3.2 Model calibration

This study modified the HEC-HMS model of Cunderlik and Simonovic (2004) with the more detailed spatial resolution within the City of London boundaries. Model modifications require calibration of parameters to allow for accurate calculation of streamflow. Cunderlik and Simonovic (2004) performed a detailed investigation of rainfall events suitable for calibration. They selected an hourly rainfall event from July 05 to July 16 of 2000 that covered almost over the entire basin. However, the observed streamflow data for the basin are limited to only few station gauges at Medway, Ealing, Dingman, and Byron stations. There are no measured streamflow data available for the Stoney and the Pottersburg Creek during the July 2000 event. The Stoney Creek is affected by the backwater effect from the North Thames River, which further complicates the selection of proper measurement data for calibration. The Upper Thames River Conservation Authority (UTRCA), therefore, recommends for Stoney Creek the flood event of October 4 – 7 in 2006 that is not affected by the backwater effect.

The HEC-HMS model provides several methods for river routing including Modified Puls, Muskingum, lag, kinematic wave, and Muskingum-Cunge (US Army Corps of Engineer, 2008). In this study, the Modified Puls method known as storage routing or level pool routing is used. It is based on a finite approximation of the continuity equation. For the Modified Puls method, the continuity equation is written as Eq. (3.3).

$$\overline{I}_t - \overline{O}_t = \frac{\Delta S_t}{\Delta t} \quad (3.3)$$

where \overline{I}_t is the average upstream flow (inflow to reach) during a period Δt ; \overline{O}_t is the average downstream flow (outflow from reach) during a period Δt ; and ΔS_t is change in storage in the reach during time t . Eq. (3.3) can be rearranged to isolate the unknown variables by a simple backward differencing scheme as shown in Eq. (3.4).

$$\left(\frac{S_t + O_t}{\Delta t}\right) = \left(\frac{I_{t-1} + I_t}{2}\right) + \left(\frac{S_{t-1} - O_{t-1}}{2}\right) \quad (3.4)$$

where I_{t-1} and I_t are inflow hydrograph ordinates at times $t-1$ and t , respectively; O_{t-1} and O_t are outflow hydrograph ordinates at times $t-1$ and t , respectively; and S_{t-1} and S_t represent storage in reach at times $t-1$ and t , respectively. In Eq. (3.4), terms on the left hand side are unknown, two unknown variables at time t : S_t and O_t . Therefore, a functional relationship equation between storage and outflow is required to solve Eq. (3.4). In this study, relationships between storage and outflow are defined for all newly added reaches utilizing the results of the UTRCA hydraulic model, HEC-RAS, calculations as shown in Figure 3.9. The flow areas and the amount of outflows for each cross-section are calculated from the HEC-RAS simulations corresponding to the various flows. The relationship between storage and outflow then can be derived from the outflow and the storage of a certain channel section calculated from multiplying the average flow area with the length of the channel section. Figures 3.10 and 3.11 show some of the relationships developed in this study.

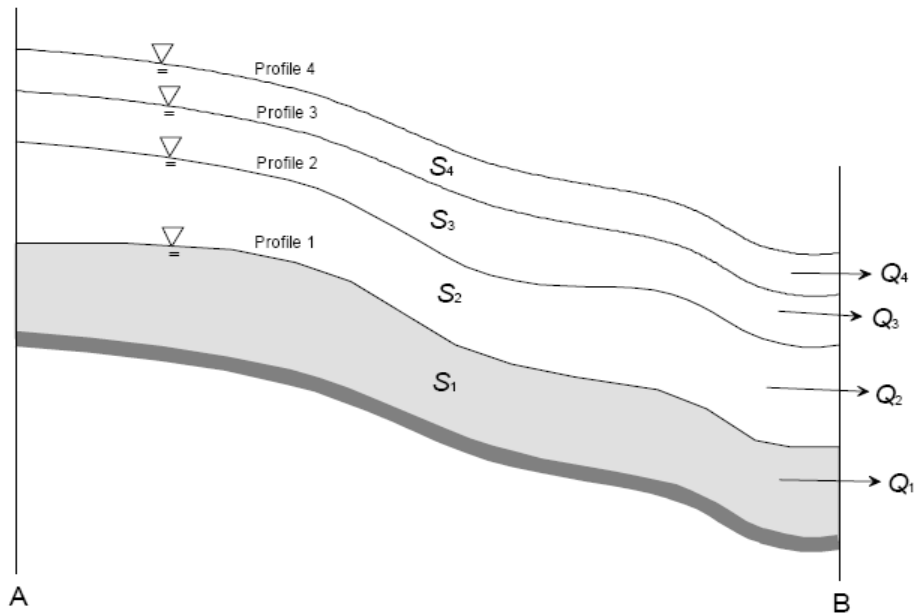
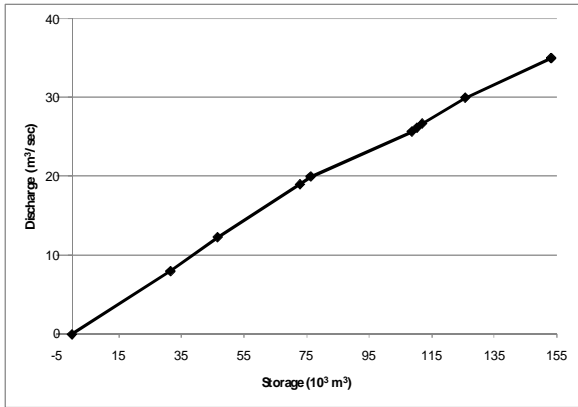
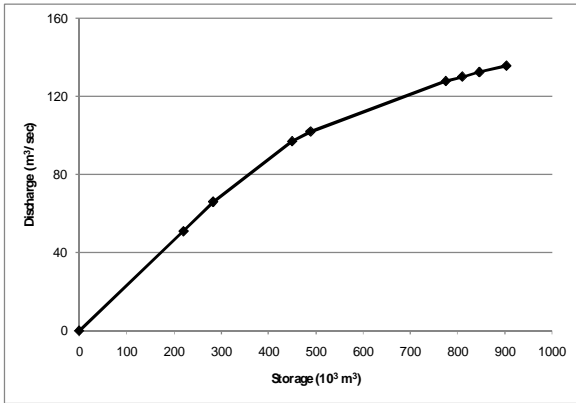


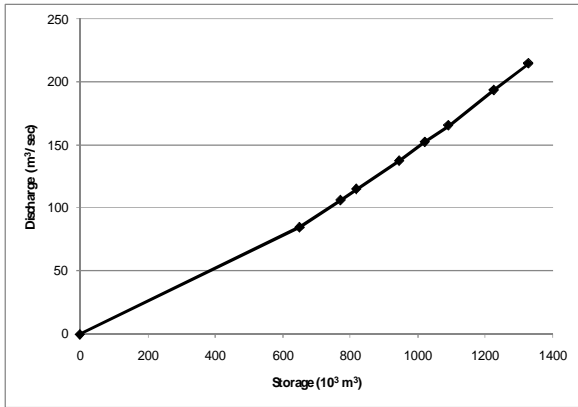
Figure 3.9 Example of a set of water-surface profiles between section A and B of a channel



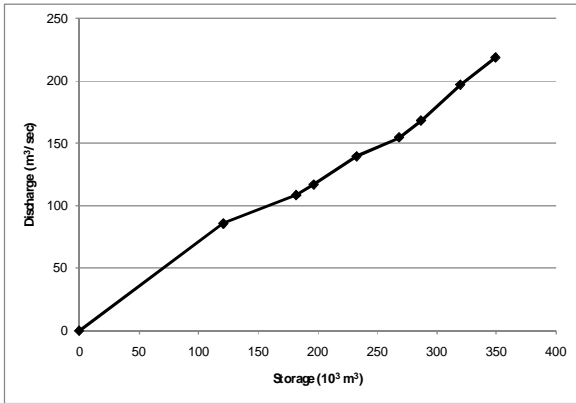
(a) R34-1(Dingman Cr.)



(b) R34-9 (Dingman Cr.)

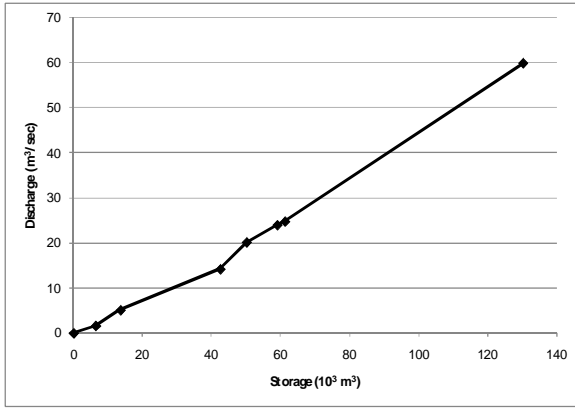


(c) R17-1(Medway Cr.)

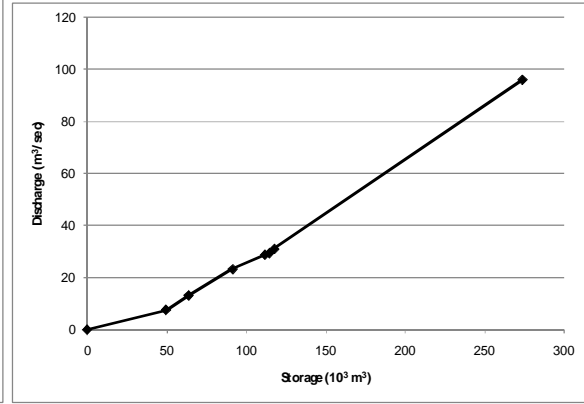


(d) R17-3 (Medway Cr.)

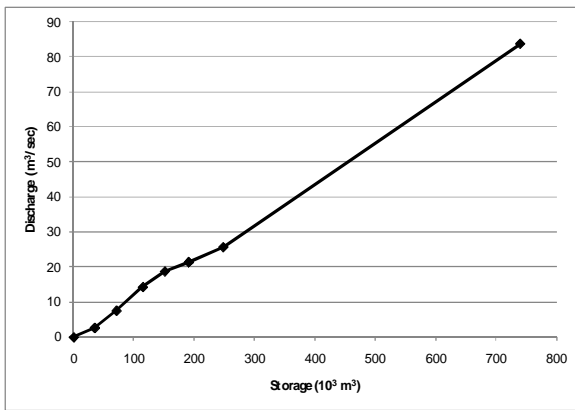
Figure 3.10 Relationships between storage and outflow for the sub-watersheds in the basin



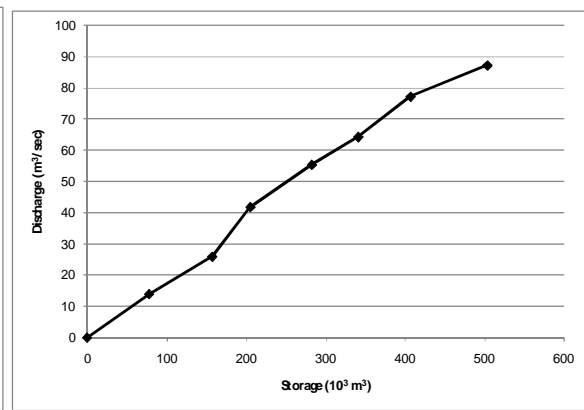
(e) R16-1(Stoney Cr.)



(f) R16-3 (Stoney Cr.)

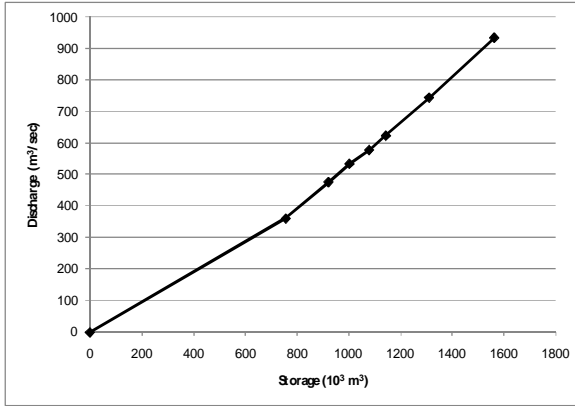


(g) R28-1(Pottersburg Cr.)

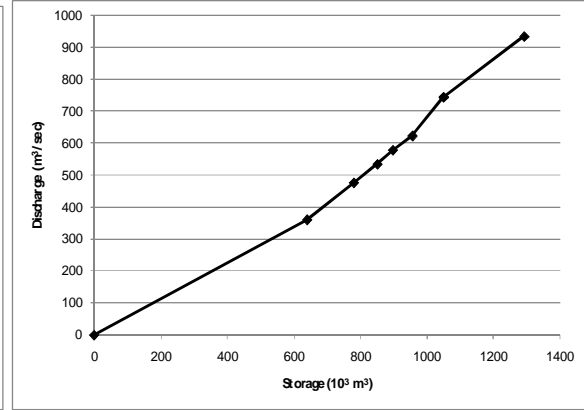


(h) R28-3 (Pottersburg Cr.)

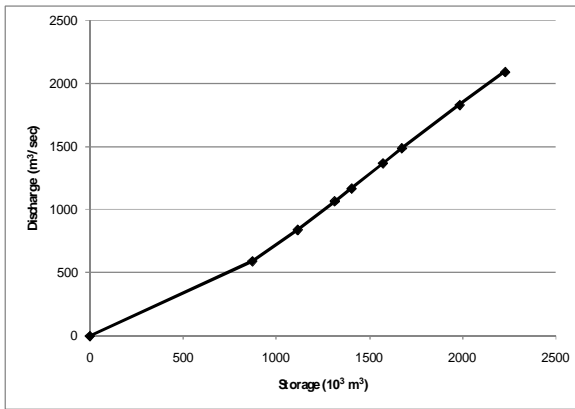
Figure 3.10 (continued)



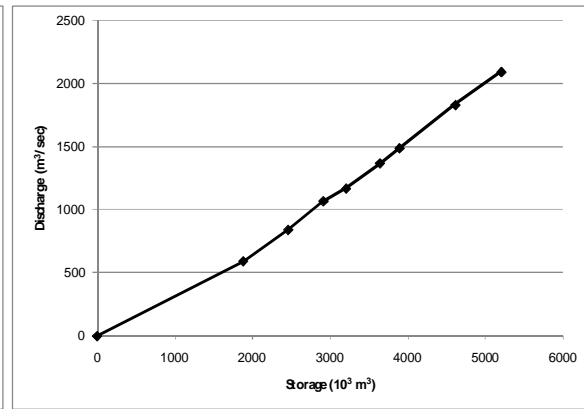
(a) R1910-1



(b) R1910-3



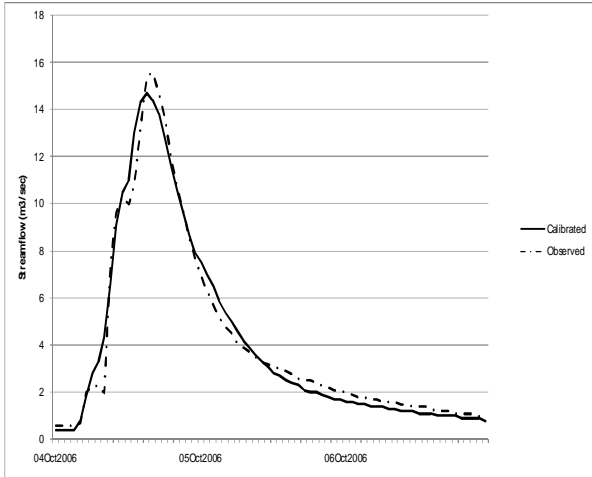
(c) R2440-1



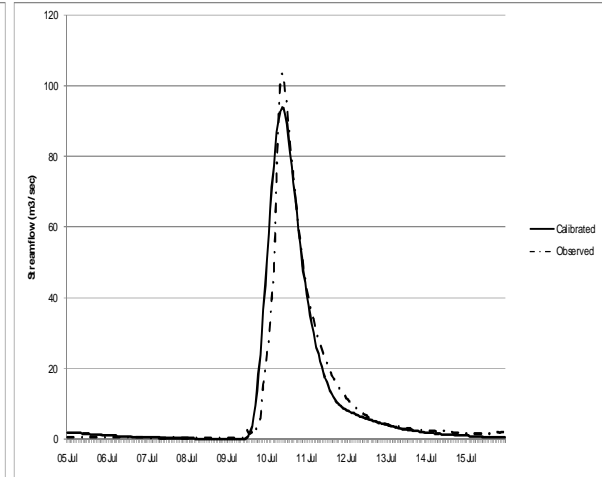
(d) R2440-3

Figure 3.11 Relationships between storage and outflow for the main stream (Upper Thames River)

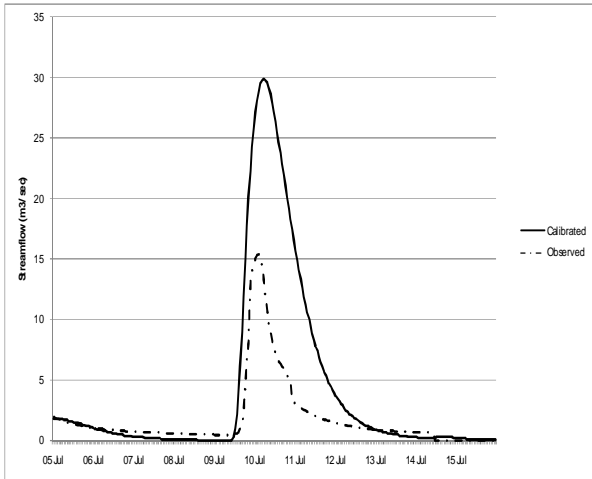
Two events, October 4-7, 2006 event for the Stoney Creek and July 5-16, 2000 for other sub-basins, are used to calibrate the HEC-HMS model parameters including time of concentration, storage coefficient, initial discharge, initial loss, and so on. The HEC-HMS provides two optimization schemes of calibration of model parameters: Nelder Mead and universal gradient search. This study used the Nelder Mead scheme to optimize the parameters for the basin. Figure 3.12 shows the calibration results for each station with available observation data. Since there are no available measurements for the Pottersburg Creek, the Ealing station located on the South Thames is used to check the calibration result for the Pottersburg Creek. The comparison between simulated and observed flows illustrates that all model parameters are calibrated well. In addition to the sub-watersheds, this study re-calibrated the parameters for the Thames River and compared the simulation result with the observed data at the Byron station for the July 2000 flood event. Comparison results shown in Fig. 3.13 demonstrate that the HEC-HMS model developed in this study is calibrated (to the best level under data limitation) for use in further hydrologic analyses.



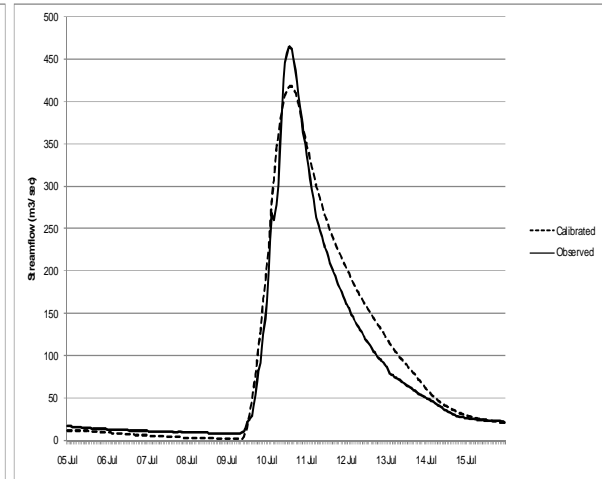
(a) Stoney station



(b) Medway station



(c) Dingman station



(d) Ealing station

Figure 3.12 Calibration results for the main stations in the basin

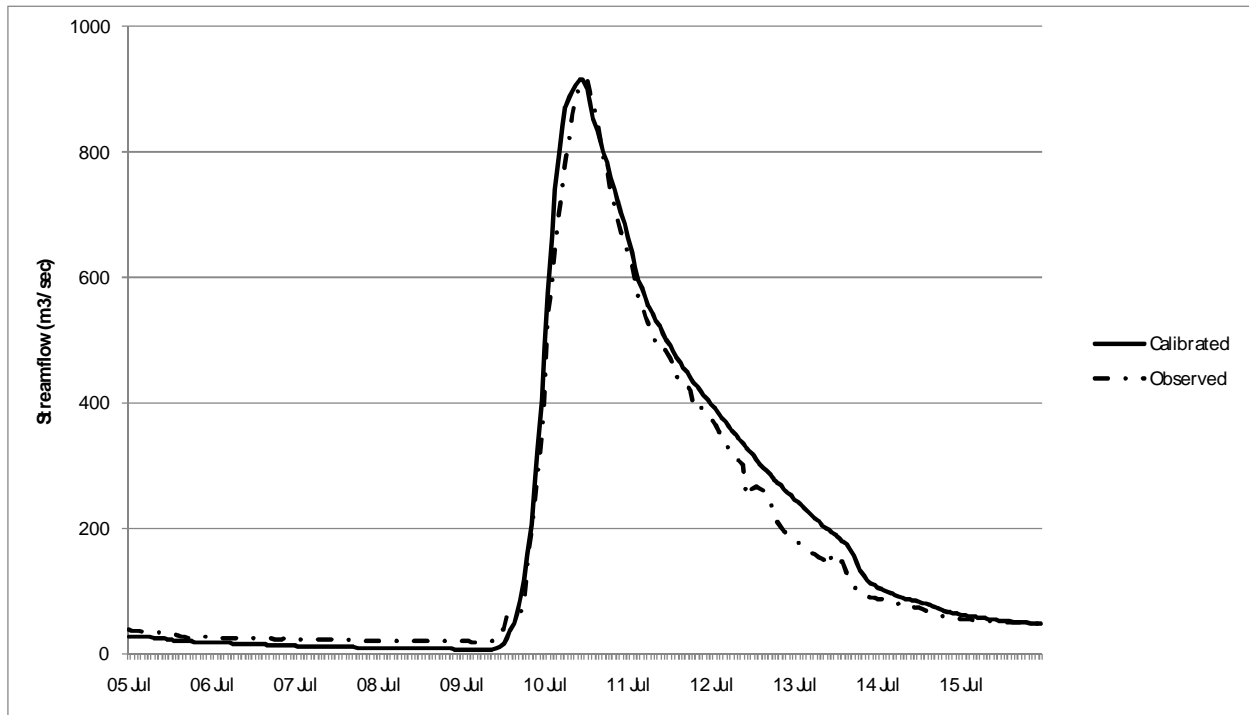


Figure 3.13 Calibration results for the Byron station (July 2000)

In order to further verify the HEC-HMS model developed in this study the simulation of synthetic storms used in the previous sub-watershed studies (Paragon Engineering Limited, 1995a; 1995b; Soil-Eng Limited, 1995, Delcan, 2005) has been done. Table 3.3 and Fig.3.14 show the characteristics of synthetic storms, the control points and the Chicago temporal distribution of precipitation with different duration time, respectively, for the three sub-watersheds: Medway, Stoney, and Pottersburg. The peak flow is computed using the OTTHYMO model (Clarifica Inc., 2002). Table 3.4 shows the comparison of the results obtained with the OTTHYMO model with the results of the HEC-HMS model using the same synthetic flood events. This comparison shows acceptable agreement in spite of the fact that these results are obtained using a very different approach.

Table 3.3 Synthetic storms and peak flows in the sub-basins

Creek	Storm			Peak flow (m ³ /sec)	
	Total precipitation (mm)	Duration (hour)	Distribution	Check point A (Point of interest)	End of Creek
Medway	25.00	4	Chicago	7.9	7.9
Pottersburg	83.22	6	Chicago	25.6	104.0
Stoney	66.11	3	Chicago	24.0	25.7

Table 3.4 Peak flow (m³/sec) simulation results

Sub-watershed	Point A		Outlet	
	OTTHYMO	HEC-HMS	OTTHYMO	HEC-HMS
Medway	7.9	7.7	7.9	7.8
Pottersburg	25.6	54.7	104.0	93.3
Stoney	24.0	29.0	25.7	37.0

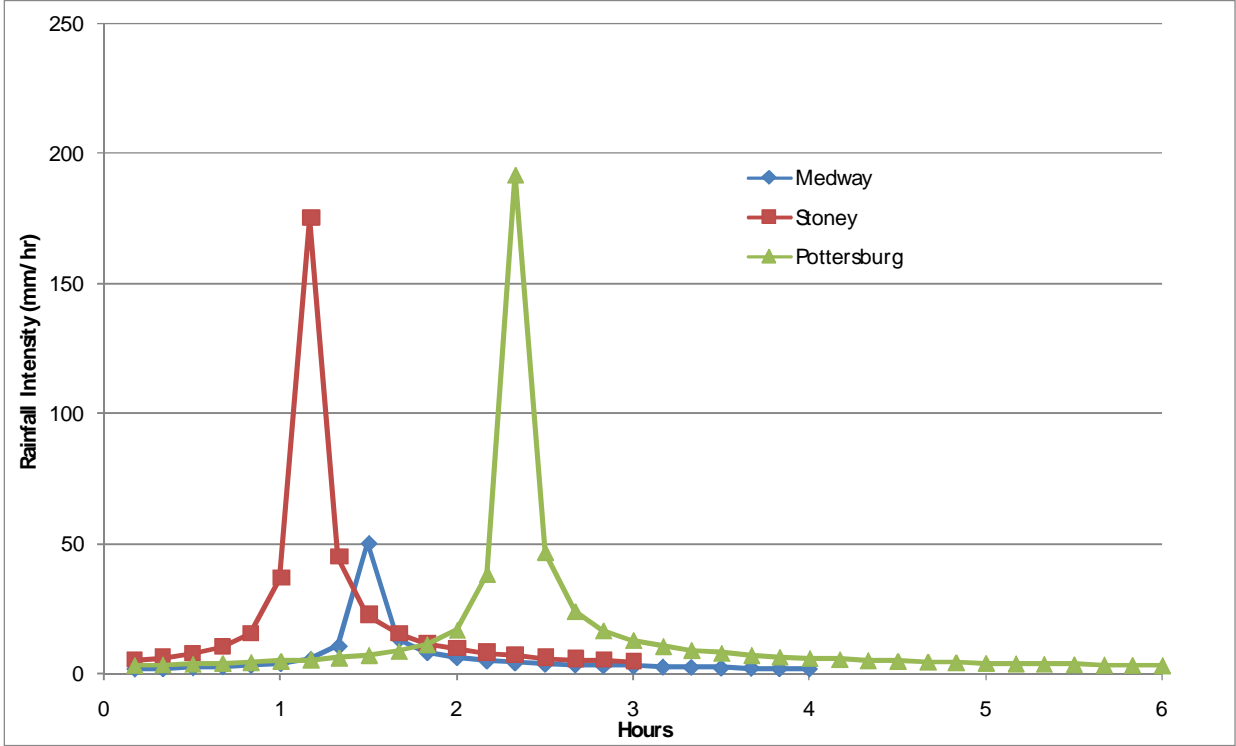


Figure 3.14 Rainfall hyetograph for three creeks

Drainage area of the Dingman Creek is the largest in the City of London, which implies that this basin is of the highest importance for this study. Fig. 3.15 represents the check points (M1 to M23) of the sub-watershed study conducted in 2005 by Delcan (2005). Therefore, in this study eight check points are selected (M1, M2, M3, M8, M9, M10, M14, and M17) and an attempt is made to provide the comparison of simulation results obtained by the HEC-HMS model with those obtained by the SWMHYMO model used in the previous study (Delcan, 2005). This comparison is based on 24 hrs SCS synthetic storm shown in Fig. 3.16. The results of this comparison for eight points selected in Table 3.5 show reasonable agreement in most cases.

From the model verification it is concluded that the HEC-HMS model is calibrated very well and is suitable for the hydrologic analyses using precipitation events generated by the WG model for two climate scenarios.

Table 3.5 Peak flow at the Dingman Creek check points

	M1		M2		M3		M8	
	SWM HYMO	HMS	SWM HYMO	HMS	SWM HYMO	HMS	SWM HYMO	HMS
Peak flow (m ³ /sec)	19.1	21.6	30.2	38.0	41.0	58.6	91.6	106.7
	M9		M10		M14		M17	
	SWM HYMO	HMS	SWM HYMO	HMS	SWM HYMO	HMS	SWM HYMO	HMS
Peak flow (m ³ /sec)	91.6	97.4	116.0	98.2	130.4	108.3	122.2	118.2

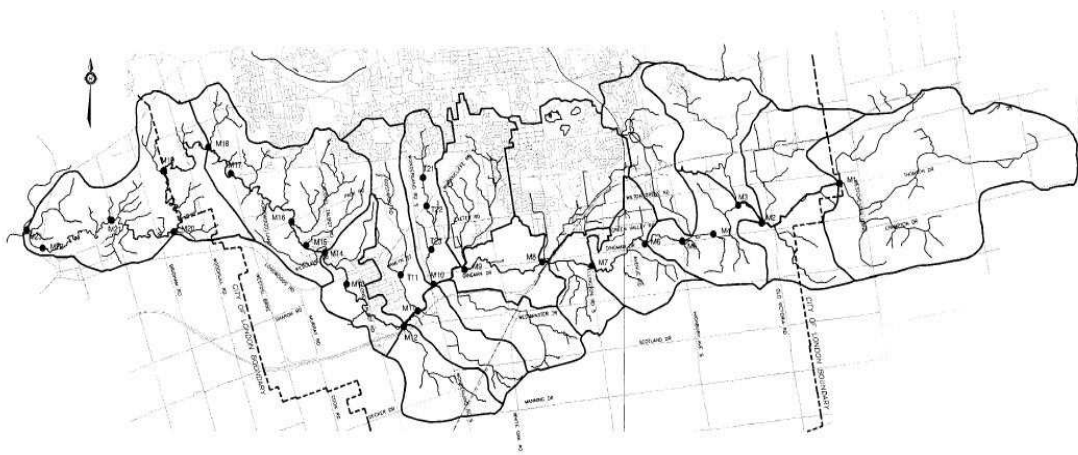


Figure 3.15 Streamflow check points of the previous sub-watershed study (Delcan, 2005)

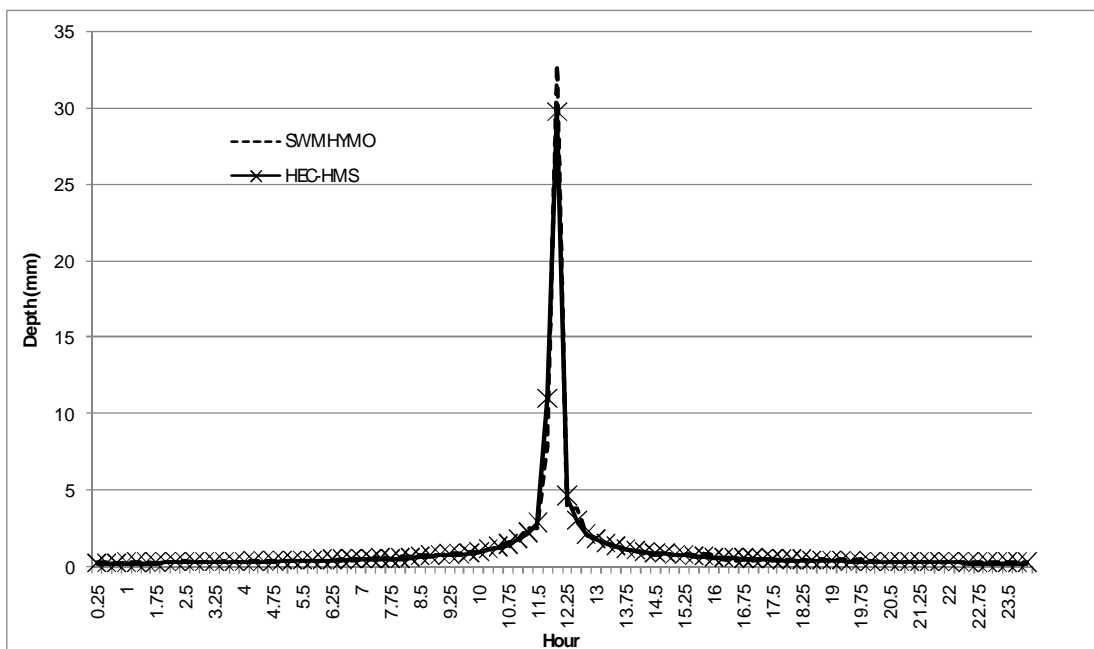
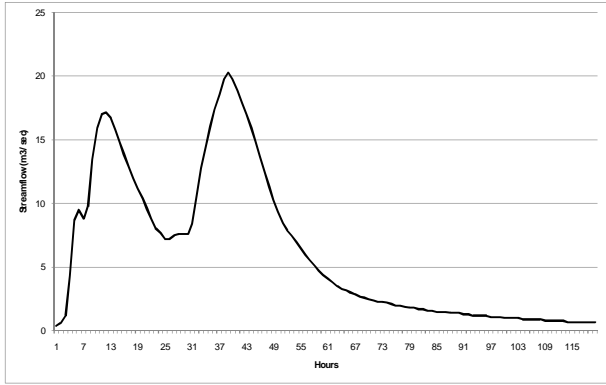


Figure 3.16 Time distribution of 24 hrs SCS synthetic storm

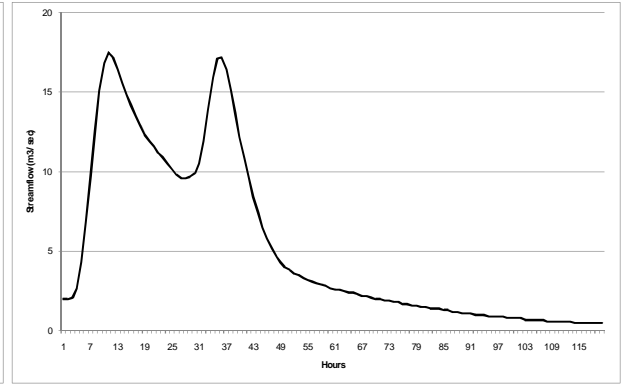
3.4 Application of the HEC-HMS model to future climate scenarios

The WG model provides as input for hydrologic analyses 200 years of daily precipitation data for two climate scenarios, historic and wet. First, the disaggregation is used to convert daily data into hourly. Then the hydrologic model, HEC-HMS, is used to convert climate input into flow data within the City of London. The annual extreme precipitation events for each of 200 years are selected and used as input into the HEC-HMS model.

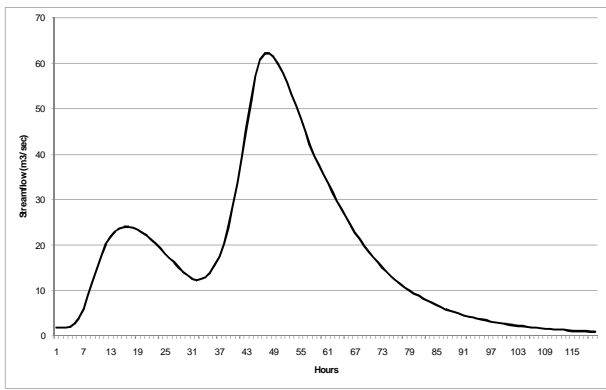
Using the selected 200 annual extreme precipitation events, this study simulates 200 flood events for two climate scenarios, total of 400 flood events. For each flood event, the streamflow values are calculated for each sub-basin and each control point. Each simulation run is done using 5-day time horizon. The simulation results provide the essential hydrologic information for each sub-basin and each control point for two climates and 200 years. Within the region of interest we have identified 171 locations of interest. From 171 locations, Figures 3.17 and 3.18 illustrate the simulation results for an event at six locations (Stoney, Dingman, Medway, Ealing, Forks, and Byron stations) for the historic and the wet climate scenarios, respectively. Three locations (Stoney, Dingman, and Medway stations) are selected to show the hydrograph for the sub-watersheds within the City of London and other three locations, i.e. Ealing, Forks, and Byron stations, are selected to present the results for the South Branch, North Branch and the main Thames, respectively.



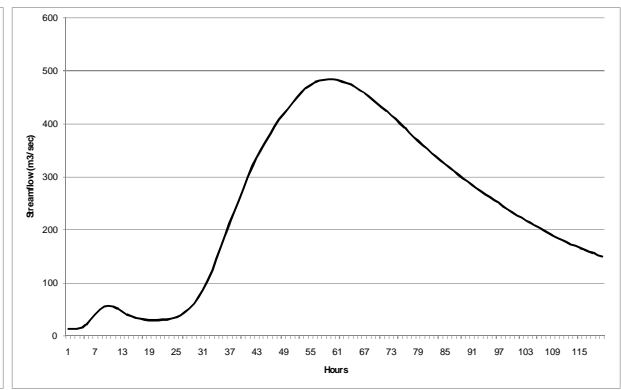
(a) Stoney station



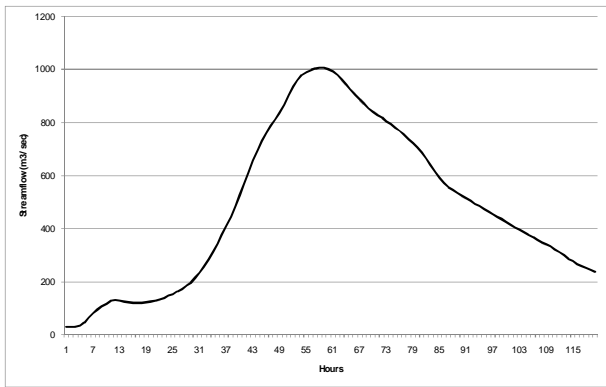
(b) Medway station



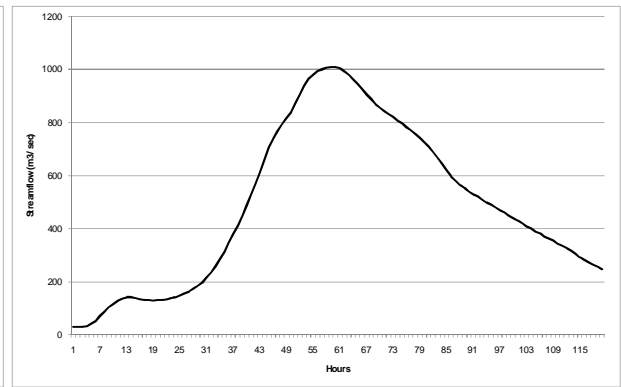
(c) Dingman station



(d) Ealing station

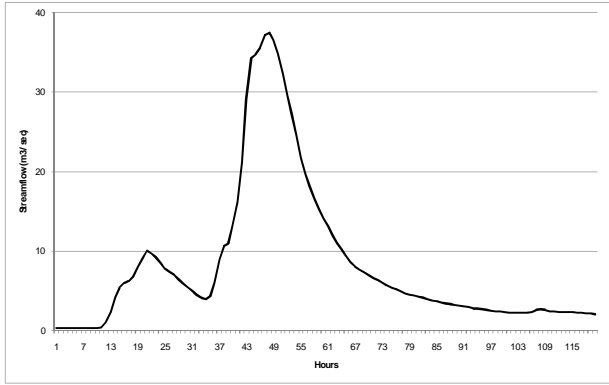


(e) Forks station

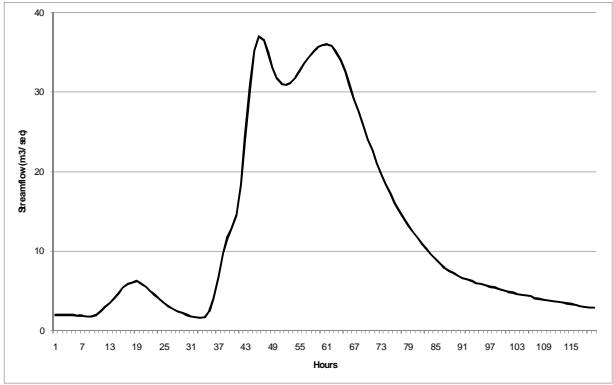


(d) Byron station

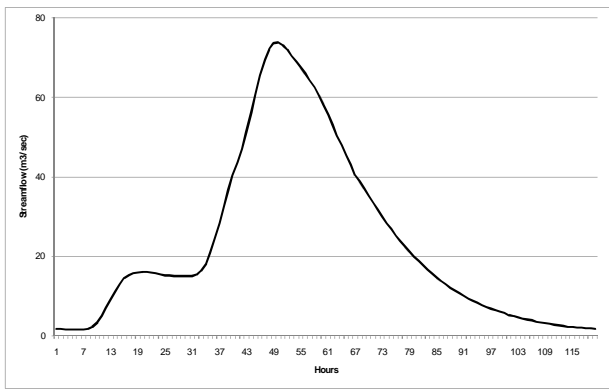
Figure 3.17 Hydrographs of an event for the historic scenario



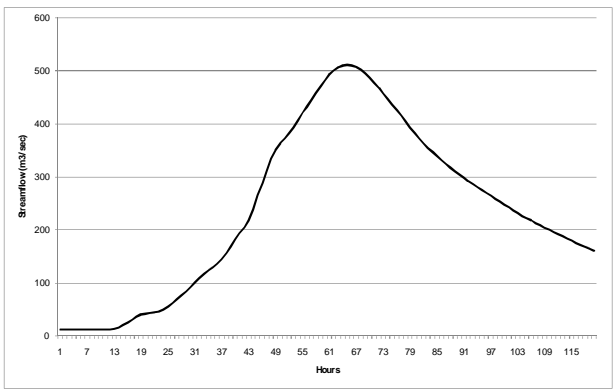
(a) Stoney station



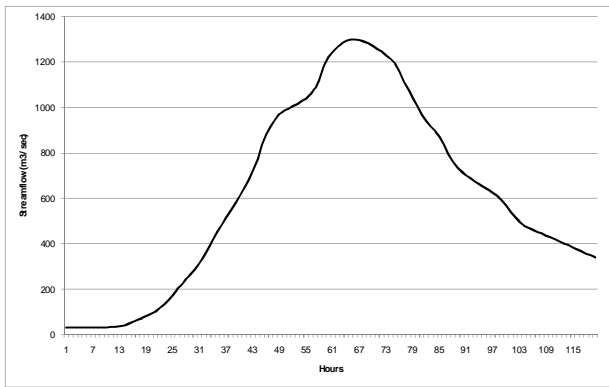
(b) Medway station



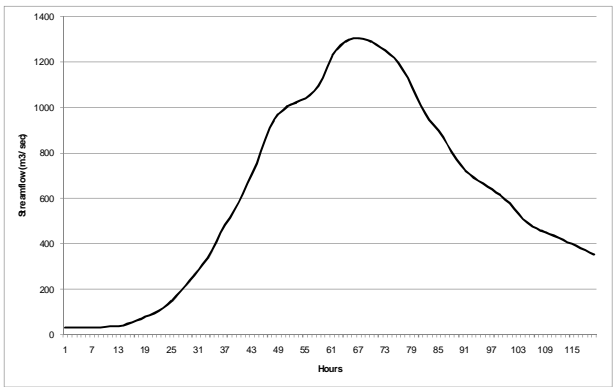
(c) Dingman station



(d) Ealing station



(e) Forks station



(d) Byron station

Figure 3.18 Hydrographs of an event for the wet scenario

3.5 Flood frequency analysis

Extreme precipitation events and corresponding floods can cause loss of life, damage to environment and significant material damage to population that may be affected by flooding. Therefore, the likelihood or probability of such severe events is the basic information for flood plain management, flood control design, and operations of flood protection infrastructure (Maidment, 1992). The frequency analysis is used to relate the magnitude of extreme events to their frequency of occurrence.

The results of the hydrologic analyses (using the HEC-HMS model) in this study are used as input into the hydraulic model (HEC-RAS) that calculates flood water levels to be used in flood plain management. For flood frequency analysis, annual extreme values should be fit to the appropriate extreme value statistical distributions such as Gumbel (less used nowadays) or Log Pearson III. The procedure of frequency analysis conducted in this study is illustrated in Fig. 3.19. First, the WG model is used to generate daily climate data for 200 years. Then, disaggregation scheme is employed to produce hourly data. Next step is to extract the annual extreme precipitation data. The annual extreme precipitation data is selected on the basis of 5-day total precipitation to capture the temporal variability of extreme precipitation events for 15 stations in the basin. 5-day moving window is selected on the basis of historic data analysis. Each extreme precipitation event, then, is simulated using the HEC-HMS hydrologic model to calculate the hydrographs at the points of interest within the basin. In the follow up step the annual peak flow is extracted from each flood hydrograph. In this study, 200 annual peak flow values at each location of interest are collected and used in the flood frequency analysis.

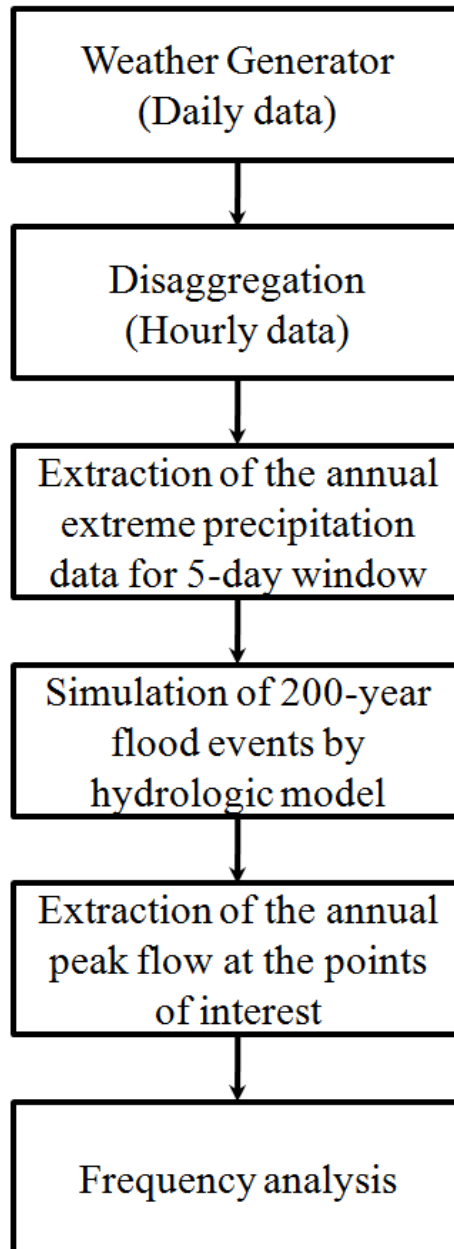


Figure 3.19 Procedure of flood frequency analysis

The annual peak flow values calculated by the HEC-HMS for successive 200 years can be considered to be independent and identically distributed. The flow data is fitted to the probability distribution to define the exceedance probability. In hydrology, the return period is more often used than the exceedance probability, e.g. 100-year flood. In general, x_p is the T -year flood for

$$T = \frac{1}{1 - p} \quad (3.5)$$

where p is cumulative probability defined from the distribution with parameters that describe the character of the probability distribution of a random variable. Moments and quantiles are used to describe the location or central tendency of a random variable. The mean (μ_X) and variance (σ_X^2), second moment about the mean, of a random variable X are defined as in Eq. (3.6) and Eq. (3.7), respectively.

$$\mu_X = E[X] \quad (3.6)$$

$$\sigma_X^2 = \text{Var}(X) = E[(X - \mu_X)^2] \quad (3.7)$$

The parameter estimation of a probability distribution is required to produce frequencies beyond the range of the available data.

There are several general approaches available for estimation of parameters: the method of moments, the method of L moment, and the maximum likelihood method. The maximum likelihood method provides very good statistical properties for large samples. This study used the method of L moment for parameter estimation of distribution. The first L-moment estimator (λ_1) is the mean as shown in Eq. (3.6). The second L moment (λ_2) is a description of scale based on the expected difference between two randomly selected observations in Eq.(3.7).

$$\lambda_2 = \frac{1}{2} E[X_{(1|2)} - X_{(2|2)}] \quad (3.7)$$

where $X_{(in)}$ is the i th largest observation in a sample size n . L-moment measures of skewness and kurtosis are

$$\lambda_3 = \frac{1}{3} E[X_{(1|3)} - 2X_{(2|3)} + X_{(3|3)}] \quad (3.8)$$

$$\lambda_4 = \frac{1}{4} E[X_{(1|4)} - 3X_{(2|4)} + 3X_{(3|4)} - X_{(4|4)}] \quad (3.9)$$

Sample estimators of L moments, therefore, are linear combinations of the ranked observation. As a result, L-moment estimators of the dimensionless coefficient of variation and skewness are almost unbiased while the product-moment estimators of the coefficients of variation and skewness are highly biased and variable in small samples. L moments can be written as functions of probability-weighted moments (PWMs) defined as Eq. (3.10).

$$\beta_r = E\{X[F(X)]^r\} \quad (3.10)$$

where $F(X)$ is cumulative density function for X . The first estimator b_0 of β_0 is the sample mean (\bar{X}).

Other unbiased PWM estimators of β_r for $r \geq 1$ are

$$b_1 = \sum_{j=1}^{n-1} \frac{(n-j)X_{(j)}}{n(n-1)} \quad (3.11)$$

$$b_2 = \sum_{j=1}^{n-2} \frac{(n-j)(n-j-1)X_{(j)}}{n(n-1)(n-2)} \quad (3.12)$$

$$b_3 = \sum_{j=1}^{n-3} \frac{(n-j)(n-j-1)(n-j-2)X_{(j)}}{n(n-1)(n-2)(n-3)} \quad (3.13)$$

For any distribution, L moments are easily calculated from Eq. (3.14).

$$\begin{aligned}
\lambda_1 &= \beta_0 \\
\lambda_2 &= 2\beta_1 - \beta_0 \\
\lambda_3 &= 6\beta_2 - 6\beta_1 + \beta_0 \\
\lambda_4 &= 20\beta_3 - 30\beta_2 + 12\beta_1 - \beta_0
\end{aligned}
\tag{3.14}$$

Using Eq. (3.14), estimates of the λ_i are obtained by replacing the unknown β_r by sample estimators b_r .

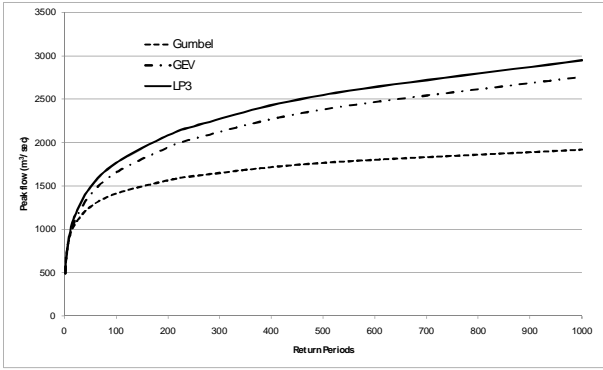
For the Gumbel distribution, for example, the estimators of L moments are represented by Eq.(3.15).

$$\begin{aligned}
\lambda_1 &= \xi + 0.5772\alpha \\
\lambda_2 &= \alpha \ln 2 \\
\lambda_3 &= 0.1699 \\
\lambda_4 &= 0.1504
\end{aligned}
\tag{3.15}$$

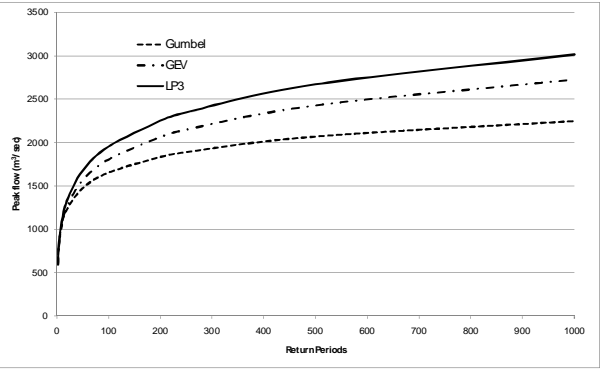
In this study, three probability distributions for extreme events are used: Gumbel, Generalized Extreme Value (GEV), and Log-Pearson type III. Fig. 3.20 shows the results of the flood frequency analysis for two climate scenarios (historic and wet scenarios) at the main locations in the basin and three probability distributions. From the visual inspection of the results it is evident that each probability distribution provides different flood frequency. In previous studies for flood plain management (Delcan, 2005), flood frequency is calculated from the peak obtained using the Chicago time distribution with the precipitation depth selected from the Intensity-Duration-Frequency (IDF) curves developed by Gumbel distribution. In addition, the Gumbel distribution is fit to the most of main locations in the basin as shown in Table 3.6 although other distributions (i.e., GEV and LP III) are also acceptable. Therefore, the Gumbel distribution is used in this study in an attempt to compare the results of flood frequency analysis in this study with those used in the current flood plain management by the City of London.

Table 3.6 Goodness-of-fit test for the main locations

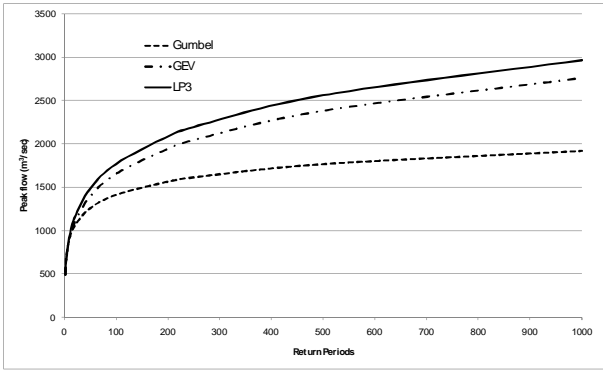
Test	Distributions	Folks	North	South	Dingman	Medway	Stoney	Pottersburg
Chi-square Test	Gumbel	20.48	46.24	16.00	10.40	13.44	17.28	19.04
	GEV	11.84	42.24	16.96	14.24	19.20	18.40	14.72
	LP III	14.40	36.32	9.29	32.16	15.36	16.46	4.80
P-value	Gumbel	0.0838	0.0001	0.2492	0.5811	0.3379	0.1868	0.1219
	GEV	0.4586	0.0001	0.1512	0.2856	0.0838	0.1041	0.2571
	LP III	0.2757	0.0003	0.6784	0.0023	0.2222	0.1711	0.9644



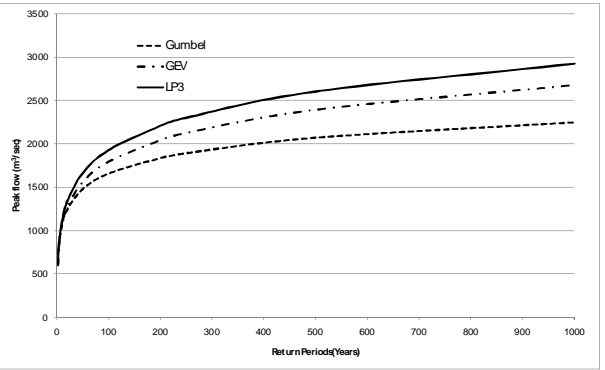
(a) Byron (Historic)



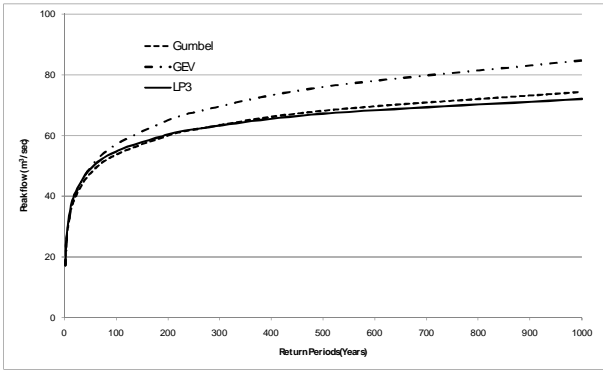
(b) Byron (Wet)



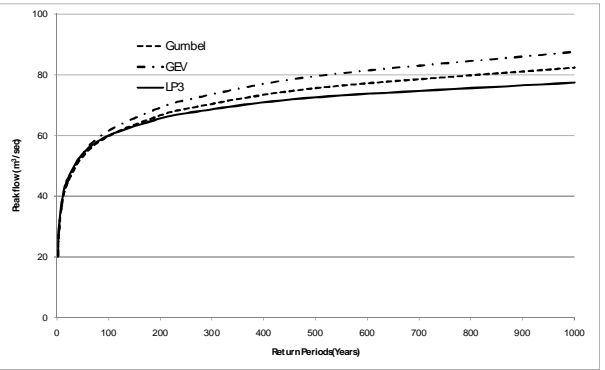
(c) Forks (Historic)



(d) Forks (Wet)

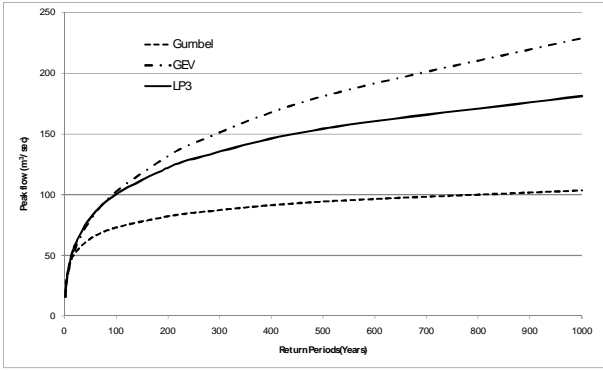


(e) Stoney (Historic)

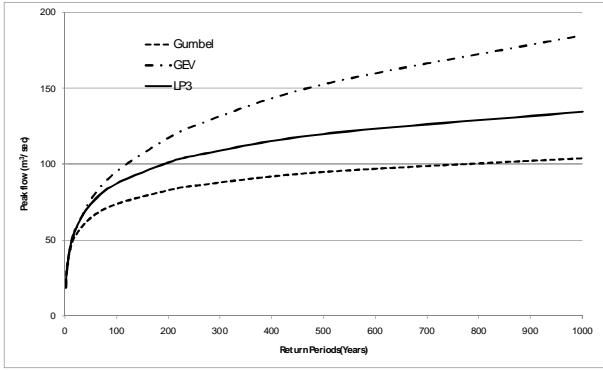


(f) Stoney (Wet)

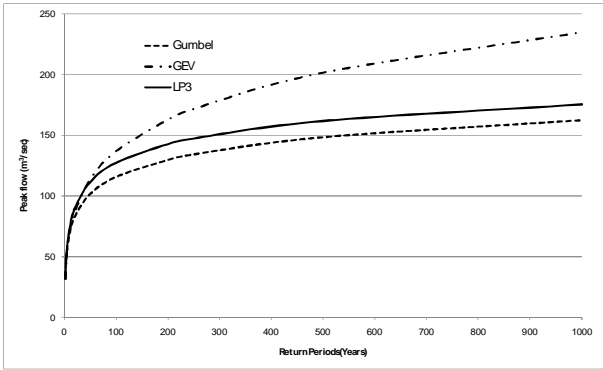
Figure 3.20 Flood frequency analyses for two climate scenarios



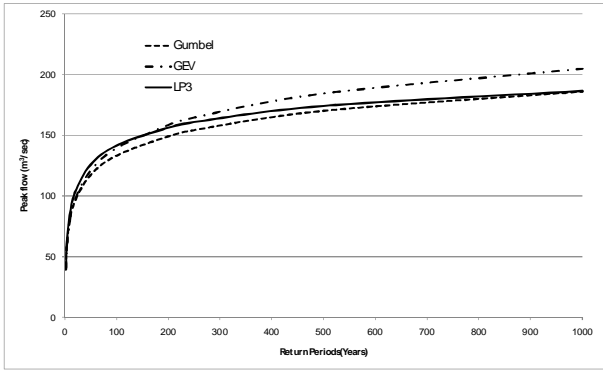
(g) Medway (Historic)



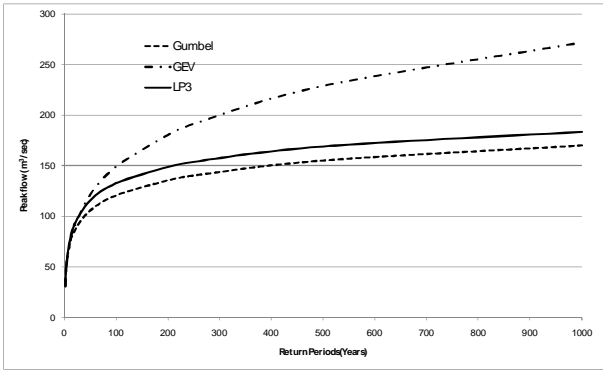
(h) Medway (Wet)



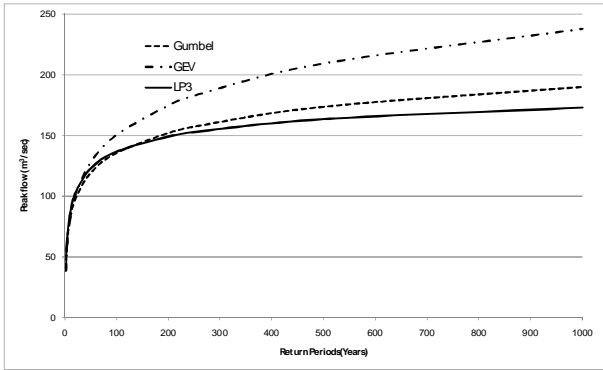
(i) Pottersburg (Historic)



(j) Pottersburg (Wet)



(i) Dingman (Historic)



(j) Dingman (Wet)

Figure 3.20 (Continued)

Fig. 3.22 provides the comparative presentation of flood frequency obtained using the Gumbel distribution and denoted as historic and wet, respectively. As expected, the flood frequency line for the wet scenario is shifted upward from the line for the historic scenario due to climate change impacts. Interestingly, the current flood flows used to build floodplain map in the previous works at some points (South Thames and Medway station) are overestimated as compared to the flood flows corresponding to the historic and wet climate scenarios while the flood flows are underestimated at the North Thames, Stoney and Pottersburg stations. For Forks and Dingman station, however, the flood frequency of the historic climate scenario is similar to the current and the wet scenario provides higher flood flows as expected.

In the previous work (Paragon Engineering Limited, 1995a; 1995b; Soil-Eng Limited, 1995, Delcan, 2005), only the IDF curve for the London station is used to calculate flood frequency for the whole territory of the City of London not reflecting the spatial heterogeneity of precipitation in the basin. However, in this study 15 stations available in the basin are used to properly capture the spatial heterogeneity of climate variables. In addition, previous flood frequency analysis is done using the peak flow from the IDF curve for one station, i.e. it is assumed that the return period for a precipitation event is equal to the return period of a corresponding flood – linear relationship. However, the hydrologic literature is pointing to the high level of non-linearity in this relationship (Pinol et al., 1997; Ceballos and Schnabel, 1998), difference can be up to 3 - 48% (Latron et al., 2008). In this study the flood flow frequency is calculated directly from the annual peak flow data simulated by the hydrologic model, not from the frequency of precipitation data. Due to the methodological difference the flood frequency results of this study should not be directly compared with the previous studies. The results of this study, as well as the previous work, should be verified by increasing flow monitoring in the basin. Based on the observed flow data that are currently insufficient, the hydrologic model can be improved and more accurately calibrated for all sub-basins. Consequently, the more accurate flood frequency can be obtained.

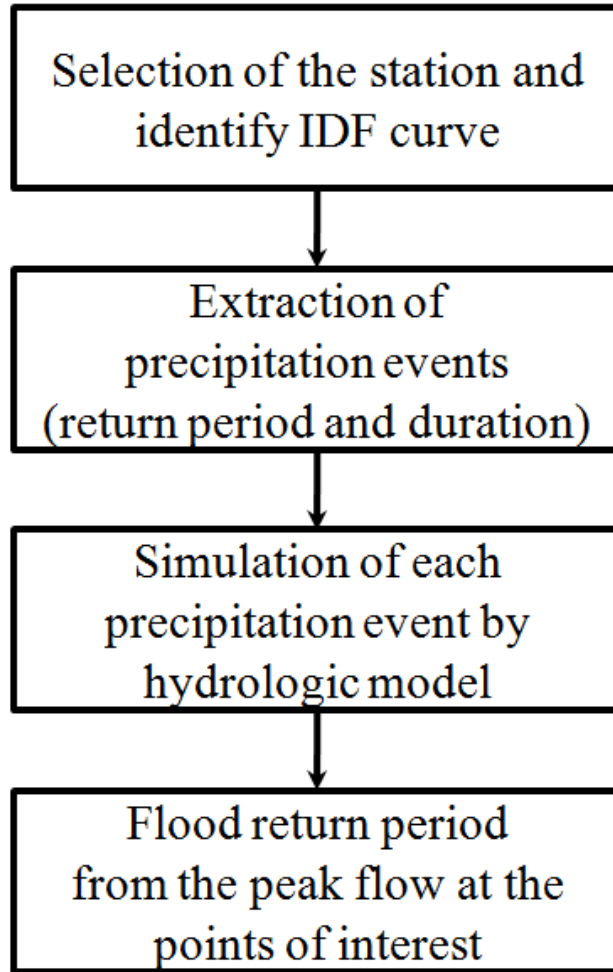
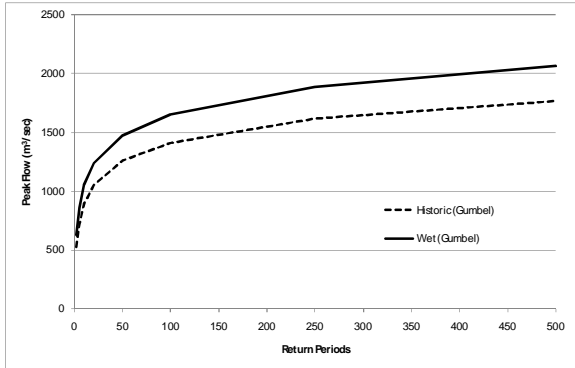
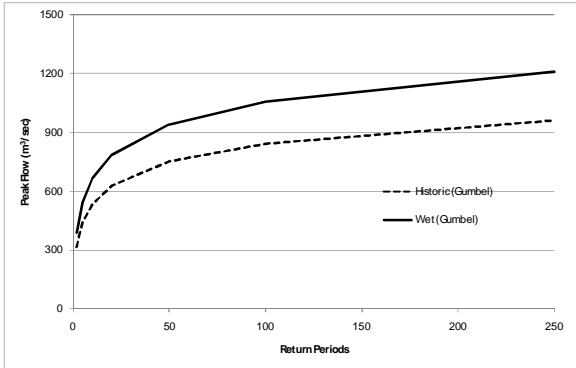


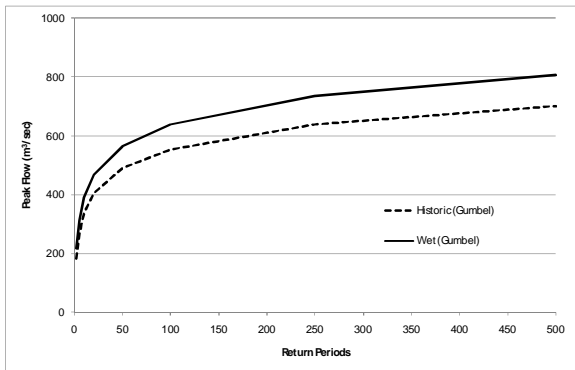
Figure 3.21 Procedure for flood frequency analysis used in the previous works



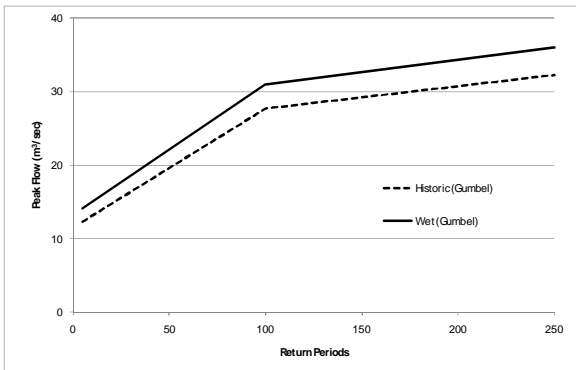
(a) Forks



(b) North Thames

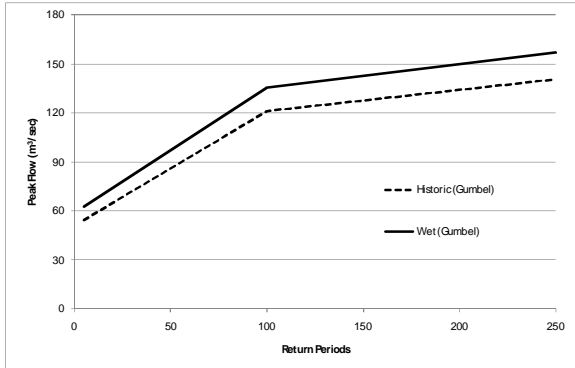


(c) South Thames

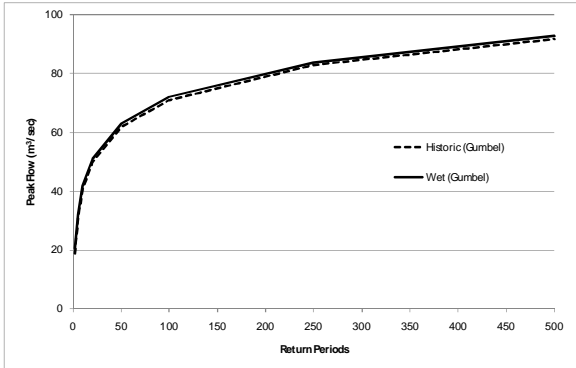


(d) Dingman(Upper)

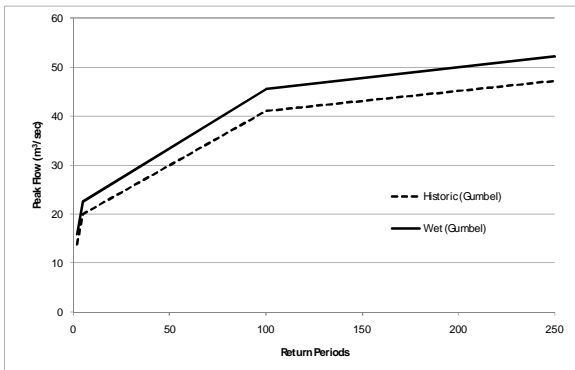
Figure 3.22 Flood frequency for two climate scenarios



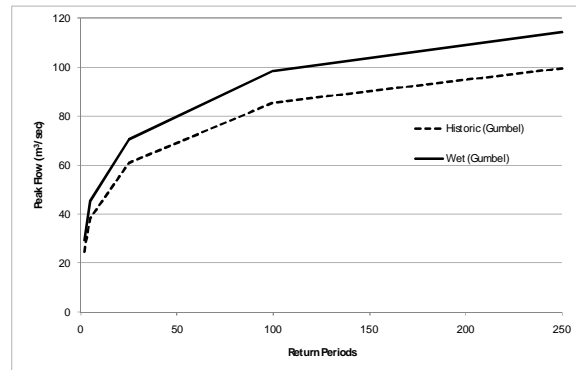
(e) Dingman station



(f) Medway station



(g) Stoney station



(f) Pottersburg (Sta. 5.51)

Figure 3.22 (Continued)

4. Conclusions

This report provides the description of the background analyses for the study “City of London: Vulnerability of the municipal infrastructure to climate change”. As the first background report this document provides description of the climate and hydrologic modeling.

The climate modeling is performed using the WG model that provides two precipitation and temperature scenarios named historic and wet. The historic scenario is assumed to be the lower bound of the potential future climate state, whereas the wet scenario represents the upper bound. The generated climate scenarios are transformed into the hydrologic variables using the HEC-HMS model to further assess the climate change impacts on the hydrologic conditions in the basin. Lastly, the frequency analysis is performed to provide flood flow frequency (return period) at various locations within the basin where flood data is required for further floodplain analyses.

Using 43 years of historic data from 1964 to 2006 at 15 stations in the basin, the WG-PCA model generates a feasible future scenario of precipitation and temperature as the historic scenario. In addition, this study employs one GCM data set (CCSRNIES B21) for time slice of 2040-2069 to generate a feasible future scenario as the wet scenario.

The results of climate modeling demonstrate that the WG-PCA model reproduces very well the historic statistical values (25th, 50th, 75th percentile). It also provides the wider range of values for climate variables by the implementation of perturbation process that generates data outside the bounds of the observed values. According to the monthly climate shift of the GCM data used with the wet climate scenario, the amount of precipitation from January to September (9 months) is higher. The significant changes are observed during the spring season from March to June and the highest change occurs in May. These results indicate that more severe and more frequent floods may occur during this period under the wet climate scenario.

In addition to precipitation, this study generates maximum and minimum temperature at 15 stations within the basin. Maximum and minimum temperature for the wet scenario increases by 5.7 °C and 5.2°C on average over all months due to the climate change. The change of maximum temperature for the winter season (6.2 °C) is larger than for the summer season (5.2°C), which indicates that floods resulting from the combined effect of snowmelt and precipitation might occur more frequently in the future.

The weather generator (WG) model results are spatially and temporally disaggregated for use with the hydrologic model. The HEC-HMS hydrologic model is developed with 72 sub-basins, 45 reaches, 49 junctions, and 3 reservoirs. It is used to simulate the annual extreme events for 200 years and provide the annual peak flows for flood frequency analysis.

Several probability distributions (Gumbel, LP3, and GEV) are tested for flood flow frequency analysis. The Gumbel distribution is selected for use with the historic and the wet climate scenarios. Results of the analyses are compared with the current flood flow frequency used by the Upper Thames River Conservation Authority (UTRCA) for flood plain management. Direct comparison of the results is not possible due to the major methodological difference between this study and previous work.

This study developed the hydrologic model with the insufficient amount of observed data for various sub-basins. This deficiency caused the difficulty in model calibration and resulted in limited ability of the model to accurately describe the hydrologic response of the system to an event. Therefore, continuous monitoring system at the various sites in the basin is needed to provide the accurate observed hydrologic information. These observations will be very valuable for the verification of flood frequency analyses performed in this study.

Acknowledgments

This work was made possible by a financial support from the City of London. The authors would like to thank the Upper Thames River Conservation Authority (UTRCA) for providing data used in this study.

References

- Buishand, T. A., and Brandsma, T. (2001). "Multisite simulation of daily precipitation and temperature in the Rhine Basin by nearest neighbor resampling." *Water Resources Research*, 37(11), 2761–2776.
- Ceballos A., and Schnabel S. (1998). "Hydrological behavior of a small catchment in the dehesa landuse system (Extremadura, SW Spain)." *Journal of Hydrology*, 210, 146–160.
- Clarifica Inc. (2002). *Visual OTTHYMO™ v2 Users Guide*.
- Cunderlik, J. and Simonovic, S. P. (2004). *Calibration, verification and sensitivity analysis of the HEC-HMS hydrologic model*. Water Resources Research Report no. 048, Facility for Intelligent Decision Support, Department of Civil and Environmental Engineering, London, Ontario, Canada.
- Cunderlik, J. M., and Simonovic, S. P. (2005). "Hydrological extremes in a south-western Ontario river basin under future climate conditions." *IAHS Hydrological Sciences Journal*, 50(4), 631–654.
- Cundelik, J.M., and Simonovic, S.P. (2007). "Inverse flood risk modelling under changing climatic conditions." *Hydrological Processes*, 21:563-577.
- DELCAN (2005). *Dingman Creek Subwatershed Study Update*, The City of London.
- Eum, H.-I., and Simonovic, S. P. (2008). "Selecting variables for the weather generator model." *Proceedings of 4th International Symposium on Flood Defence*, Institute for Catastrophic Loss Reduction (ICLR), Toronto, Canada.
- Fisher, N.I. (1993). *Statistical Analysis of Circular Data*. Cambridge Univ. Press, New York.
- Hashimoto, T., Stedinger, J. R., and Loucks, D. P. (1982). "Reliability, resiliency, and vulnerability criteria for water resource system performance evaluation." *Water Resources Research*, 18(1), 14-20.
- IPCC (2000). *Special Report on Emissions Scenarios*. Cambridge University Press, Cambridge.

- IPCC (2007). *Summary for Policymakers. Climate Change 2007: The physical science basis. Contribution of the Working Group I to the Fourth Assessment Report of the Intergovernmental Panel on Climate Change*. Cambridge University Press, Cambridge, United Kingdom.
- Lall, U., and Sharma, A. (1996). "A nearest neighbour bootstrap for time series resampling." *Water Resources Research*, 32 (3), 679–693.
- Lall, U., Rajagopalan, B., and Torboton, D. G., (1996). "A nonparametric wet/dry spell model for resampling daily precipitation." *Water Resources Research*, 32 (9), 2803–2823.
- Lapen, D. R. and Hayhoe, H. N. (2003). "Spatial analysis of seasonal and annual temperature and precipitation normals in Southern Ontario, Canada." *Journal of Great Lakes Research*, 29(4), 529-544.
- Latron J., Soler, M., Llorens, P., and Gallart, F. (2008). "Spatial and temporal variability of the hydrological response in a small Mediterranean research catchment (Vallcebre, Eastern Pyrenees)." *Hydrological Processes*, 22, 775-787.
- Maidment, D. R. (1992). *Handbook of Hydrology*. McGraw-Hill, New York.
- Mehrotra, R; and Sharma, A. (2007). "Preserving low-frequency variability in generated daily rainfall sequences." *Journal of Hydrology*, 345, 102-120.
- Milly, P.C.D., J. Betancourt, M. Falkenmark, R.M. Hirsch, Z.W. Kundzewicz, D.P. Lettenmaier, and R.J. Stouffer (2008), "Stationarity is Dead: Whiter Water Management?", *Science*, 319, 573-574.
- Nicks, A. D., Richardson, C. W., and Williams, J. R., (1990). "Evaluation of EPIC model weather generator: erosion/productivity impact calculator, 1. Model documentation." In: Sharpley, A.N., Williams, J.R., (Eds.), *USDA-ARS Tech. Bull.*, 1768, 235.
- Paragon Engineering Limited (1995a). *Pottersburg Creek and Crumlin Creek Drain Subwatershed Study*, City of London.

- Paragon Engineering Limited (1995b). *Stoney Creek Subwatershed Study*, City of London. Parlange, M. B., and Katz, R. W. (2000). "An extended version of the Richardson model for simulating daily weather variables." *Journal of Applied Meteorology*, 39, 610–622.
- Pinol J., Beven K., and Freer J. (1997). "Modeling the hydrological response of mediterranean catchments, Prades, Catalonia. The use of distributed models as aids to hypothesis formulation." *Hydrological Processes*, 11, 1287–1306.
- Porter, J. W. and Pink, B. J. "A method of synthetic fragments for disaggregation in stochastic data generation." *International Hydrology and Water Resources Symposium*, Perth, Australia, 781-786.
- Prodanovic, P., and Simonovic, S. P. (2006a). *Inverse Flood Risk Modelling of The Upper Thames River Basin*, Water Resources Research Report no. 052, Facility for Intelligent Decision Support, Department of Civil and Environmental Engineering, London, Ontario, Canada.
- Prodanovic, P., and Simonovic, S. P. (2006b). *Inverse Drought Risk Modelling of The Upper Thames River Basin*, Water Resources Research Report no. 053, Facility for Intelligent Decision Support, Department of Civil and Environmental Engineering, London, Ontario, Canada.
- Rajagopalan, B., and Lall, U. (1999). "A k-nearest neighbour simulator for daily precipitation and other variables." *Water Resources Research*, 35(10), 3089–3101.
- Sharif, M., and Burn, D. H. (2006). "Simulating climate change scenarios using an improved K-nearest neighbor model." *Journal of Hydrology*, 325, 179-196.
- Sharma, A., Tarboton, D. G., and Lall, U. (1997). "Streamflow simulation: A nonparametric approach." *Water Resources Research*, 33(2), 291-308.
- Sharma, A., and O'Neill R. (2002). "A nonparametric approach for representing interannual dependence in monthly streamflow sequences." *Water Resources Research*, 38(7), doi 10.1029/2001WR000953.
- Soil-Eng Limited (1995). *City of London Subwatershed Studies Group 1 Subwatersheds*, City of London.

- Srikanthan, R. and McMahon, T. A. (1982). "Stochastic generation of monthly streamflows." *Proceedings of the American Society of Civil Engineers. Journal of the Hydraulics Division*, 108(3), 419-441.
- Svanidze, G. G. (1977). *Mathematical Modeling of Hydrologic Series*, Water Resources Publications, Littleton, Colorado.
- US Army Corps of Engineers (2008). *Hydrologic Modeling System HEC-HMS User's Manual*. Hydrologic Engineer Center.
- Wey, K. M. (2006). *Temporal Disaggregation of Daily Precipitation Data in a Changing Climate*. Master thesis, University of Waterloo.
- Wilks, D. S., and Wilby, R. L. (1999). "The weather generation game: a review of stochastic weather models." *Progress in Physical Geography*, 23(3), 329-357.
- Wójcik, J., and Buishand, T. A. (2003). "Simulation of 6-hourly rainfall and temperature by two resampling schemes." *Journal of Hydrology*, 273, 69-80.
- Yates, D., Gangopadhyay, S., Rajagopalan, B., and Strzepek, K. (2003). "A technique for generating regional climate scenarios using a nearest-neighbor algorithm." *Water Resources Research*, 39(7), SWC 7-1–SWC 7-14.
- Young, K.C. (1994). "A multivariate chain model for simulating climatic parameters with daily data." *Journal of Applied Meteorology*, 33, 661–671.

Appendix 1: Flood frequency at various locations

1. 100 yr frequency (Unit: m³/sec)

River	Number of River Station in HEC-RAS ⁽¹⁾	Historic (1)	Wet (2)	UTRCA (3)	Difference between Historic and UTRCA (1) – (3)	Difference between Wet and UTRCA (2) – (3)
Ballymonte	2511.324	11.5	12.6	5.4	6.1	7.2
Ballymonte	788.7309	16.0	17.6	6.5	9.5	11.1
Northdale	1114.278	1.1	1.2	1.0	0.1	0.2
Northdale	457.1955	3.5	4.0	2.6	0.9	1.4
Powell Drain	1355.036	2.6	2.9	2.6	-0.1	0.3
Powell Drain	699.343	3.1	3.5	2.8	0.3	0.7
Powell Drain	269.5363	7.8	8.8	5.9	1.9	2.9
Stoney Creek	10028.42	15.9	19.8	8.4	7.5	11.4
Stoney Creek	9182.6	17.1	19.1	8.4	8.7	10.7
Stoney Creek	6862.462	23.7	26.5	8.4	15.3	18.1
Stoney Creek	6242.931	41.0	45.4	14.3	26.7	31.1
Stoney Creek	4736.068	42.3	46.9	13.3	29.0	33.6
Stoney Creek	2881.127	51.3	57.1	14.3	37.0	42.8
Stoney Creek	1564.418	55.9	62.2	31.0	24.9	31.2
Pottersburg	14213.43	33.42	39.81	18.8	14.6	21.0
Pottersburg	9600.814	68.17	79.41	20.1	48.1	59.3
Pottersburg	8049.473	74.86	86.95	30.75	44.1	56.2
Pottersburg	6780.69	83.28	96.42	50.49	32.8	45.9
Pottersburg	5799.997	85.51	98.47	55.47	30.0	43.0
Pottersburg	2696.997	109.71	125.87	55.5	54.2	70.4
Pottersburg	1771.452	120.69	138.31	73	47.7	65.3
Pottersburg	899.4334	123.45	141.43	89.6	33.9	51.8
South Thames	10634.24	572.7	660.0	705.7	-133.0	-45.6
North Thames	14281.62	842.5	1056.6	745.0	97.5	311.6
North Thames	4364.224	902.4	1099.5	815.0	87.4	284.5
Main Thames	11187.99	1412.3	1656.0	1489.0	-76.7	167.0
Medway Creek	12534.02	64.1	66.4	157.1	-93.0	-90.7

⁽¹⁾ represents the distance from the end of river

River	Number of River Station in HEC-RAS*	Historic (1)	Wet (2)	UTRCA (3)	Difference between Historic and UTRCA (1) – (3)	Difference between Wet and UTRCA (2) – (3)
Medway Creek	8340.125	65.8	68.3	166.0	-100.1	-97.7
Medway Creek	6814.245	65.8	68.3	165.5	-99.7	-97.3
Medway Creek	4401.77	68.8	70.6	165.7	-96.8	-95.1
Medway Creek	2502.589	71.0	72.1	168.6	-97.6	-96.4
Mud Creek	2397.303	0.8	0.8	6.7	-6.0	-5.9
Mud Creek	1400.737	3.9	4.3	15.5	-11.6	-11.3
Mud Creek	655.1806	6.3	6.9	15.5	-9.2	-8.6
Mud Creek	263.5877	9.4	10.2	20.1	-10.7	-9.8
Dingman (Main)	29643.436	71.5	80.8	25.7	45.8	55.1
Dingman(Main)	29282.363	71.7	81.1	26.7	45.0	54.4
Dingman(Main)	28760.541	71.4	80.8	28.3	43.1	52.5
Dingman(Main)	27123.502	74.7	84.4	31.2	43.5	53.2
Dingman(Main)	24269.293	87.4	98.0	34.0	53.4	64.0
Dingman(Main)	22443.02	106.2	119.4	72.0	34.2	47.4
Dingman(Main)	18841.631	105.9	118.8	80.3	25.6	38.5
Dingman(Main)	17717.428	113.0	126.4	90.0	23.0	36.4
Dingman(Main)	15770.021	110.5	123.6	112.3	-1.8	11.3
Dingman(Main)	12864.36	110.1	123.1	113.7	-3.6	9.4
Dingman(Main)	5712.2881	118.9	133.1	127.8	-8.9	5.3
Dingman(Trib.6)	2622.8225	6.4	7.2	0.9	5.5	6.3
Dingman (Trib.5)	1429.6442	7.7	8.6	48.6	-40.9	-40.0
Dingman (Trib.5)	2181.5747	12.1	13.5	57.7	-45.6	-44.2
Dingman (Trib.4)	895.04858	2.5	2.7	5.2	-2.7	-2.5
Dingman (Trib.4)	2394.6248	11.6	12.6	5.2	6.4	7.4
Dingman (Trib.4)	2006.9204	12.1	13.2	6.1	6.0	7.1
Dingman (Trib.4)	751.81909	13.5	14.8	11.0	2.5	3.8
Dingman (Trib.4)	588.14539	18.3	20.0	11.0	7.3	9.0
Dingman (Trib.3)	4832.0176	2.2	2.4	9.4	-7.2	-7.0
Dingman (Trib.3)	3164.4568	7.1	7.7	8.6	-1.5	-0.9
Dingman (Trib.3)	1062.6754	10.7	11.6	10.4	0.3	1.2
Dingman (Trib.11)	3514.9307	5.2	5.4	4.0	1.2	1.4
Dingman (Trib.11)	610.84808	12.1	12.7	8.1	4.0	4.6
Dingman (Trib.2)	5177.5825	3.3	3.6	14.4	-11.1	-10.8
Dingman (Trib.2)	3926.3052	5.8	6.2	21.2	-15.4	-15.0

River	Number of River Station in HEC-RAS*	Historic (1)	Wet (2)	UTRCA (3)	Difference between Historic and UTRCA (1) – (3)	Difference between Wet and UTRCA (2) – (3)
Dingman (Trib.2)	1458.7761	8.4	9.0	23.8	-15.4	-14.8
Dingman (Trib.10)	784.34576	5.4	5.8	5.0	0.4	0.8
Dingman (Trib.9)	1649.277	0.8	0.8	4.3	-3.5	-3.5
Dingman (Trib.8)	1354.2716	3.3	3.5	4.5	-1.2	-1.0
Dingman (Trib.7)	2297.6155	5.3	5.7	9.8	-4.5	-4.1
	sum	6272.8 (*1.7 %)	7310.8 (*18.6 %)	6165.2 (-)	**1.6	**17.4

* represents the percentage of change in flow as compared to current UTRCA

** represents the average flow

2. 250 yr frequency

River	Number of River Station in HEC-RAS	Historic (1)	Wet (2)	UTRCA (3)	Difference between Historic and UTRCA (1) – (3)	Difference between Wet and UTRCA (2) – (3)
Ballymonte	2511.324	13.1	14.4	6.6	6.5	7.8
Ballymonte	788.7309	18.3	20.1	8.0	10.3	12.1
Northdale	1114.278	1.3	1.4	1.3	-0.1	0.1
Northdale	457.1955	4.1	4.6	3.2	0.9	1.4
Powell Drain	1355.036	3.0	3.3	3.1	-0.1	0.2
Powell Drain	699.343	3.6	4.0	3.6	0.0	0.4
Powell Drain	269.5363	9.1	10.1	7.1	2.0	3.0
Stoney Creek	10028.42	18.4	20.5	10.0	8.4	10.5
Stoney Creek	9182.6	19.8	22.1	10.0	9.8	12.1
Stoney Creek	6862.462	27.4	30.6	10.2	17.2	20.4
Stoney Creek	6242.931	47.7	52.2	17.5	30.2	34.7
Stoney Creek	4736.068	48.7	53.9	16.2	32.5	37.7
Stoney Creek	2881.127	59.2	65.7	17.2	42.0	48.5
Stoney Creek	1564.418	64.5	71.5	35.9	28.6	35.6
Pottersburg	14213.43	39.3	46.6	21.4	17.9	25.2
Pottersburg	9600.814	79.5	92.3	23.6	55.9	68.8
Pottersburg	8049.473	87.2	101.0	35.9	51.3	65.1
Pottersburg	6780.69	96.9	111.9	67.0	29.9	44.9
Pottersburg	5799.997	99.5	114.2	64.4	35.1	49.8
Pottersburg	2696.997	127.4	145.8	64.4	63.0	81.4
Pottersburg	1771.452	140.1	160.1	87.4	52.7	72.7
Pottersburg	899.4334	143.3	163.7	103.2	40.1	60.5
South Thames	10634.24	660.3	760.0	849.5	-189.2	-89.6
North Thames	14281.62	962.4	1209.2	935.0	27.4	274.2
North Thames	4364.224	1031.5	1258.1	1107.0	-75.5	151.1
Main Thames	11187.99	1614.9	1891.9	1834.0	-219.0	57.9
Medway Creek	12534.02	75.6	78.1	182.3	-106.7	-104.2
Medway Creek	8340.125	77.3	79.9	193.6	-116.2	-113.6
Medway Creek	6814.245	77.3	79.9	193.4	-116.1	-113.5
Medway Creek	4401.77	80.6	82.3	193.7	-113.1	-111.3
Medway Creek	2502.589	82.9	84.0	197.2	-114.3	-113.2
Mud Creek	2397.303	0.9	1.0	9.0	-8.2	-8.1
Mud Creek	1400.737	4.5	4.9	21.0	-16.5	-16.1
Mud Creek	655.1806	7.3	7.9	21.0	-13.8	-13.1
Mud Creek	263.5877	10.8	11.7	27.6	-16.8	-15.9

River	Number of River Station in HEC-RAS	Historic (1)	Wet (2)	UTRCA (3)	Difference between Historic and UTRCA (1) – (3)	Difference between Wet and UTRCA (2) – (3)
Dingman(Main)	29643.436	83.3	93.7	26.7	56.6	67.0
Dingman(Main)	29282.363	83.5	94.0	26.7	56.8	67.3
Dingman(Main)	28760.541	83.1	93.7	29.4	53.7	64.3
Dingman(Main)	27123.502	87.0	97.9	32.4	54.6	65.5
Dingman(Main)	24269.293	101.8	113.8	35.3	66.5	78.5
Dingman(Main)	22443.02	123.7	138.7	102.5	21.2	36.2
Dingman(Main)	18841.631	123.3	137.9	113.5	9.8	24.4
Dingman(Main)	17717.428	131.5	146.6	127.2	4.2	19.4
Dingman(Main)	15770.021	128.5	143.3	125.3	3.2	18.0
Dingman(Main)	12864.36	128.0	142.8	125.2	2.8	17.6
Dingman(Main)	5712.2881	138.2	154.4	132.4	5.8	22.0
Dingman (Trib.13)	3457.2783	3.3	3.8	2.9	0.4	0.9
Dingman (Trib.12)	1080.8469	11.3	12.6	2.1	9.2	10.5
Dingman (Trib.12)	3098.6504	4.2	4.7	1.7	2.5	3.0
Dingman (Trib.12)	2213.1494	19.9	22.2	3.8	16.1	18.4
Dingman (Trib.12)	1148.9613	28.5	31.9	6.2	22.3	25.7
Dingman (Trib.6)	2622.8225	7.5	8.4	0.9	6.6	7.5
Dingman (Trib.5)	1429.6442	9.0	10.0	76.8	-67.8	-66.8
Dingman (Trib.5)	2181.5747	14.1	15.7	100.5	-86.4	-84.8
Dingman (Trib.4)	895.04858	2.9	3.1	5.5	-2.6	-2.4
Dingman (Trib.4)	2394.6248	13.5	14.6	7.7	5.8	6.9
Dingman (Trib.4)	2006.9204	14.1	15.3	7.9	6.2	7.4
Dingman (Trib.4)	751.81909	15.8	17.1	12.5	3.3	4.6
Dingman (Trib.4)	588.14539	21.3	23.2	12.5	8.8	10.7
Dingman (Trib.3)	4832.0176	2.5	2.7	12.9	-10.4	-10.2
Dingman (Trib.3)	3164.4568	8.3	8.9	10.5	-2.2	-1.6
Dingman (Trib.3)	1062.6754	12.4	13.4	12.1	0.3	1.3
Dingman (Trib.11)	3514.9307	6.0	6.3	4.2	1.8	2.1
Dingman (Trib.11)	610.84808	14.1	14.8	8.4	5.7	6.4
Dingman (Trib.2)	5177.5825	3.9	4.1	21.1	-17.2	-17.0
Dingman (Trib.2)	3926.3052	6.7	7.2	29.3	-22.6	-22.1

River	Number of River Station in HEC-RAS	Historic (1)	Wet (2)	UTRCA (3)	Difference between Historic and UTRCA (1) – (3)	Difference between Wet and UTRCA (2) – (3)
Dingman (Trib.2)	5177.5825	3.9	4.1	21.1	-17.2	-17.0
Dingman (Trib.2)	3926.3052	6.7	7.2	29.3	-22.6	-22.1
Dingman (Trib.2)	1458.7761	9.7	10.4	32.6	-22.9	-22.2
Dingman (Trib.10)	784.34576	6.3	6.7	5.1	1.2	1.6
Dingman (Trib.9)	1649.277	0.9	1.0	5.7	-4.8	-4.7
Dingman (Trib.8)	1354.2716	3.8	4.1	5.5	-1.7	-1.4
Dingman (Trib.7)	2297.6155	6.2	6.6	12.4	-6.2	-5.8
	Sum	7295.8 (-4.7 %)	8484.5 (10.8 %)	7658.9 (-)	** -5.1	** 11.6

* represents the percentage of change in flow as compared to current UTRCA

** represents the average flow

Appendix 2: HEC-HMS hydrologic model parameters.

Sub-basin*	Basin Area (km ²)	Time of Concentration (Hr)	Storage Coefficient (Hr)	Initial loss (mm)	Constant rate (mm/hr)	Initial discharge (m ³ /s/km ²)
1	175.98	8.0	10.0	5.0	1.00	0.01
10	141.12	13.0	9.0	5.0	1.10	0.01
11	28.94	9.0	5.0	5.0	1.20	0.01
12	35.47	10.0	8.0	5.0	1.30	0.01
13	153.72	13.0	14.0	5.0	1.00	0.01
14	84.54	14.0	10.0	5.0	1.50	0.01
15	94.20	15.0	20.0	5.0	2.00	0.01
16-1	14.54	6.0	18.0	6.7	1.66	0.01
16-10	14.99	16.0	24.0	5.0	2.00	0.01
16-2	4.89	4.5	10.0	7.0	1.26	0.01
16-3	9.17	6.5	7.8	5.0	0.50	0.01
16-4	3.68	7.0	6.0	5.0	1.80	0.01
16-5	2.01	3.0	9.0	4.5	1.30	0.02
16-6	3.29	2.0	2.0	2.2	0.50	0.02
16-7	7.30	6.0	8.0	5.0	2.00	0.01
16-8	10.84	6.0	8.0	5.0	2.00	0.01
16-9	6.49	17.0	23.0	5.0	2.00	0.01
17-1	177.67	21.0	13.0	8.0	8.50	0.01
17-2	12.73	3.5	7.0	5.6	3.00	0.01
17-3	7.92	4.9	6.0	5.6	3.00	0.01
17-4	3.23	7.0	3.0	5.6	3.00	0.01
17-5	3.15	3.0	5.0	5.6	3.00	0.01
18	148.32	10.0	9.0	5.0	1.00	0.01
19	96.84	15.0	9.0	5.0	1.10	0.01
2	129.52	10.0	12.0	5.0	1.00	0.01
20	97.91	18.0	3.0	5.0	1.00	0.01
21	170.70	24.0	12.0	5.0	1.30	0.01
22	42.86	24.0	9.0	5.0	1.30	0.01
23	291.08	30.0	35.0	10.0	3.00	0.01
24	35.86	25.0	8.0	5.0	1.40	0.01
25	165.97	26.0	35.0	10.0	2.00	0.01

* refer to Figure 3.8 in this report.

Sub-basin	Basin Area (km ²)	Time of Concentration (Hr)	Storage Coefficient (Hr)	Initial loss (mm)	Constant rate (mm/hr)	Initial discharge (m ³ /s/km ²)
26	120.94	27.0	30.0	10.0	3.00	0.01
27	104.95	15.0	16.0	22.0	3.50	0.01
28-1	16.29	7.0	4.0	10.0	5.00	0.01
28-2	11.16	4.0	2.0	10.0	2.00	0.01
28-3	5.95	7.0	2.0	3.0	1.00	0.01
28-4	12.00	9.0	2.0	2.0	1.00	0.01
28-5	15.15	9.0	8.0	5.0	2.00	0.01
29	22.56	4.0	6.0	5.0	2.20	0.01
3	47.75	12.0	6.0	5.0	1.10	0.01
30-1	2.09	6.0	10.0	5.0	2.30	0.01
30-2	6.69	5.0	11.0	5.0	2.30	0.01
30-3	6.89	5.0	10.0	5.0	2.30	0.01
30-4	0.60	2.0	7.0	5.0	2.30	0.01
30-5	13.02	3.0	7.0	5.0	2.30	0.01
30-6	3.23	4.0	9.0	5.0	2.30	0.01
31-1	4.93	6.0	6.0	5.0	2.20	0.01
31-2	8.18	6.0	6.0	5.0	2.20	0.01
31-3	15.14	6.0	6.0	5.0	2.20	0.01
32	88.85	40.0	14.0	5.0	4.00	0.01
33	50.49	8.0	7.0	5.0	2.40	0.01
34-1	28.67	12.0	15.0	5.0	3.00	0.0117
34-10	7.73	5.0	3.0	5.0	3.00	0.0117
34-11	5.85	5.0	4.0	5.0	3.00	0.0117
34-12	7.92	5.0	4.0	5.0	3.00	0.0117
34-13	22.25	8.0	4.0	5.0	3.00	0.0117
34-14	15.94	8.8	4.9	5.0	3.00	0.0117
34-15	4.63	4.0	3.0	5.0	3.00	0.0117
34-16	14.06	6.0	4.0	5.0	3.00	0.0117
34-2	5.45	4.0	3.5	5.0	3.00	0.0117
34-3	5.92	3.7	2.5	5.0	3.00	0.0117
34-4	8.37	4.0	3.0	5.0	3.00	0.0117
34-5	1.78	2.5	1.5	5.0	3.00	0.0117
34-6	11.40	7.0	5.0	5.0	3.00	0.0117
34-7	14.45	7.0	4.0	5.0	3.00	0.0117
34-8	12.10	5.0	3.0	5.0	3.00	0.0117
34-9	3.47	3.0	2.0	5.0	3.00	0.0117

Sub-basin	Basin Area (km ²)	Time of Concentration (Hr)	Storage Coefficient (Hr)	Initial loss (mm)	Constant rate (mm/hr)	Initial discharge (m ³ /s/km ²)
4	151.19	12.0	10.0	5.0	1.00	0.01
5	76.82	7.0	6.0	5.0	1.10	0.01
7	144.00	5.0	10.0	5.0	1.00	0.01
8	88.36	11.0	7.0	5.0	1.00	0.01
9	78.48	7.0	6.0	5.0	1.10	0.01

Appendix 3: Description of CD enclosed

Folder	File	Description
WG-PCA\	JAVA files (MainWG.java etc)	The sources files for the weatehr generator model
WG-PCA\	WG model(Read me).doc	Instructions for Weather Generator to install, run, and check the results
	'StationNames'PPT_1964-2006.txt	
WG-PCA\DATA\B21	'StationNames'TempMax_1964- 2006.txt	Precipitation, maximum temperature, and minimum temperature data for the wet scenario (Input data of the WG model)
	'StationNames'TempMin_1964- 2006.txt	
	'StationNames'PPT_1964-2006.txt	
WG- PCA\DATA\Historical	'StationNames'TempMax_1964- 2006.txt	Observed precipitation, maximum temperature, and minimum temperature data (Input data of the WG model)
	'StationNames'TempMin_1964- 2006.txt	
	'StationNames'PPT_1964-2006.txt	
WG-PCA\Output\B21	'StationNames'TempMax_1964- 2006.txt	Output of precipitation, maximum temperature, and minimum temperature values for the wet scenario
	'StationNames'TempMin_1964- 2006.txt	

Folder	File	Description
WG- PCA\Output\Historical	'StationNames'PPT_1964-2006.txt	Output of precipitation, maximum temperature, and minimum temperature values for the historic scenario
	'StationNames'TempMax_1964-2006.txt	
	'StationNames'TempMin_1964-2006.txt	
hmsproj\	UTRb_EVENT(Read me).doc	Instructions for the hydrologic model to install, run, and check the results
hmsproj\ UTRb_EVENT	UTR_ClimateChange(B21).dss	Wet scenario part I
	UTR_ClimateChange(B21-2).dss	Wet scenario part II
	UTR_ClimateChange(Historical).dss	Historic scenario part I
	UTR_ClimateChange(Historical2).dss	Historic scenario part II
	UTR_Oct2006Gauges.dss	Observed data on Oct, 2006
hmsproj\ UTRb_EVENT	*.basin (e.g., EVENT.basin)	Basin components in HEC-HMS
hmsproj\ UTRb_EVENT	*.control (e.g., Event1.control)	Control components in HEC-HMS
hmsproj\ UTRb_EVENT	*.met (e.g., IDM_CC.met)	Meteorologic components in HEC-HMS

Appendix 4: List of Previous Reports in Series

ISSN: (print) 1913-3200; (online) 1913-3219

(1) Slobodan P. Simonovic (2001). Assessment of the Impact of Climate Variability and Change on the Reliability, Resiliency and Vulnerability of Complex Flood Protection Systems. Water Resources Research Report no. 038, Facility for Intelligent Decision Support, Department of Civil and Environmental Engineering, London, Ontario, Canada, 91 pages. ISBN: (print) 978-0-7714-2606-3; (online) 978-0-7714-2607-0.

(2) Predrag Prodanovic (2001). Fuzzy Set Ranking Methods and Multiple Expert Decision Making. Water Resources Research Report no. 039, Facility for Intelligent Decision Support, Department of Civil and Environmental Engineering, London, Ontario, Canada, 68 pages. ISBN: (print) 978-0-7714-2608-7; (online) 978-0-7714-2609-4.

(3) Nirupama and Slobodan P. Simonovic (2002). Role of Remote Sensing in Disaster Management. Water Resources Research Report no. 040, Facility for Intelligent Decision Support, Department of Civil and Environmental Engineering, London, Ontario, Canada, 107 pages. ISBN: (print) 978-0-7714-2610-0; (online) 978-0-7714-2611-7.

(4) Taslima Akter and Slobodan P. Simonovic (2002). A General Overview of Multiobjective Multiple-Participant Decision Making for Flood Management. Water Resources Research Report no. 041, Facility for Intelligent Decision Support, Department of Civil and Environmental Engineering, London, Ontario, Canada, 65 pages. ISBN: (print) 978-0-7714-2612-4; (online) 978-0-7714-2613-1.

(5) Nirupama and Slobodan P. Simonovic (2002). A Spatial Fuzzy Compromise Approach for Flood Disaster Management. Water Resources Research Report no. 042, Facility for Intelligent Decision Support, Department of Civil and Environmental Engineering, London, Ontario, Canada, 138 pages. ISBN: (print) 978-0-7714-2614-8; (online) 978-0-7714-2615-5.

(6) K. D. W. Nandalal and Slobodan P. Simonovic (2002). State-of-the-Art Report on Systems Analysis Methods for Resolution of Conflicts in Water Resources Management. Water Resources Research Report no. 043, Facility for Intelligent Decision Support, Department of Civil and Environmental Engineering, London, Ontario, Canada, 216 pages. ISBN: (print) 978-0-7714-2616-2; (online) 978-0-7714-2617-9.

(7) K. D. W. Nandalal and Slobodan P. Simonovic (2003). Conflict Resolution Support System – A Software for the Resolution of Conflicts in Water Resource Management. Water Resources Research Report no. 044, Facility for Intelligent Decision Support, Department of Civil and Environmental Engineering, London, Ontario, Canada, 144 pages. ISBN: (print) 978-0-7714-2618-6; (online) 978-0-7714-2619-3.

- (8) Ibrahim El-Baroudy and Slobodan P. Simonovic (2003). New Fuzzy Performance Indices for Reliability Analysis of Water Supply Systems. Water Resources Research Report no. 045, Facility for Intelligent Decision Support, Department of Civil and Environmental Engineering, London, Ontario, Canada, 90 pages. ISBN: (print) 978-0-7714-2620-9; (online) 978-0-7714-2621-6.
- (9) Juraj Cunderlik (2003). Hydrologic Model Selection for the CFCAS Project: Assessment of Water Resources Risk and Vulnerability to Changing Climatic Conditions. Water Resources Research Report no. 046, Facility for Intelligent Decision Support, Department of Civil and Environmental Engineering, London, Ontario, Canada, 40 pages. ISBN: (print) 978-0-7714-2622-3; (online) 978-0-7714-2623-0.
- (10) Juraj Cunderlik and Slobodan P. Simonovic (2004). Selection of Calibration and Verification Data for the HEC-HMS Hydrologic Model. Water Resources Research Report no. 047, Facility for Intelligent Decision Support, Department of Civil and Environmental Engineering, London, Ontario, Canada, 29 pages. ISBN: (print) 978-0-7714-2624-7; (online) 978-0-7714-2625-4.
- (11) Juraj Cunderlik and Slobodan P. Simonovic (2004). Calibration, Verification and Sensitivity Analysis of the HEC-HMS Hydrologic Model. Water Resources Research Report no. 048, Facility for Intelligent Decision Support, Department of Civil and Environmental Engineering, London, Ontario, Canada, 113 pages. ISBN: (print) 978-0-7714-2626-1; (online) 978-0-7714-2627-8.
- (12) Predrag Prodanovic and Slobodan P. Simonovic (2004). Generation of Synthetic Design Storms for the Upper Thames River basin. Water Resources Research Report no. 049, Facility for Intelligent Decision Support, Department of Civil and Environmental Engineering, London, Ontario, Canada, 20 pages. ISBN: (print) 978-0-7714-2628-5; (online) 978-0-7714-2629-2.
- (13) Ibrahim El-Baroudy and Slobodan P. Simonovic (2005). Application of the Fuzzy Performance Indices to the City of London Water Supply System. Water Resources Research Report no. 050, Facility for Intelligent Decision Support, Department of Civil and Environmental Engineering, London, Ontario, Canada, 137 pages. ISBN: (print) 978-0-7714-2630-8; (online) 978-0-7714-2631-5.
- (14) Ibrahim El-Baroudy and Slobodan P. Simonovic (2006). A Decision Support System for Integrated Risk Management. Water Resources Research Report no. 051, Facility for Intelligent Decision Support, Department of Civil and Environmental Engineering, London, Ontario, Canada, 146 pages. ISBN: (print) 978-0-7714-2632-2; (online) 978-0-7714-2633-9.
- (15) Predrag Prodanovic and Slobodan P. Simonovic (2006). Inverse Flood Risk Modelling of The Upper Thames River Basin. Water Resources Research Report no. 052, Facility for Intelligent Decision Support, Department of Civil and Environmental Engineering, London, Ontario, Canada, 163 pages. ISBN: (print) 978-0-7714-2634-6; (online) 978-0-7714-2635-3.

- (16) Predrag Prodanovic and Slobodan P. Simonovic (2006). Inverse Drought Risk Modelling of The Upper Thames River Basin. Water Resources Research Report no. 053, Facility for Intelligent Decision Support, Department of Civil and Environmental Engineering, London, Ontario, Canada, 252 pages. ISBN: (print) 978-0-7714-2636-0; (online) 978-0-7714-2637-7.
- (17) Predrag Prodanovic and Slobodan P. Simonovic (2007). Dynamic Feedback Coupling of Continuous Hydrologic and Socio-Economic Model Components of the Upper Thames River Basin. Water Resources Research Report no. 054, Facility for Intelligent Decision Support, Department of Civil and Environmental Engineering, London, Ontario, Canada, 437 pages. ISBN: (print) 978-0-7714-2638-4; (online) 978-0-7714-2639-1.
- (18) Subhankar Karmakar and Slobodan P. Simonovic (2007). Flood Frequency Analysis Using Copula with Mixed Marginal Distributions. Water Resources Research Report no. 055, Facility for Intelligent Decision Support, Department of Civil and Environmental Engineering, London, Ontario, Canada, 144 pages. ISBN: (print) 978-0-7714-2658-2; (online) 978-0-7714-2659-9.
- (19) Jordan Black, Subhankar Karmakar and Slobodan P. Simonovic (2007). A Web-Based Flood Information System. Water Resources Research Report no. 056, Facility for Intelligent Decision Support, Department of Civil and Environmental Engineering, London, Ontario, Canada, 133 pages. ISBN: (print) 978-0-7714-2660-5; (online) 978-0-7714-2661-2.
- (20) Angela Peck, Subhankar Karmakar and Slobodan P. Simonovic (2007). Physical, Economical, Infrastructural and Social Flood Risk – Vulnerability Analyses in GIS. Water Resources Research Report no. 057, Facility for Intelligent Decision Support, Department of Civil and Environmental Engineering, London, Ontario, Canada, 80 pages. ISBN: (print) 978-0-7714-2662-9; (online) 978-0-7714-2663-6.
- (21) Predrag Prodanovic and Slobodan P. Simonovic (2007). Development of Rainfall Intensity Duration Frequency Curves for the City of London Under the Changing Climate. Water Resources Research Report no. 058, Facility for Intelligent Decision Support, Department of Civil and Environmental Engineering, London, Ontario, Canada, 51 pages. ISBN: (print) 978-0-7714-2667-4; (online) 978-0-7714-2668-1.
- (22) Evan G. R. Davies and Slobodan P. Simonovic (2008). An integrated system dynamics model for analyzing behaviour of the social-economic-climatic system: Model description and model use guide. Water Resources Research Report no. 059, Facility for Intelligent Decision Support, Department of Civil and Environmental Engineering, London, Ontario, Canada, 233 pages. ISBN: (print) 978-0-7714-2679-7; (online) 978-0-7714-2680-3.
- (23) Vasan Arunachalam (2008). Optimization Using Differential Evolution. Water Resources Research Report no. 060, Facility for Intelligent Decision Support, Department of Civil and Environmental Engineering, London, Ontario, Canada, 42 pages. ISBN: (print) 978-0-7714-2689-6; (online) 978-0-7714-2690-2.

- (24) Rajesh Shrestha and Slobodan P. Simonovic (2009). A Fuzzy Set Theory Based Methodology for Analysis of Uncertainties in Stage-Discharge Measurements and Rating Curve. Water Resources Research Report no. 061, Facility for Intelligent Decision Support, Department of Civil and Environmental Engineering, London, Ontario, Canada, 104 pages. ISBN: (print) 978-0-7714-2707-7; (online) 978-0-7714-2708-4.
- (25) Hyung-II Eum, Vasan Arunachalam and Slobodan P. Simonovic (2009). Integrated Reservoir Management System for Adaptation to Climate Change Impacts in the Upper Thames River Basin. Water Resources Research Report no. 062, Facility for Intelligent Decision Support, Department of Civil and Environmental Engineering, London, Ontario, Canada, 81 pages. ISBN: (print) 978-0-7714-2710-7; (online) 978-0-7714-2711-4.
- (26) Evan G. R. Davies and Slobodan P. Simonovic (2009). Energy Sector for the Integrated System Dynamics Model for Analyzing Behaviour of the Social- Economic-Climatic Model. Water Resources Research Report no. 063. Facility for Intelligent Decision Support, Department of Civil and Environmental Engineering, London, Ontario, Canada. 191 pages. ISBN: (print) 978-0-7714-2712-1; (online) 978-0-7714-2713-8.
- (27) Leanna King, Tarana Solaiman, and Slobodan P. Simonovic (2009). Assessment of Climatic Vulnerability in the Upper Thames River Basin. Water Resources Research Report no. 064, Facility for Intelligent Decision Support, Department of Civil and Environmental Engineering, London, Ontario, Canada, 61pages. ISBN: (print) 978-0-7714-2816-6; (online) 978-0-7714-2817-3.
- (28) Slobodan P. Simonovic and Angela Peck (2009). Updated Rainfall Intensity Duration Frequency Curves for the City of London under Changing Climate. Water Resources Research Report no. 065, Facility for Intelligent Decision Support, Department of Civil and Environmental Engineering, London, Ontario, Canada, 64pages. ISBN: (print) 978-0-7714-2819-7; (online) 987-0-7714-2820-3.
- (29) Leanna King, Tarana Solaiman, and Slobodan P. Simonovic (2010). Assessment of Climatic Vulnerability in the Upper Thames River Basin: Part 2. Water Resources Research Report no. 066, Facility for Intelligent Decision Support, Department of Civil and Environmental Engineering, London, Ontario, Canada, 72pages. ISBN: (print) 978-0-7714-2834-0; (online) 978-0-7714-2835-7.
- (30) Christopher J. Popovich, Slobodan P. Simonovic and Gordon A. McBean (2010). Use of an Integrated System Dynamics Model for Analyzing Behaviour of the Social-Economic-Climatic System in Policy Development. Water Resources Research Report no. 067, Facility for Intelligent Decision Support, Department of Civil and Environmental Engineering, London, Ontario, Canada, 37 pages. ISBN: (print) 978-0-7714-2838-8; (online) 978-0-7714-2839-5.